TECHNISCHE UNIVERSITÄT MÜNCHEN
Lehrstuhl für Carbon Composites

Cure and Viscosity Measurement of Thermosetting Epoxy Resin with Fresnel Reflectometer Sensors

Jonathan Fabio Oelhafen

Vollständiger Abdruck der von der Fakultät für Maschinenwesen der Technischen Universität München zur Erlangung des akademischen Grades eines

Doktor-Ingenieurs

genehmigten Dissertation.

Vorsitzender:	Prof. Dr.-Ing. Karsten Stahl
Prüfer der Dissertation:	Prof. Dr.-Ing. Klaus Drechsler
	Prof. Dr.-Ing. habil. Dr. h.c. Alexander W. Koch

Die Dissertation wurde am 09.05.2019 bei der Technischen Universität München eingereicht und durch die Fakultät für Maschinenwesen am 02.10.2019 angenommen.

Technische Universität München
Fakultät für Maschinenwesen
Lehrstuhl für Carbon Composites
Boltzmannstraße 15
D-85748 Garching bei München

Tel.:+ 49 (0) 89 / 289 - 15092
Fax: + 49 (0) 89 / 289 - 15097
Email: info@lcc.mw.tum.de
Web: www.lcc.mw.tum.de

Declaration

Ich erkläre hiermit ehrenwörtlich, dass ich die vorliegende Arbeit selbstständig und ohne Benutzung anderer als der angegebenen Hilfsmittel angefertigt habe; die aus fremden Quellen (einschließlich elektronischer Quellen) direkt oder indirekt übernommenen Gedanken sind ausnahmslos als solche kenntlich gemacht. Die Arbeit wurde in gleicher oder änlicher Form noch keiner anderen Prüfungsbehörde vorgelegt.

Ort, Datum	Jonathan Oelhafen

Acknowledgement

This work would not have been possible without the support of several people who I would like to express my gratitude to:

- Prof. Klaus Drechsler of the Institute of Carbon Composites (LCC) for providing me the opportunity to write this thesis and my second supervisor Prof. Alexander W. Koch.
- Dr. Elisabeth Ladstätter and Dr. Swen Zaremba of the LCC for always having an open door, for their support and for the flexibility they provided during this work; but also during our REXUS campaign.
- Dr. Mathias Müller who mentored me and who was a great source of knowledge and encouragement during the whole time.
- The people of fos4X GmbH who create smart measurement solutions and especially Dr. Lars Hoffmann, Dr. Markus Schmid, Maximilian Raith, Fabian Zelenka, Dominik Wetzel and Florian Muschawechk for their unselfish support.
- Prof. Kostas Moutzouris of the University of West Attica and Prof. Johannes Roths of the University of Applied Sciences Munich provided valuable input for the calibration procedure and were always open for a discussion.
- All the students I had the pleasure to work with, especially Daniel Dickes and Tobias Mayr, who contributed greatly to the success of this thesis.
- My colleagues at the LCC who I shared a joyful time with and above all my room mate Tobias Wehrkamp-Trichter for having been an endless source of Matlab tricks and Ralf Engelhardt for the exciting REXUS adventure and beyond.
- My proof readers Mathias, Swen and Sophie Bruce.
- My parents, Peter und Britta, who created an environment during my upbringing that allowed me to thrive and follow my own path.

Abstract

Process monitoring is a means to increase the performance of composite manufacturing. Fibre optic sensors are suitable for process monitoring because they are versatile and provide a way to overcome the size and material limitations of electrical sensors. Earlier research results show that fibre optic sensors and measurement systems are capable of measuring a variety of process parameters. Two sensor types stick out at this as they are able to measure the most relevant process parameters: Fibre Bragg Grating (FBG) sensors for strain or temperature measurement e.g. of the composite laminate and Fresnel sensors for refractive index measurement e.g. of the polymer resin. Dual-sensing fibre optic sensor systems exploiting the versatile nature of these sensors are not available. However, most commercial FBG interrogators are equipped with the required hardware to also interrogate Fresnel sensors. Therefore, it is investigated whether this sensing scheme is able to measure the degree of curing and the viscosity of thermosetting epoxy resin during curing with Fresnel sensors. For that reason, the refractive index measurement uncertainty of said sensing scheme was investigated. Moreover, the degree of cure and viscosity of curing resin was correlated with its refractive index under isothermal and non-isothermal conditions to deduct analytical models for both parameters. This thesis describes the method to measure the refractive index with Fresnel sensors in combination with an FBG interrogator and it describes the applied calibration procedure. Additionally, two models are proposed to measure the degree of cure and the viscosity of curing thermosetting epoxy resin based on its resin refractive index and temperature; and their application is presented during composite manufacturing.

The observed refractive index measurement uncertainty is sufficiently low to measure curing of thermosetting epoxy resins typical to composite manufacturing. Further, it was found that the proposed models reproduce curing and viscosity behaviour well. This shows that the FBG interrogator is suitable to interrogate Fresnel sensors for cure monitoring during composite manufacturing. This ability opens new possibilities for process monitoring of composite manufacturing.

Kurzfassung

Prozessüberwachung kann zur Ertragssteigerung des Herstellungsprozesses von Verbundwerkstoffen beitragen. Insbesondere faseroptische Sensoren eignen sich dafür, da sie vielseitig einsetzbar sind und die Größen- und Materialbeschränkungen elektrischer Sensoren überwinden können. Frühere Forschungsergebnisse zeigen, dass sich faseroptischen Sensoren und Messsystemen dazu eigenen eine Vielzahl an Prozessparametern zu messen. Dabei ragen zwei Sensortypen heraus die in der Lage sind die wichtigsten Prozessparameter zu messen: FBG Sensoren zur Dehnungs- oder Temperaturmessung, z.B. des Laminats, und Fresnelsensoren zur Brechungsindexmessung, z.B. des Harzes. Multifunktionale faseroptische Sensorsysteme, die die Vielseitigkeit dieser Sensoren nutzen, sind nicht verfügbar. Die meisten kommerziellen FBG Messgeräte sind jedoch mit der erforderlichen Hardware ausgestattet, um Fresnelsensoren zu verwenden. Daher wird untersucht ob sich diese Messanordnung eigenet den Aushärtungsgrad und die Viskosität von duroplastischem Epoxidharz während der Aushärtung mit Hilfe von Fresnelsensoren zu messen. Aus diesem Grund wurde die Unsicherheit der Brechungsindexmessung der Messanordnung untersucht. Darüber hinaus wurde der Aushärtungsgrad und die Viskosität des aushärtenden Harzes mit seinem Brechungsindex unter isothermen und nicht-isothermen Bedingungen korreliert, mit dem Ziel analytische Modelle für beide Parameter basierend auf Fresnelsensormessungen abzuleiten. Die vorliegende Arbeit beschreibt das Verfahren zur Brechungsindexmessung mittels Fresnelsensoren mit einem FBG Messgerät, sowie das angewandte Kalibrierverfahren. Zusätzlich werden zwei Modelle zur Messung des Aushärtungsgrads und der Viskosität von aushärtendem duroplastischen Epoxidharzes vorgestellt, die auf dessen Brechungsindex und Temperatur basieren. Zuletzt wird die Anwendung der Sensoren während des Herstellungsprozesses von Verbundwerkstoffen gezeigt.

Die beobachtete Messunsicherheit der Brechungsindexmessung ist ausreichend niedrig, um die Aushärtung von duroplastischen Epoxidharzen zu messen, die für die Herstellung von Verbundwerkstoffen typisch sind. Weiterhin wurde festgestellt, dass die vorgeschlagenen Modelle das Aushärtungs- und Viskositätsverhalten gut reproduzieren. Dies eröffnet neue Möglichkeiten für die Überwachung des Herstellungsprozesses von Verbundwerkstoffen.

Table of Contents

List of Figures

List of Tables

Nomenclature

List of symbols

General notation

∇	Gradient
$\parallel$	parallel to the plane of incident
$\perp$	perpendicular to the plane of incident

Arabic letters

A	Molar refractivity	$\mathrm{m^3\,mol^{-1}}$
A_i	Amplitude of the incident electric field vector	$\mathrm{V\,m^{-1}}$
A_r	Amplitude of the reflected electric field	$\mathrm{V\,m^{-1}}$
A_t	Amplitude of the transmitted electric field	$\mathrm{V\,m^{-1}}$
A_1	Constant of refractive-index-based viscosity model	Pa·s
A_2	Constant of refractive-index-based viscosity model	Pa·s
a	Attenuation coefficient	$\mathrm{m^{-1}}$
a_i	Parameter of refractive-index-based degree of cure model	-
b_i	Parameter of refractive-index-based degree of cure model	-
C_a	Calibration constant	-
C_b	Calibration constant	-
C_i	Sellmeier coefficient	-
c_1	Parameter of refractive-index-based degree of cure model	-
c_0	Vacuum velocity of light	$\mathrm{m\,s^{-1}}$
D_i	Sellmeier coefficient	$\mathrm{nm^2}$
d_i	Parameter of refractive-index-based viscosity model	
E_1	Constant of refractive-index-based viscosity model	$\mathrm{J\,mol^{-1}}$

E_2	Constant of refractive-index-based viscosity model	$\mathrm{J\,mol^{-1}}$
$G^{'}$	Storage modulus	Pa
$G^{''}$	Loss modulus	Pa
G^{*}	Complex shear modulus	Pa
h	Gap height	mm
I	Light intensity	arb. unit
I_z	Light intensity at position z	arb. unit
I_i	Incident light intensity	arb. unit
I_0	Zero intensity	arb. unit
I_r	Reflected light intensity	arb. unit
$I_{r,air}$	I_r during air reference measurement	arb. unit
K	Permeability	$\mathrm{m^2}$
k	Factor	-
k_T	Temperature coefficient	$\mathrm{K^{-1}}$
K_a	Temperature-dependent parameter	-
K_b	Temperature-dependent parameter	-
K_1	Temperature-dependent parameter	$\mathrm{kg\,m^{-3}}$
K_2	Temperature-dependent parameter	$\mathrm{kg\,m^{-3}}$
k_0	Free space wavenumber	$\mathrm{nm^{-1}}$
l	Bragg grating length	mm
M	Molar mass	$\mathrm{g\,mol^{-1}}$
M_R	Torque	mN m
N	Number of molecules per unit volume	$\mathrm{m^{-3}}$
N_m	Avogadro number	$\mathrm{mol^{-1}}$
n_{rot}	Rotational speed	$\mathrm{s^{-1}}$
n	Refractive index	-
n_{air}	Air refractive index	-
n_{cal}	Refractive index of calibration fluid measured with refractometer	-
Δn_{cal}	Offset between n_{theo} and n_{corr}	-
n_{corr}	Corrected refractive index by calibration	-
n_{co}	Core refractive index	-
n_{cl}	Cladding refractive index	-
Δn_{cure}	Resin refractive index increase during curing	-
n_{eff}	Effective fibre refractive index	-
$n_{eff,0}$	n_{eff} at ambient temperature	-
n_f	Fibre refractive index	-
$n_{f,air}$	n_f during air reference measurement	-

n_{fluid}	Refractive index of calibration fluid measured fibre optically	-
$\overline{n}_{fluid}$	Mean refractive index of calibration fluid measured fibre optically	-
Δn_{off}	Offset between $\overline{n}_{fluid}$ and respective n_{cal}	-
n_p	Prism refractive index	-
n_{theo}	Refractive index calculated based on generic reflectivity input	-
p	Pressure	Pa
p	probability value	-
Q	Heat	J
$\dot{Q}$	Heat flow	mW
$\Delta Q(t)$	Heat, released or consumed	J
ΔQ_{tot}	Heat, total released	J
q	Volume averaged Darcy velocity	$\mathrm{m\,s^{-1}}$
R	Reflectivity	-
RE	Resolution	-
r	Radius	mm
r_α	Residual of refractive-index-based degree of cure model	-
r_η	Residual of refractive-index-based viscosity model	Pa·s
T	Temperature	°C
T_0	Ambient temperature	°C
T_{air}	Air temperature during reference measurement	°C
T_{fluid}	Water basin temperature	°C
T_g	Glass transition temperature	°C
$T_{g,0}$	Initial glass transition temperature	°C
$T_{g,\infty}$	Final glass transition temperature	°C
ΔT	Temperature difference	K
T_{Ref}	Reference temperature	°C
T_{Sample}	Sample temperature	°C
t	Time	s or min
t_{end}	Time at end of cure	s
t_0	Time at beginning of cure	s
u	Uncertainty	-
u_{BI}	Uncertainty of the offset from the calibration reference	-
u_{CAL}	Uncertainty of the calibration reference	-
u_{EVR}	Uncertainty of the equipment variation	-
$u_{EVR,max}$	Maximum value of u_{EVR} over all channels	-

u_{MP}	Uncertainty of the measurement process	-
u_{MS}	Uncertainty of the measurement system	-
$u_{MS.min}$	Required uncertainty of the measurement system	-
u_{RE}	Uncertainty of the measurement device resolution	-
v_{ph}	Phase velocity of light	$\mathrm{m\,s^{-1}}$
X	Random value	-
z	Length	m

Greek letters

α	Degree of cure	-
α_{hyp}	Level of significance	-
α_p	Mean polarisability	$\mathrm{m^3}$
α_{gel}	Degree of cure at gel point	-
α_Λ	Thermal expansion coefficient	$\mathrm{K^{-1}}$
α_n	termo-optic coefficient	$\mathrm{K^{-1}}$
β	Phase constant	$\mathrm{nm^{-1}}$
γ	Shear strain	%
γ_a	Shear strain amplitude	%
$\dot{\gamma}$	Shear strain rate	$\mathrm{s^{-1}}$
δ	Phase shift angle	°
η	Viscosity	Pa·s
η^*	Complex viscosity	Pa·s
η_1	First term of refractive-index-based viscosity model	Pa·s
η_2	First term of refractive-index-based viscosity model	Pa·s
Θ	Cone angle	°
Θ_i	Incident angle	°
Θ_t	Refraction angle	°
Θ_r	Reflection angle	°
Θ_c	Critical angle	°
Λ	FBG grating period	nm
λ	Wavelength	nm
λ_c	Centre wavelength of the light source	nm
λ_B	Bragg wavelength	nm
μ	Mean value of sample with outliers	-
μ_{sub}	Mean value of subsample without outliers	-
ρ	Density	$\mathrm{kg\,m^{-3}}$

ρ_0	Resin density in the uncured state	$\mathrm{kg\,m^{-3}}$
ρ_{max}	Resin density at full cure	$\mathrm{kg\,m^{-3}}$
σ	Standard deviation of sample with outliers	-
σ_n	Standard deviation of fluid refractive indices	-
$\sigma_{\overline{n}}$	Standard deviation of $\overline{n}$	-
σ_{sub}	Standard deviation of subsample without outliers	-
τ	Shear stress	Pa
τ_a	Shear stress amplitude	Pa
ω	Angular frequency	$\mathrm{rad\,s^{-1}}$
ω	Angular velocity	$\mathrm{rad\,s^{-1}}$

Physical constants

N_m	Avogadro number	$\mathrm{mol^{-1}}$
R	Universal gas constant	$\mathrm{J\,K\,mol^{-1}}$

List of abbreviations

ASE Amplified Spontaneous Emission

CFRP Carbon Fibre Reinforced Plastic

DC Direct Current

DEA Dielectric Analysis

DSC Differential Scanning Calorimetry

EFPI Extrinsic Fabry-Perot Interferometer

EPON 828 EPON™ Resin 828

EPS 600 HEXION® EPIKOTE™ System 600 resin

FBG Fibre Bragg Grating

FOS Fibre Optic Sensor

FRP Fibre Reinforced Plastic

FT-IR Fourier Transform Infrared Spectroscopy

FT-Raman Fourier Transform Raman Spectroscopy

GUM Guide to the Expression of Uncertainty in Measurement

IR Infrared

ISO International Organization for Standardization

LC Lucent Connector

LCM Liquid Composite Moulding

LPG Long Periode Grating

LVE Linear Viscoelastic Region

NCF Non-Crimp Fabric

NIR Near Infrared

PLC Planar Lightwave Circuit

RTM Resin Transfer Moulding

RTM 6 HexFlow® RTM 6 resin

TOC Thermo-Optic Coefficient

UV Ultraviolet

VARI Vacuum Assisted Resin Infusion

WDM Wavelength-Division Multiplexing

1 Introduction

In times of increasing fuel costs, generally growing awareness of the CO_2 footprint of air travel and tighter competition on the aviation market in the last two decades, the demand for more fuel-efficient aircrafts has raised. Weight reduction potential of traditional steel and aluminium alloys was exhausted and in the 1980s aircraft manufacturers started to replace metal structures with Fibre Reinforced Plastics (FRPs) due to their enhanced specific strength and stiffness [126].

However, developing and ramping up a FRP manufacturing process is time and material consuming because it is often developed on a trial and error basis [73]. Manufacturers are commonly challenged with highly variable parts, unpredictable part yield, high cost, and inefficient use of resin systems [4]. In an already competitive market, emerging aircraft manufacturers from Russia and China will further challenge the established manufacturers to stay competitive and cost efficient. The need is to reduce cycle time, waste and to improve the manufacturing quality [73]. Process monitoring technology provides valuable insights in the occurring effects and can improve process control.

Integrated sensors can provide valuable information on the process state, e.g. resin degree of cure, because the conditions inside the laminate or under core structures can differ strongly from the conditions on the laminate surface [16]. Many process monitoring systems and sensors are available on the market. However, few sensors are suited for FRP laminate integration. Integrated sensors must be small and non-intrusive in order to not affect the mechanical properties of the final FRP structure negatively. Additionally, these sensors shall be inexpensive since they remain in the structure and cannot be reused. These requirements speak for fibre optic sensors. A fibre optic sensor consist of an optical fibre that acts as a guide for light which is modulated by external perturbations. Fibre optic Fresnel reflectometer sensors are particularly suited for structural integration because they are inexpensive and have been applied previously to measure a variety of resin properties [7, 32, 92].

Fresnel sensors are characterised by a planar face at the end of an optical fibre. This face acts as the sensor because it reflects parts of the incident light back into the fibre depending on the surrounding medium.

For other important process parameters (e.g. temperature) further measurement systems are necessary. In order to reduce equipment cost and to ease merging of sensor data, it is favourable to have a multifunctional measurement system that can measure all or most process parameters. Commercial fibre optic Fibre Bragg Grating (FBG) measurement systems are designed to measure strain and temperature based on the associated wavelength shift of an FBG. These measurement systems possess the necessary hardware to interrogate Fresnel sensors. Early investigations in that field have been performed with laboratory equipment by Cusano et al. [32]. However, it has not been investigated to what extend it is possible to add this sensing functionality to a commercial fibre optic FBG measurement system. If successful it would allow to interrogating two different fibre optic sensors simultaneously. This would create a powerful and inexpensive measurement system for process monitoring of composite structures.

1.1 Objectives

The aim of this work is to expand the capabilities of fibre optic process monitoring during composite manufacturing. One focus is to investigate the capability of a commercial fibre optic FBG measurement system to measure the refractive index with Fresnel sensors. Being capable of that would provide the ability to perform *dual-sensing* which means to interrogate two different sensor types with one measurement system. The other is to develop new analytical models to measure resin properties, such as degree of cure and viscosity, based on Fresnel sensor measurements of the resin refractive index. The objectives to reach this aim are to:

- Calibrate a simplified refractive index measurement scheme that provides no means to measure the incident light intensity; and to set the determined measurement uncertainty in relation to previous studies and the requirements of epoxy resin cure monitoring.

- Model the relationship between refractive index and epoxy resin properties, such as degree of cure and viscosity, during isothermal and non-isothermal curing.

- Apply the fibre optic Fresnel sensors during composite manufacturing to measure the resin properties degree of cure and viscosity in the laminate.

1.2 Structure

Chapter 2: Describes aspects of composite manufacturing and the governing process parameters. A literature review is provided on the advances in process monitoring with a focus on fibre optic sensors. It is shown that fibre optic Fresnel sensors for refractive index measurement are very versatile. The underlying equations for refractive index measurements are introduced.
Chapter 3: Assesses the potential of the fibre optic FBG measurement system to measure the resin refractive index with Fresnel sensors. At first, the applied calibration method and procedure is introduced. Then, the calibration measurements are performed and the system is calibrated subsequently. At last, the refractive index measurement uncertainty is calculated.
Chapter 4: An analytical model to measure the degree of cure based on the resin refractive index and temperature is introduced. Isothermal and non-isothermal measurements of the degree of cure and the refractive index are performed and subsequently correlated. Based on these correlations, the model is derived and fitting parameters are determined. At last, the model is validated and the quality is assessed based on the analysis of the model residuals.
Chapter 5: This chapter introduces an analytical model to measure the resin viscosity based on the resin refractive index. The model is a combination of a state-of-the-art kinetic viscosity model and the previously determined degree of cure model. The model is fitted to isothermal viscosity measurements obtained from rheometer measurements. At last, the model is validated with isothermal and non-isothermal viscosity data and the quality is assessed based on the model residuals.
Chapter 6: The applicability of the fibre optic FBG measurement system in a *dual-sensing* application is demonstrated during composite manufacturing. Fresnel sensors are integrated in a composite laminate and the resin degree of cure and viscosity is monitored during curing. At the same time a mould-integrated FBG temperature sensor is interrogated with the same measurement device to track the mould temperature.
Chapter 7: A summary of the conducted work is provided and conclusions are drawn. Additionally, the contributions to the knowledge and literature on fibre optic process monitoring are stated.
Chapter 8: This chapter evaluates potential future work and applications of the presented Fresnel sensors and the fibre optic measurement system.

2 Theory and state of the art

The content of this chapter includes an introduction to composite manufacturing (Sec. 2.1) and presents the governing process parameters of composite manufacturing. Furthermore, background information is given on polymer curing and the resulting process parameters. Sec. 2.2 details and reviews the state of the art in process monitoring of two governing process parameters: degree of cure and viscosity. Sec. 2.3 introduces the standard laboratory methods to analyse the increase in degree of cure and viscosity during curing of polymer resins. In Sec. 2.4 fibre optic sensor technology is introduced. This section also provides a detailed literature review on fibre optic process monitoring. In addition, the fundamental equations for refractive index measurements with Fresnel sensors are introduced. A summary of the chapter is given in Sec. 2.5 and the gaps found in the literature regarding fibre optic process monitoring are presented.

2.1 Composite manufacturing

This section provides an overview on composite manufacturing technology, in particular Liquid Composite Moulding (LCM) in Sec. 2.1.1, and the governing process parameters in Sec. 2.1.3. The necessary background regarding resin curing and polymer properties is addressed in Sec. 2.1.2.

2.1.1 Liquid Composite Moulding

Composites are a composition of two or more materials, where one material carries structural loads (reinforcing phase) and the other material primarily binds the reinforcing phase (matrix). This has the purpose to increase the overall mechanical properties compared to the bulk properties of the individual components, such as weight-specific stiffness or thermal expansion.

Long before mankind discovered the structural advantages of reinforced concrete or polymers, nature had created specialised composite materials such as wood or bone. Nowadays, the composition of reinforcing fibres with polymer resin, also

known as FRP, is a typical composite application in mechanical engineering. In the context of this work, the term composite will be used to refer to FRPs.

Characteristic reinforcing fibre materials include glass, carbon, aramid or natural fibres. The fibre material is commonly processed into standardised textiles, by braiding, weaving or by binding large yarn bundles with knitting threads. Using textiles has several advantages for composite manufacturers: textiles can be handled easier and stacking of multiple layers is facilitated.

Polymer resins consist of long molecules that are entangled and linked with each other. The most relevant polymer matrix materials in engineering can generally be distinguished in thermosetting and thermoplastic materials. The former is a viscous liquid that solidifies due to chemical cross-linking to form an infusible mass. The latter becomes liquid and processible when heated over a threshold temperature and solidifies when cooled below. This process is reversible, in contrast to cross-linking. [109]

This work relates only to thermosetting resins, since they are the most relevant resins in composite manufacturing. Most common thermosetting resins are polyester (80 %) and epoxies (10 %) with market shares given in parenthesis [21]. Epoxy resins are used in advanced composites, due to their unique combination of low viscosity which eases infusion, fast curing, low shrinkage, high adhesive strength, high mechanical properties, good chemical resistance and versatility [98].

Today, FRP manufacturing is generally done by: hand lay-up, filament winding, autoclave, pultrusion and LCM [159]. LCM processes are favourable for high throughput and complex geometries at relatively low invest. This is due to low costs for the semi-finished products and easily drapeable dry textile stacks, which are also known as preform.

A variety of LCM infusion processes exist for thermosetting composites. Generally, they can be classified in matched-mould processes with two rigid moulds that shape the part, and single-sided mould processes with only one rigid mould and a flexible membrane that shapes the part when vacuum is applied. Which process is applied depends mainly on part size, quantity and quality. [4, 54, 159] Single-sided moulds are suitable for larger parts, in lower quantities and with lower surface quality requirements. All LCM processes have in common that the preform is compacted to the desired part thickness and that resin is infused by applying a pressure difference between the preform and the exterior.

A common single-sided LCM variant is the Vacuum Assisted Resin Infusion (VARI) process. A schematic of the VARI setup is shown in Fig. 2.1. The layup process is started by applying a volatile release agent that eases demoulding after curing. Then, the preform is placed on the mould. A peel ply layer covers the

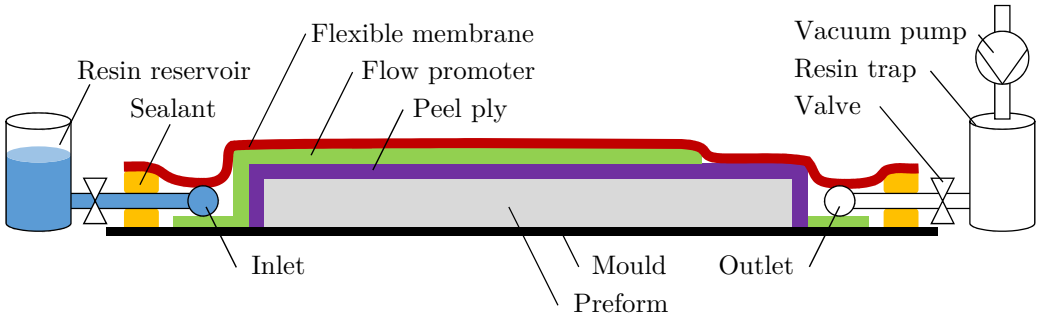

Figure 2.1: Schematic of the VARI process.

preform to ease demoulding. It has a similar function as the release agent. A flow promoter fabric is placed on top of the peel ply to enable fast resin distribution. The layup process ends by covering the whole stack with an airtight flexible membrane which is sealed against the mould with sealant tape. A vacuum pump is attached to the outlet and the whole setup is evacuated. When an appropriate pressure level is reached[1], the preform is infused by opening the valve at the resin inlet. The infusion is typically completed when the resin reaches the outlet. By metering the amount of resin infused in the preform, the fraction of fibre material in the composite (fibre volume fraction) can be controlled. A greater fibre volume fraction typically leads to greater mechanical properties. In order to reach high fibre volume fractions excessive resin can be removed from the preform through the outlet. After infusion is completed remaining pressure differences between inlet and outlet can be equalised by short-circuiting both, in order to homogenise the part thickness. The on-going resin polymerisation (curing) eventually solidifies the resin and the composite is formed. Depending on the resin system applied, additional heat is introduced to accelerate resin curing.

The aforementioned cross-linking process of epoxy resins can be accelerated by raising the resin temperature. The recommended processing temperatures are specific to each resin system. In the context of this work HEXION® EPIKOTE™ System 600 resin (EPS 600) was used. It is an unmodified premixed epoxy resin based on methylenedianiline and aromatic amine [70]. It was developed for aerospace applications as an alternative for the widely used HexFlow® RTM 6 resin (RTM 6) which has similar properties [69]. The data sheets of both resin systems are provided in the appendix in Sec. A.2 and Sec. A.3, respectively

When processing premixed epoxy resins in an infusion process, the resin is heated to several different temperature levels in order to allow resin flow and to reach the desired mechanical properties. Fig. 2.2 shows a typical mould temperature profile

[1] Typically $< 0.05\,\text{bar}$ [9].

during FRP manufacturing. Prior to resin infusion, of e.g. EPS 600 or RTM 6,

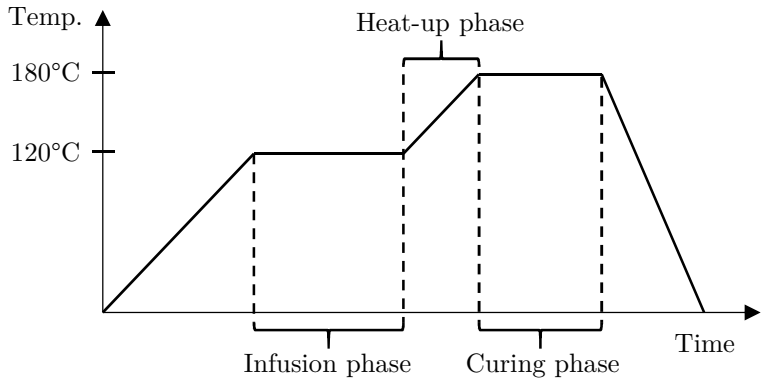

Figure 2.2: Mould temperature profile during a generic FRP manufacturing process. (After [9])

the mould is preheated at 120 °C because elevated temperatures lower the resin viscosity which eases infusion. In the mean time the resin is heated from storage temperature −18 °C to 80 °C (not shown in the image). During this phase the resin transfers from a solid to a liquid phase. When the liquid resin enters the preheated mould, the resin viscosity drops further. After infusion is finalised, a heat-up phase follows where the mould is heated to the curing temperature of 180 °C. The final resin properties are strongly influenced by the process temperatures [69]. Therefore, process temperatures and heating rates are specified in process specifications to assure constant production quality. For example: the heating rate must be below 2.5 K/ min and the isothermal plateaus must be held within ±5 °C when processing RTM 6 according to aerospace specifications [9].

2.1.2 Polymerisation

Polymers are cross-linked macromolecules that consists of many repeating units. Their structure consist mainly of carbon atoms. Macromolecules are generated by the chemical reaction (polymerisation) of low molecular base materials (monomers). Chemical cross-linking of the macromolecules by strong, covalent bond leads to a polymer network. A substantial factor for polymer properties are the number and type of cross-links, because they affect molecular size and shape [109].

Thermosetting epoxy resins, as used in this work, are highly cross-linked which explains their distinct thermal, mechanical and chemical properties [4]. The ability of carbon atoms to undergo a variety of chemical bondings explains the vast number of monomers and molecular bonds which make several so called polyreactions possible. The formation of macromolecules is controlled by environmental conditions (e.g. temperature, pressure, concentration, etc.) and regulating additives such as catalysts, activators or inhibitors. In many cases the exact formulation and

concentration of the reacting partners is not known. For that reason different polyreactions may occur at different moments during curing. For a detailed description of polymer reactions the reader is referred to the following books [98, 146]. A detailed insight into the reaction process is difficult to achieve. Ellis [47] states that for a comprehensive description of the extend of cure, it is required:

- to determine the concentration of reacting groups (e.g. by spectroscopy),
- to estimate the extent or progress of chemical reaction (e.g. by thermal analysis), and
- to measure changes in physical and mechanical properties (e.g. by rheometry).

One can see that it is elaborate to describe the curing reaction comprehensively and for most questions it is not necessary. Commonly, one settles for determining the conversion of the reacting partners which is also known as the degree of cure. Conversion is the fraction of reacted molecules to the overall amount of reactive molecules and takes the value of 0 at the beginning of cure and rises towards 1 at the end. In case of thermosetting polymers, the curing reaction is accompanied by heat release due to exothermic reaction. It is common to track conversion by detecting the released heat during polymerisation, e.g. by Differential Scanning Calorimetry (DSC). This measurement method is described in detail in Sec. 2.3.1.

In material science, the state of matter is commonly described by phases (solid, liquid, gas) with distinct phase boundaries (defined by e.g. temperature or pressure). This idea cannot simply be transferred to polymers due to their composition. Their material characteristics are mainly determined by their molecular structure which in turn determines their molecular mobility. Temperature is the main facilitator for molecular mobility which leads to softening, changes in volume and enthalpy, mechanical dampening and so forth [146]. For this reason, polymer properties, thermal states and phase transitions have been described as functions of temperature.

During curing, thermosetting polymers pass through three distinct stages. At the beginning the material is liquid. With ongoing conversion of the reactive partners, a three dimensional network forms and the material becomes rubbery. In the last stage, the material becomes glassy and forms a solid [67]. These stages are separated by two characteristic transitions: the transition from the liquid to the rubbery stage is called gelation. At this point an infinite network is formed and the (weight average) molecular weight and subsequently the resin viscosity diverges to infinity [94, 106, 166]. Resulting from that, polymers at the gel point lose their ability to flow and are no longer processible. Therefore, chemical shrinkage of the

polymer cannot be compensated by further resin flow and stress induced through chemical shrinking cannot be relieved. This is important because process-induced stress is a common cause for deformations [117]. The chemical curing reaction, however, is unaffected by gelation and proceeds well beyond the gel point [94]. For that reason gelation can only be measured by mechanical or mechanical means, e.g. by rheometry (Sec. 2.3.2), and not by thermal analysis methods such as DSC [106]. It is worth noting that, independent of curing temperature, the gel point of a given resin system occurs at the same degree of cure [128]. This fact is used in some viscosity models where it confines the applicability of the respective models [64].

During the glass transition the polymer changes from the rubbery to the glassy state. In the rubbery state the molecular backbone of the polymer is mobile and it changes place rapidly. During the transition, molecular segments become immobile. This is accompanied by drastic changes in material properties, such as specific volume (Fig. 2.3), density, heat capacity and modulus [67, 109, 150, 161]. These changes allow measurements of the glass transition by mechanical and thermal means such as rheology or DSC [94, 157]. As the name suggests, the glass transition occurs over a temperature range. For practical use the term glass transition temperature (T_g) was coined for the temperature at which the property changes most rapidly. In many cases T_g sets the upper limit of the temperature application window of the final part. During curing, T_g rises from an initial glass transition $T_{g,0}$ in the uncured state (typically $< 0\,°C$), to the final glass transition temperature $T_{g,\infty}$ at full cure ($> 200\,°C$ possible). When the polymer solidifies the curing

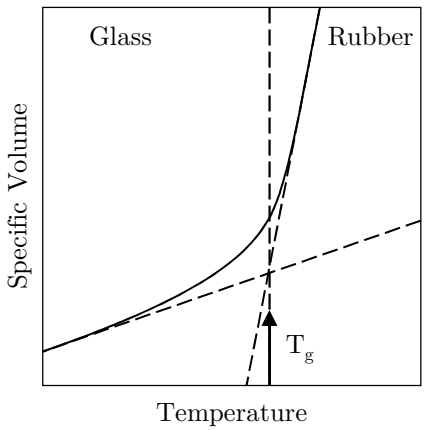

Figure 2.3: Deflection of specific volume at glass transition during temperature change, after [109]. The intersection between the asymptotes indicates the approximate location of the glass transition temperature and divides the image in glassy and a rubbery region.

reaction slows down drastically because molecular mobility is inhibited. However, curing still progresses on a small scale through diffusion.

As a side note: the glass transition is reversible, in contrast to gelation. Therefore, curing of uncured reaction partners can be continued by heating the polymer above the glass transition thus re-enabling molecular mobility for further cross-linking [167].

2.1.3 Process parameters of liquid composite moulding

A (manufacturing) process is a series of interrelated tasks that transforms inputs into outputs [114]. The efficiency of a process, also called productivity, is expressed as the quotient of output and input. The greater the quotient, the better the efficiency. Efficiency is a challenge in composite manufacturing because its production requires complex manufacturing processes which can lead to process variability. This is time and material consuming and results in unpredictable part yield and high cost as a consequence [4, 73, 169]. The variability originates from various causes such as: preform material, preform handling and storage, resin impregnation, curing behaviour and equipment malfunction [117, 137]. Efficiency is not only an issue during production but also during process development and production ramp-up. Many times, development and ramp-up is performed empirically because the process of resin infusion and curing cannot be monitored visually inside the mould [58]. Furthermore, the process is determined by parameters that are dependent on each other and affect the process and the part quality [95]. In order to stay competitive there is a need for constant increase of productivity and reliability of the processing cycles[2]. Efficiency increase can be achieved by minimising the process input in terms of material, energy, time and man hours to generate the desired output. Therefore, the goal for every composite manufacturer is to achieve a robust process, that produces completely cured parts in the desired shape, with uniform resin content and minimized void content, in the shortest time possible [73, 88]. Bringing light to the underlying effects during processing by measuring characteristic process and material properties serves the purpose:

- to document product quality and manufacturing process,
- to monitor product quality and manufacturing process, and
- to generate input parameters for process control,

[2] A cycle is a predetermined sequence of temperatures, pressures, flow rates, etc. to produce a part in a given time frame [73].

as Hochrein and Alig [72] and Doyle et al. [43] point out. As a possible result, process development and production ramp-up can be accelerated, and productivity can be increased. Since the underlying effects are literally invisible, the LCM process can be seen as a black box. This black box process is characterised by process parameters, e.g. temperature and pressure, and by quality parameters of the finished part, e.g. rheologic quantities or degree of cure. Process parameters are generally strongly linked to quality parameters in polymer processing [72]. This might explain why both parameters are often not differentiated and why there is no unanimous opinion about the full extend of all process parameters.

An overview of common LCM process and quality parameters is shown in Fig. 2.4. This overview is extracted from several sources [4, 95, 142] and lists the input, disturbance and target values that characterise the LCM process. The input values are determined by the process parameters, the mould design and the specific composite materials. The resulting quality parameters and process properties are a function of the input values and disturbance values that result from deviations in the material, the processing equipment or originate from environmental impacts such as ambient temperature. The presented list raises no claim to completeness since the definitions are subjective to the observer and the specific process.

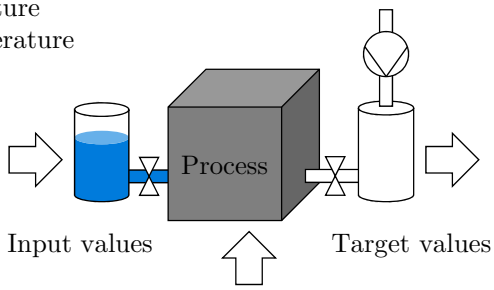

Process parameters
- Initial resin temperature
- Resin (Mould) temperature
- Injection pressure
- Mould pressure
- Viscosity
- Permeability
- Flow front
- ...

Quality parameter
- Degree of cure
- T_g
- Density
- Porosity
- Fibre volume content
- Dimensions
- ...

Tool and material
- Location of gates and vents
- Fabric type
- Resin system
- ...

Disturbance values

Deviations
- Material
- Process parameters
- Environmental
- ...

Process
- Cycle time
- Energy consumption
- Material consumption
- ...

Figure 2.4: Input, disturbance and target values of an LCM process.

For composite manufacturing, the two most important parameters are temperature and pressure [72, 73, 137]. This is easily comprehensible when considering the fundamental equation that describes resin flow q during infusion:

$$q = -\frac{K}{\eta} \cdot \nabla p \,. \tag{2.1}$$

The so called Darcy equation[3] relates resin flow to the applied pressure gradient in the mould ∇p, to the preform permeability K - a proportional constant that describes the porosity, and to the resin viscosity η [4]. Pressure difference and permeability are mainly controlled by the infusion equipment and preform properties, leaving viscosity as the only property of the flowing medium (here: resin).

Viscosity is defined as the resistance of fluids against deformation. Besides temperature and cure, viscosity is a function of pressure, shear rate, particle volume and particle fraction [64]. During composite manufacturing the resin cures and its viscosity increases gradually from 0 Pa·s to infinity. Eventually, this brings the resin flow to a halt. As a rule of thumb: resin flow halts when it reaches the non-injection point at 1 Pa·s [138]. The gradual viscosity increase during curing can be temporarily stopped or reversed due to its temperature dependence. For example: raising the resin temperature increases the molecular mobility, thus reduces resistance to deformation, which results in a lower viscosity [4]. This effect is exploited in composite manufacturing by processing the resin at different temperature levels to ease infusion and preform impregnation (cf. Fig. 2.2).

The central role of viscosity is due to the fact that it controls resin flow and its strong dependence on temperature and cure. Also worth noting: the rheological properties of curing resins govern the extent to which residual stresses occur during processing, as Woerdeman et al. [169] point out. In light of these facts it is obvious that the parameters viscosity and degree of cure belong to the governing parameters in composite manufacturing [32, 73, 101, 103, 137, 169]. Monitoring both can contribute to increased productivity.

2.2 Review of process monitoring technology for curing and viscosity

The previous chapter showed that composite manufacturing is dependent on manifold parameters. As was pointed out in Sec. 2.1.3, the most important parameters are pressure and temperature. For these parameters, a wide array of monitoring solutions are available on the market [72]. It was also pointed out, that the parameters curing and viscosity, play a similarly important role in composite manufacturing. Therefore, the focus of this work shall be on monitoring these two parameters. The following chapter gives an overview of the state of the art in monitoring curing (Sec. 2.2.1) and viscosity (Sec. 2.2.2).

[3] Henry Darcy (1803-1858), a French engineer who performed water flow experiments in beds of sand [37].

2.2.1 Conversion

Polymer curing is the central processing step in producing composites with thermosetting resins. Several methodologies have been developed to characterize aspects of the cure process. The following list gives an overview of these methodologies and provides references of their application:

- DSC [25, 66, 76, 158, 160]
- rheometry [123, 158, 166]
- Dielectric Analysis (DEA) [66, 90, 111, 129, 148, 156]
- Direct Current (DC) [35, 88, 147]
- dynamical mechanical analysis [22, 106]
- torsional braid analysis [53]
- ultrasonic measurements [25, 158]
- piezoelectric sensors [156]
- refractometry [36]
- Fourier Transform Infrared Spectroscopy (FT-IR) [38, 44, 55, 57, 76, 101, 158, 166]
- Fourier Transform Raman Spectroscopy (FT-Raman) [38, 66]
- Fibre Optic Sensor (FOS) applications [25, 55, 140, 160, 169] (cf. Sec. 2.4)

Most of the above cited methodologies can measure curing but are not capable of measurements during the composite manufacturing process ("online"). This is mainly due to the size or measurement principle that prohibits process integration. Online methods need to be non-invasive and non-destructive so that the manufacturing process is not influenced or disturbed. Among the methods cited above, mainly electrical methods (DEA and DC) and optical methods (FOS, FT-IR and FT-Raman) are able to perform online curing measurements [66, 143, 160].

Using electrical sensors for cure monitoring of polymers has a long history dating back to the 1930s [148, 164]. Commercial DEA measurement equipment for mould-integrated measurement of resin properties has been developed e.g. by Netzsch GmbH. The addressed mould sensors measure the resin properties at the part surface. However, during composite manufacturing it is also of interest to measure

the properties in between the laminate layers or under core structures, e.g. for the purpose of validating process simulations or to detect undesired effects such as race tracking or dry spots. To overcome this disadvantage, electrical DEA sensors have been miniaturized and successfully embedded in laminates [111]. However, electric sensors need insulation against conductive reinforcing fibres, e.g. carbon fibres, that may lead to bulkier sensor designs. In addition, metallic wiring is needed, which may induce interference in the electrically noisy production environment as George et al. [55] point out.

Spectroscopy has been used to analyse thermosetting resin curing [36]. The measurement principle relies on analysing changes in the intensity of reflection peaks. Since these peaks relate to specific functional groups of the polymer, this method is useful to monitor compositional changes during curing [158]. With the evolution of new Fourier transform sampling techniques, spectroscopy became a particularly useful method for online process monitoring [158]. One big advantage of spectroscopy is that these methodologies can be used in stationary devices but also in combination with optical fibres. Archibald et al. [14] and George et al. [55] obtained Near Infrared (NIR) spectra during resin curing with embedded FOS. Dunkers et al. [44] did so with a mould-integrated attenuated total internal reflection sensor in combination with FT-IR. Due to the spectral cut-off of commercial optical fibres, the measurement is restricted to the NIR spectrum (700 nm to 3000 nm) [14]. However, this spectrum is ideal for monitoring changes during cure, due to increased molecular excitation [43]. The disadvantage of spectroscopic methods is, that they rely on relative changes of spectral peaks and that no absolute measurement is possible.

Other optical methods for cure monitoring during composite manufacturing are fibre optic sensors which are discussed in detail in Sec. 2.4.

2.2.2 Viscosity

Viscosity measurements are classically performed with rheometers (see Sec. 2.3.2). Due to their size and measurement principle, conventional rheometers cannot be used for online viscosity measurement during manufacturing. For polymer extrusion processes, different approaches have been suggested to measure the viscosity in a bypass of the polymer melt with capillary rheometers [72]. Anton Paar, Austria, developed the L-Vis 510 device that is immersed directly in the production liquid to measure viscosity of asphalt polymer blends or lubricants. However, the aforementioned solutions have little relevance to online monitoring of composite manufacturing because they cannot be integrated in the mould.

Acoustic wave sensors may have the potential to conquer that problem by using piezoelectric materials to shear material on a microscopic scale. The Vectron ViSmart sensor for example uses surface acoustic waves for online viscosity measurement of oils, lubricants and fuels. Several researchers have shown their application as biosensors in fluids [51, 62, 113].

Electrical sensors such as DEA sensor [148] and the DC sensor [164] have been used to measure resin properties during curing. Maistros and Bucknall [110] found that an inversely proportional relationship exists between viscosity and DEA ionic conductivity, as resin viscosity reflects molecular mobility in the growing network. In other previous studies, rheometer data has been correlated with data from DEA sensors [87, 90, 152] and DC sensors [54, 88].

Solutions for optical process monitoring of viscosity are scarce in literature [163]. Ton-That et al. [158] showed a correlation of zero shear viscosity to the degree of cure calculated from FT-IR measurements. Levy and Schwab [101] used fibre-optic flourimetry by utilising viscosity-dependent fluorescence compounds dispersed in the resin. Other contributions have applied FBG to measure viscosity of liquids [96, 133]. However, these solutions rely on excitation of mechanical parts which makes integration into moulds difficult and they have not been applied to curing resins.

In summary, DEA sensors are the most advanced sensors for online viscosity measurement during composite manufacturing. FOS, however, show good potential if the measurement principle does not rely on mechanical interaction. Typically, viscosity sensors are validated with values obtained in rheometer measurements (cf. Sec. 2.3.2).

2.3 Curing reaction analysis

Curing reaction can be characterised by several means as pointed out in Sec. 2.1.2. This section focuses on two methods: thermal analysis with DSC to derive the degree of cure (Sec. 2.3.1) and rheometry to derive e.g. viscosity (Sec. 2.3.2).

2.3.1 Thermal analysis with DSC

Thermal analysis measures the amount of heat that is necessary for a physical or chemical transformation of material, e.g. curing or glass transition. Depending on if energy (heat) is released or consumed one distinguishes between exothermic and endothermic reactions. Thermosetting epoxy curing is typically exothermic [68, 79]. The most established method to measure heat flow during composite curing is

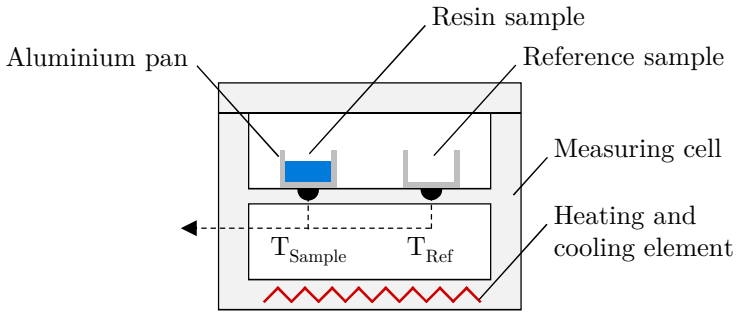

Figure 2.5: Schematic of DSC measuring cell with resin sample pan and reference sample pan.

Differential Scanning Calorimetry (DSC). The specific measurement procedures for polymer applications are provided in the ISO 11357-1:2009 standard [41].

Generally, DSC devices consist of a measuring cell to measure the released heat of a curing sample under controlled thermal and atmospheric conditions, see Fig. 2.5. Measurements are performed by measuring the temperature difference between an aluminium pan filled with the resin sample and an empty aluminium pan as reference ($\Delta T = T_{Sample} - T_{Ref}$). Both samples are subjected to the same thermal cycle. Any temperature difference between resin and reference is based on their varying heat capacities and can be related to the curing reaction or to phase transitions that consume or release heat. Based on the temperature difference, the sample heat flow is deducted. Due to the differential measuring principle, pan mass ($\pm 0.01\,\mathrm{mg}$) and sample mass ($\pm 0.1\,\mathrm{mg}$) have to be determined precisely, to ensure accurate measurements [41]. The recommended precision is given in parenthesis. The released or consumed heat $\Delta Q(t)$ in a time interval between t_0 and t is given by

$$\Delta Q(t) = \int_{t_0}^{t} \frac{dQ}{dt} dt\,, \tag{2.2}$$

with the heat flow $\frac{dQ}{dt} = \dot{Q}$ and the time differential dt. It is assumed, that the released heat during exothermic curing is proportional to the amount of chemical reactions currently occurring. Hence, the released heat $\Delta Q(t)$ is proportional to the degree of cure $\alpha(t)$:

$$\alpha(t) = \frac{\Delta Q(t)}{\Delta Q_{tot}}\,. \tag{2.3}$$

The total released heat at full conversion ΔQ_{tot} is determined in non-isothermal curing runs in order to allow full conversion of the reactants and to prevent vitrification. In non-isothermal curing runs the sample is cooled below $T_{g,0}$. Then the temperature is increased at a constant heating rate and the resin is cured until no further heat is released. This point marks the curing end time t_{end}. Typical heating rates are between $5\,\mathrm{K\,min^{-1}}$ and $20\,\mathrm{K\,min^{-1}}$ [41]. Fig. 2.6 shows an exem-

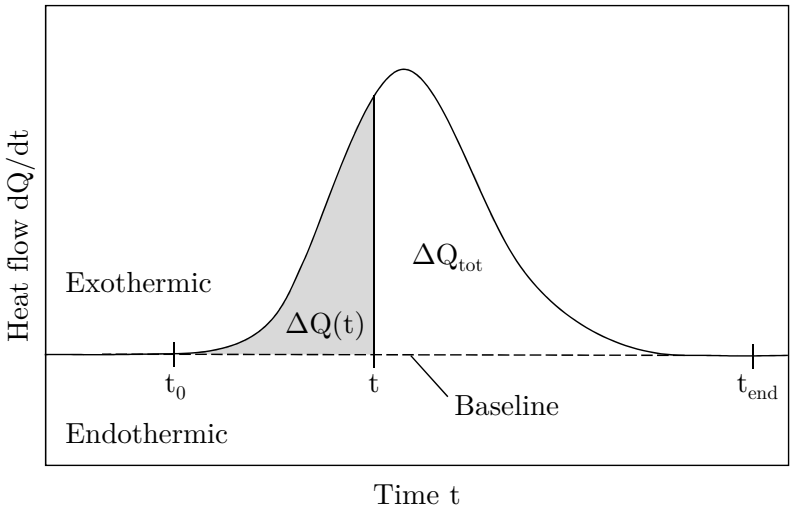

Figure 2.6: Exemplary heat flow measurement during resin curing in DSC. The degree of cure α is the ratio of the released heat $\Delta Q(t)$ at a given time t and the total released heat ΔQ_{tot}.

plary heat flow curve obtained during exothermic curing. When the curing reaction starts and excess energy is set free, the curve starts to deviate from the baseline at t_0. The total released heat ΔQ_{tot} is represented by the area between the curve and a material specific baseline between t_0 and t_{end}. The released heat $\Delta Q(t)$ at a given time t is highlighted in grey.

2.3.2 Rheologic analysis with rheometry

Viscosity η is the resistance of fluids against deformation. The behaviour of an ideal viscous material is expressed in Newton's law of viscosity by the ratio of shear stress τ to shear rate $\dot{\gamma}$ [134]:

$$\eta = \frac{\tau}{\dot{\gamma}} \,. \tag{2.4}$$

It is typically measured in stationary rheometers. Depending on the phenomenon of interest or the processing technology, different rheometer instruments are available on the market [118, 134]. In this work, a rotational rheometer has been used due to its versatility. Rotational rheometers are usually used in a cone-plate or parallel-plate configuration where a fluid is sheared between a static and a rotating surface (see Fig. 2.7). In the parallel-plate configuration, the shear stress τ and shear rate $\dot{\gamma}$ for Newtonian liquids is calculated by [42]

$$\tau = \frac{2M_R}{\pi r^3} \,, \text{ and} \tag{2.5}$$

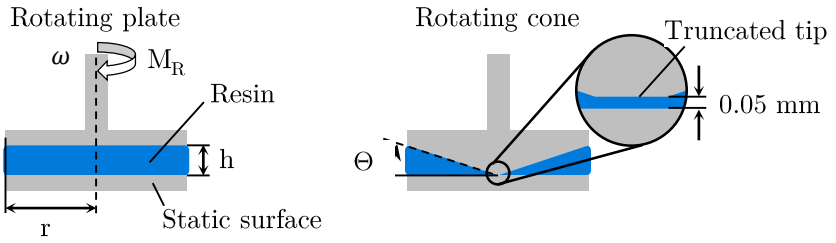

Figure 2.7: Schematic of two rotational rheometer configurations: parallel-plate (left) and cone-plate (right) with detail of truncated cone tip.

$$\dot{\gamma} = \frac{\omega r}{h}\,, \tag{2.6}$$

with rheometer torque M_R, plate radius r and gap distance h. The angular velocity $\omega = \frac{2\pi \cdot n_{rot}}{60}$ is related to the rotational speed n_{rot}. In the parallel-plate configuration the shear rate is not constant in the gap, instead it increases from 0 at the centre to the maximum at the outer radius. For viscosity analysis the outer radius is incorporated in Eq. 2.5 and Eq. 2.6. The cone-plate configuration, in contrast, generates a constant shear rate over the radius for a given cone angle Θ. Due to that, the equations for shear stress and shear rate differ slightly for this configuration:

$$\tau = \frac{3M_R}{2\pi r^3}\,, \text{ and} \tag{2.7}$$

$$\dot{\gamma} = \frac{\omega}{\tan\Theta} \underbrace{\approx}_{\text{for} < \Theta} \frac{\omega}{\Theta}\,. \tag{2.8}$$

The simplification made in Eq. 2.8 is valid for small cone angles $\Theta < 3\,^\circ$ [118]. In order to prevent contact between the cone tip and the plate, the cone is truncated, see detail in Fig. 2.7. In order to satisfy the constant shear rate condition, a 0.05 mm gap is maintained between cone and plate. Since volume shrinkage might alter the gap height and influence the viscosity measurement, special attention must be paid when investigating resin curing in the cone-plate configuration [134].

Rheometers can either perform rotational measurements where the plate spins constantly, or oscillatory measurement where the plate rotates back and forth. Rotational measurements are typically performed under isothermal temperatures. One distinguishes tests that are performed at a given shear rate $\dot{\gamma}$ ($\omega = const.$) resulting in a measured torque M_R and tests performed at a given shear stress τ ($M_R = const.$) resulting in a measured angular velocity ω. The former yields the shear stress τ which can be calculated according to Eq. 2.5 or Eq. 2.7. The latter yields the shear rate $\dot{\gamma}$ according to Eq. 2.6 or Eq. 2.8.

The viscosity of most polymers is dependent on the shear rate. This phenomenon is called shear thinning behaviour. It is due to disentanglement of the polymer chains under the influence of shear, resulting in lower viscosity due to easier sliding of the molecule chains. The dependence of viscosity on shear rate is typically investigated in *shear rate sweeps*. There, the viscosity is measured while increasing or decreasing the shear rate. Ideally, a region can be identified where the viscosity stays constant with increasing shear rate. Rotational measurements should be performed within this region.

Curing thermosetting resins change their viscosity from a liquid, viscous state that can be described by Newton's law of viscosity to a solid, elastic state that is described by Hooke's law[4]. During this transition the material properties are somewhat in between and show viscoelastic behaviour. Rotational measurements are inappropriate to capture this transition because the rotation damages the solidifying polymer. Instead, oscillatory measurements are performed to reduce the applied shear.

During oscillatory measurements the material is subjected to deformation or torque. Based on that input, shear stress τ or shear strain γ can be deducted as well as the lag between input and material responds. The lag is also expressed by the so called phase shift angle δ. By evaluating shear strain, stress and phase shift angle, further parameters can be deducted. Most importantly, the storage modulus $G^{'}$ that describes the elastic behaviour. It is a measure of the stored, reversible, deformation energy introduced in the material during shearing. In contrast, the loss modulus $G^{''}$ describes the viscous behaviour. It is a measure of the lost, dissipated energy during shearing. The moduli are described by

$$G^{'} = \frac{\tau_a}{\gamma_a} \cdot \cos(\delta)\,, \text{ and} \tag{2.9}$$

$$G^{''} = \underbrace{\frac{\tau_a}{\gamma_a}}_{\mathrm{G^*}} \cdot \sin(\delta)\,, \tag{2.10}$$

with shear stress amplitude τ_a and shear strain amplitude γ_a and the complex shear modulus G^*. The ratio of loss to storage modulus is referred to as loss factor $\tan(\delta)$:

$$\tan(\delta) = \frac{G^{''}}{G^{'}}\,. \tag{2.11}$$

[4] $\varepsilon = k\sigma$. The strain ε of an object is proportional k to the stress σ applied to it. Named after the British physicist Robert Hooke (1635-1703).

Evaluating G' and G'' can give indication of e.g. the gel point during curing thermosetting polymers. This occurs when $G' = G''$ which is equivalent to $\tan(\delta) = 1$ [166]. In addition, the viscosity can be determined in oscillatory measurements, where it is referred to as complex viscosity η^*. It is also described by Newton's law of viscosity (compare Eq. 2.4):

$$\eta^* = \frac{\tau(t)}{\dot{\gamma}(t)}\,. \tag{2.12}$$

Although oscillatory and rotational measurements are performed under different conditions, the obtained viscosity values are comparable according to the Cox-Merz rule, if the values of the shear strain rate $\dot{\gamma}$ in the rotational measurement match the value of the angular frequency ω of the oscillating measurement: $\eta(\dot{\gamma}) = |\eta^*(\omega)|$. [29, 118]

Taking into account the findings of Cox and Merz, allows to generate continuous viscosity slopes from combined rotational and oscillatory measurements. This is useful to extend viscosity measurements e.g. beyond gelation where rotational measurements cannot be performed. The Cox-Merz rule has shown its validity in the Linear Viscoelastic Region (LVE), where Hooke's and Newton's laws apply. This region is characterised by proportional behaviour of rheometer input and material output. Beyond that, the underlying rheometric equations are not valid. Therefore, it is highly recommended to determine the LVE by performing *amplitude sweeps*. During a sweep, τ_a or γ_a are increased while the temperature and angular frequency ω are kept constant. As long as the resulting values for G' and G'' remain constant the material is in the LVE. Mezger [118] recommends to evaluate the G'- curve since it has shown the tendency to leave the LVE before the G''- curve. It has to be stressed, that the results from the amplitude sweep are only valid for the applied angular frequency. Many materials exhibit elevated stiffness (G') at elevated angular frequencies [118]. Therefore, it is also recommended to perform a *frequency sweep* (within the LVE) to investigate the time-dependent deformation behaviour of the resin. The interpretation of frequency sweeps is often material specific and for a detailed discussion the reader is kindly referred to the literature [118].

2.4 Fibre optical process monitoring

The literature review in Sec. 2.2 showed, that optical methods are particularly suited to perform online cure measurements. Utilising optical approaches to measure polymer properties during curing can overcome the short comings of electrical sensors. Since the early 1980's quantitative non-destructive evaluation of compos-

ite materials with FOS has been the subject of research. FOS are advantageous because they are made of inert fused silica (glass). This has the positive effect that optical fibres do not corrode the composite, are electromagnetically compatible and are insensitive to conductive carbon fibres. In addition, FOS are small. Modern optical fibres have coating diameters below 250 µm, see Fig. 2.8. Reports show, that fibres with coating diameters low as 52 µm have been developed [155]. Due to their size, FOS are suitable for integration into laminates while having minor effects on the laminate's mechanical properties and its infusion characteristic [89, 144]. Another advantage of FOS is their variability that results in a large variety of sensing schemes. A good overview of state of the art in fibre optic sensing schemes has been presented in several reviews [28, 59, 82, 97, 141, 153].

2.4.1 Introduction to optical fibres and their composition

In general optical fibres are waveguides for light. Their structure typically consists of a round *core* and several concentric layers called *cladding*, *coating* and *buffer*. The light guiding properties of a fibre are determined by the core and the cladding. Fused silica is used for some optical fibres, due to its low attenuation in the visible and NIR spectral range, see Fig. 2.10. The coating serves the purpose to increase the mechanical resistance of the glass fibre. Moreover, it increases its resistance against environmental influences such as humidity or oxygen, which are known sources for premature failure due to microcracking [1, 61]. For additional protection, glass fibres can be covered by a polymer layer, called *buffer*.

Optical fibres are made from a glass preform. The light guiding properties are introduced into the preform by different vapour phase techniques. Most techniques have in common that a rotating silica seed material is doped by vaporised raw materials. Depending on the choice of dopant, the refractive index can be decreased or increased. The most popular dopant for increasing the refractive index of the fibre core is GeO_2 [1, 48]. After preform fabrication, fibres are drawn from the preform at approx. 2100 °C. The desired fibre diameter is controlled by adjusting the drawing speed. Protective coating layers are applied immediately after fibre drawing, in order to protect the optical fibre from the aforementioned environmental influences [1]. Large preforms typically provide enough material to produce optical fibres in excess of 300 km.

The production process allows to manufacture fibres with different dimensions and light-guiding properties. In this work, so called singlemode fibres are used that are widely applied in telecommunications, sensor application and fibre lasers. In Fig. 2.8 a sectional view of a singlemode glass fibre is presented together with

typical dimensions. The light-guiding properties of optical fibres rely on a mismatch

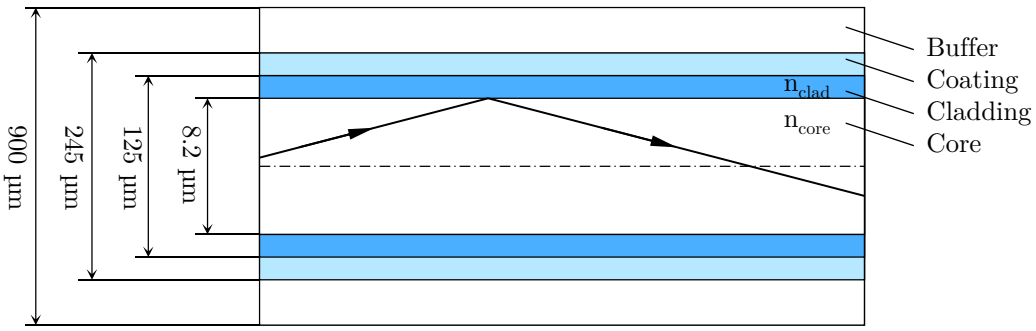

Figure 2.8: Sectional view of a step index optical fibre with path of incident and reflected light (→) at the core-cladding interface. (not drawn to scale)

between refractive indices in the fibre core and cladding. The core refractive index is approx. 0.3 % greater than the cladding refractive index [1]. The refractive index n is a dimensionless physical material property. It is defined as the ratio of vacuum velocity of light c_0 to the phase velocity of light v_{ph} in the material:

$$n = \frac{c_0}{v_{ph}} \,. \tag{2.13}$$

Light propagation in optical fibre occurs due to total internal reflection of the incident light at the core-cladding interface, see Fig. 2.9. The occurring effects in single mode fibres can be phenomenologically explained by geometrical optics. When an incident light wave falls onto the boundary between two homogeneous, transparent media with different refractive indices n_1 and n_2, the light wave gets split into a transmitted and a reflected wave. The reflection angle Θ_r is determined by the incident angle Θ_i according to the *law of reflection*:

$$\Theta_i = \pi - \Theta_r \,. \tag{2.14}$$

The refraction angle Θ_t is described by the *law of refraction*, also known as *Snell's law* [20]:

$$\frac{\sin(\Theta_i)}{\sin(\Theta_t)} = \frac{n_2}{n_1} \,. \tag{2.15}$$

Above a critical angle of incident Θ_c, all incident light is reflected due to total internal reflection. The critical angle occurs for $\sin(\Theta_t = 90° = 1)$ and is determined by:

$$\Theta_c = \sin^{-1}\left(\frac{n_2}{n_1}\right) . \tag{2.16}$$

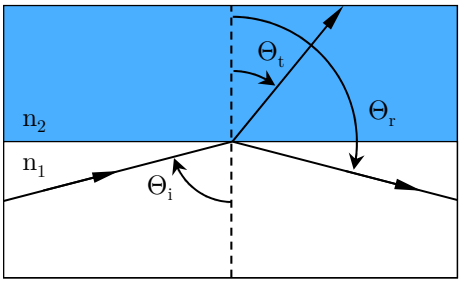

Figure 2.9: Refraction and reflection of incident light at the boundary between two bulk media with differing refractive indices n_1 and n_2.

Two of the most important parameters of optical fibres is *attenuation* (also referred to as transition loss) and *dispersion*. Attenuation leads to power loss in the optical fibre and it increases exponentially with fibre length according to the Beer-Lambert law[5]. These losses are due to Rayleigh scattering, intrinsic absorption in the Infrared (IR) and Ultraviolet (UV) region caused by excitation of molecular structures and electron transitions, and due to absorption bands caused by vibration of the OH^--radical[6], see Fig. 2.10. Other causes for absorption include structural imperfections and macro bending. Due to the mentioned effects, GeO_2-doped silica fibres have two wavelength windows around 1.31 μm and 1.55 μm that exhibit low attenuation. Most fibre optic components are optimised for those wavelength windows [1, 19, 48].

Dispersion of propagating light describes the frequency dependence of the phase velocity. One distinguishes *mode dispersion* and *chromatic dispersion* [1, 19, 48]. Mode dispersion means, that certain modes[7] spread out differently, which can lead to distorted transmitted light pulses. In this work, only singlemode fibres with a continuous light source are used, therefore only chromatic dispersion is relevant. In waveguides, such as optical fibres, light propagation is not strictly confined to the core. Therefore, the effective fibre refractive index n_{eff}[8] is used instead of the refractive index n of the core and cladding bulk materials. Generally speaking: n_{eff} is in-between n_f and n_{cl}. Chromatic dispersion describes the vacuum wavelength dependence of the effective refractive index of the waveguide $n_{eff}(\lambda)$ [48]. The cause for chromatic dispersion can be split in material dispersion and

[5] $I(z) = I_0 \cdot e^{-az}$, with z the length, I_z the light intensity at position z, and a the attenuation coefficient . Named after Swiss scientist Johann H. Lambert (1728-1777) and German physicist August Beer (1825-1863) [48].

[6] OH^--radicals can occur during silica glass manufacturing due to contamination of process gases with water vapour or hydrogen [48].

[7] Modes are solutions of the electromagnetic wave equation, that maintain the geometric structure of their electromagnetic field. The geometry of singlemode fibres allows propagation of only one fundamental mode (LP_{01}) [48].

[8] $n_{eff} = \frac{\beta}{k_0}$, with the phase constant β and the free-space wave number k_0 [48].

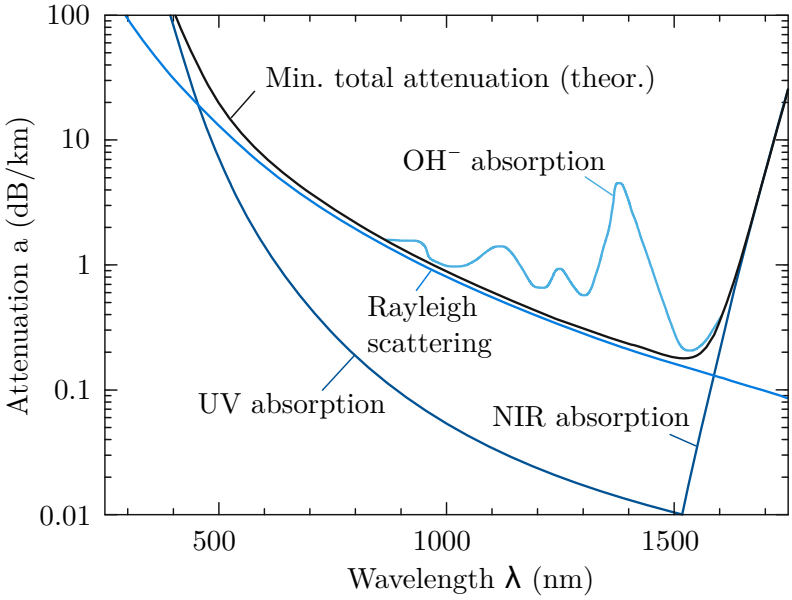

Figure 2.10: Mechanisms of attenuation in SiO_2 glass fibres after [48].

waveguide dispersion. Material dispersion results from the wavelength dependence of the material's refractive index $n(\lambda)$. The wavelength dependence of bulk material can be described by the *Sellmeier equation*[9]. According to that equation, the refractive index of bulk fused silica is plotted over the wavelength in Fig. 2.11. It can be seen, that the material has a strong wavelength dependence of the refractive index below 500 nm. In the wavelength regions relevant for singlemode applications around 1310 nm and 1550 nm the material dispersion is relatively low with $\frac{dn}{d\lambda} = -1.19 \times 10^{-5}\,\mathrm{nm}^{-1}$.

Waveguide dispersion results from the wavelength dependence of the effective refractive index $n_{eff}(\lambda)$. Taking into account chromatic dispersion, the effective refractive index n_{eff} of a standard singlemode fibre (here: Corning SMF-28e) is shown in Fig. 2.12.

Around the centre wavelength of the applied light source $\lambda_c = 1550\,\mathrm{nm}$, the refractive index wavelength-dependence of bulk fused silica is low[10]. Since the emitted spectrum of the light source is small (approx. 60 nm), it is assumed that chromatic dispersion of the fibre refractive index is negligible in this work. For a

[9] Proposed 1871 by Wilhelm Sellmeier, the equation is an empirical relationship between refractive index and wavelength and describes the dispersion of light in transparent media. It is usually given as a function of λ and material specific parameters C_i and D_i:
$n(\lambda) = \sqrt{1 + \sum_{i=1}^{3} \frac{C_i \lambda^2}{\lambda^2 - D_i^2}}$.
Parameters for fused silica have been previously determined by Malitson [112]. A Sellmeier plot based on his data can be found in Fig. 2.11.

[10] $\frac{dn_{eff}}{d\lambda} \approx -1.5 \times 10^{-5}\,\mathrm{nm}^{-1}$

detailed description of the derivation of the waveguide dispersion the author refers to the literature [48].

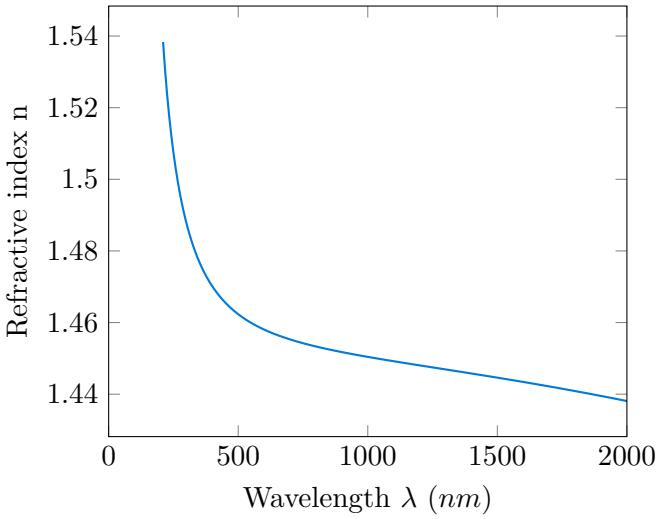

Figure 2.11: Refractive index wavelength dependence of fused silica calculated from Sellmeier equation. (Data obtained from [119])

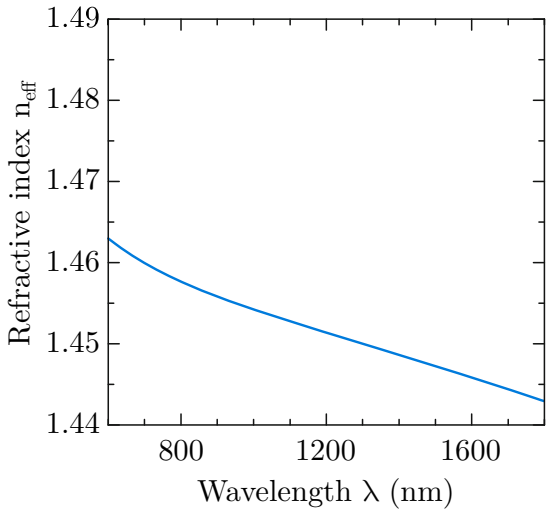

Figure 2.12: Effect of waveguide dispersion and material dispersion on the effective refractive index n_{eff}, after [48].

2.4.2 Review of fibre optic process monitoring

Fibre optic sensors are commonly classified in extrinsic and intrinsic sensors. The term extrinsic describes that sensing takes place outside of the optical fibre and the fibre acts merely as a light guide [28, 153]. Intrinsic sensors interact directly with external influences which leads to light modulation in the fibre. Further sensor

classification can be done by their spatial distribution. Point sensors for example determine the measurand at one specific point. Whereas quasi-distributed sensors measure along the fibre at specific points and distributed sensors measure along the whole length of the fibre. Other classifications rely on the modulation scheme of the optical signal, e.g. intensimetric, polarimetric, interferometric, or spectroscopic [15, 59, 153, 171].

Process monitoring with fibre optic sensors relies mainly on four approaches: intensity measurement, interferometry, spectrum analysis and fibre grating interrogation. The following list provides an overview on the application of these approaches in the context of composite manufacturing.

- Intensity measurements are performed based on refraction of light at boundaries between two media with different refractive indices. This has been used in optical fibres by measuring Fresnel reflection [3, 7, 10, 12, 17, 32–34, 43, 56, 92, 93, 104, 143, 160] and by measuring the light loss achieved by removing the cladding [63, 103] or by inserting high-index fibre segments in the light path [6]. Intensity sensors have the advantage that they are inherently simple. The disadvantage is that erroneous measurements might occur when the output level of the light source fluctuates or fibre loss varies over time.

- Interferometric measurements are used to analyse the interference pattern caused by Fresnel reflection between two semi-translucent boundaries. Fibre optic interferometry has been applied to composite manufacturing mainly by interrogating Extrinsic Fabry-Perot Interferometer (EFPI) sensors [13, 27, 80, 100, 156].

- Spectrum analysis relies on the interaction of light with matter, in this case the curing polymer. When a polymer is illuminated by a certain wavelength spectrum — typically NIR [14] — certain groups of the polymeric chain can be excited, which result in a characteristic spectral response. Depending on the state of cure the spectral response may change. This change has been tracked during composite manufacturing with different techniques such as FT-Raman [14, 55], FT-IR [30, 31, 43], evanescence wave sensing by deploying high-index fibres[11] [30, 31, 43, 140], and evanescent wave fluorescence sensing by adding fluorescence dyes to the resin [168, 169].

- Fibre gratings are a periodic perturbations of the refractive index of the optical fibre that act as filters for incident light. Fibre grating interrogation

[11] Fibre refractive index of 1.65 compared to 1.46 in conventional fibres.

is performed by sending broadband light through an optical fibre and subsequently analysing the spectral response of the grating. Fibre gratings have a strong strain and temperature sensitivity. In composite manufacturing FBG sensors [11, 15, 23, 49, 56, 63, 86, 97, 100, 102, 121, 123, 127, 129] and Long Periode Grating (LPG) sensors [45, 172] have been applied to process monitoring. Different grating interrogator types are possible and can be found in the literature [97].

Fibre optic process monitoring has been applied to several different composite manufacturing processes. Most commonly FOS have been applied to the VARI process (see Sec. 2.1.1) [13, 15, 17, 23, 49, 63, 121, 127, 129, 172]. This might be due to the relatively inexpensive process equipment and uncomplicated ingress of the optical fibre through the sealing tape. Other authors applied FOS to Resin Transfer Moulding (RTM) [84, 86, 103, 168, 169], autoclave processes [80, 123, 125], resin film infusion [10] and microwave process [102]. Besides the applications in composite manufacturing processes, many authors have applied FOS in neat resin to study the sensor responses [3, 6, 7, 11, 12, 30–34, 43, 44, 56, 92, 93, 104, 140, 143, 160].

Since FOS and their interrogation schemes are so versatile, different sensors for LCM process monitoring have been developed that are sensitive to a variety of parameters. The following list provides an overview of the different parameters and sensors used:

- temperature: FBG [102, 125], hybrid EFPI-FBG [100] and luminescing phosphor-coated fibre end tip sensor [153],
- strain: FBG [11, 12, 23, 56, 86, 100, 121, 123, 125, 127, 129], EFPI [13, 125, 156] and hybrid EFPI-FBG [100],
- curing: Fresnel sensor [3, 7, 12, 32–34, 56, 92, 93, 143, 160], intensity-based [6, 7, 31], FT-IR [14, 30, 31, 55, 125], evanescence wave spectroscopy [30, 31], evanescent wave fluorescence sensing [168, 169] and FBG [49],
- flow: Fresnel sensor [10, 17], Intensity-based sensor [63, 84, 103], FBG [15, 49, 63, 127] and LPG [45, 172],
- Glass transition: Fresnel sensor [3, 34, 56],
- Gel point: FBG [12, 56, 121].

It is obvious that two FOS are particularly suited to measure most LCM parameters: FBG and Fresnel sensors. This is because both sensors signals can be directly

related to material properties. Combining both sensor types in a *dual-sensing* application is appealing and was first suggested by Cusano et al. [34]. Soon after, Giordano et al. [56] practically implemented the idea and applied two separate light sources to interrogate an FBG and a Fresnel sensor for simultaneous T_g and gel point monitoring.

This work focuses on Fresnel sensors due to their versatility and inexpensiveness. Fig. 2.13 shows a schematic of a Fresnel sensor submerged in resin. Fresnel sensors are made from fused silica singlemode fibres by cutting the fibre with a specific fibre cutting device (cleaver) to create a planar tip surface. The tip surface acts as point sensors that can measure the refractive index of polymers when it is immersed in resin. The resulting tip surface after cleaving is shown in the scanning electron microscopy image in Fig. 2.14 on the right. For comparison the result after using an ordinary blade is shown on the left.

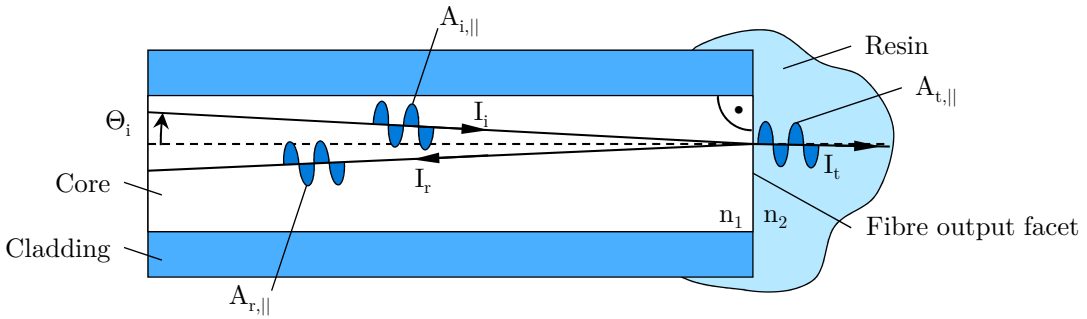

Figure 2.13: Schematic of a Fresnel sensor submerged in a resin sample. At the fibre output facet, incident light is partly reflected back into the core and partly transmitted into the resin. The proportion between reflected and transmitted light is described by the simplified Fresnel equations under the assumption of normal incidence and transparent media.

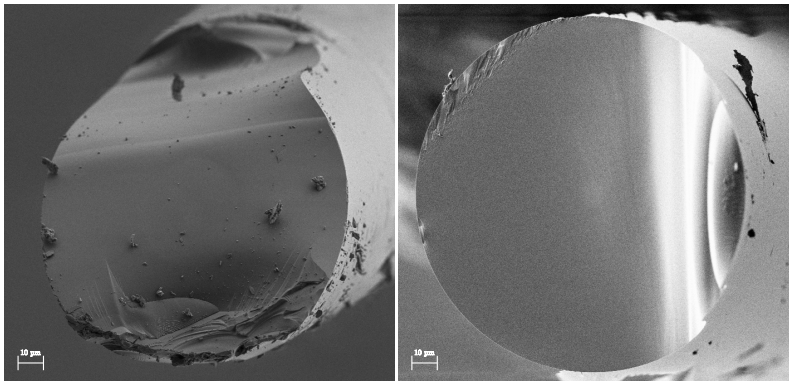

Figure 2.14: Scanning electron microscopy images of broken (left) and cleaved optical fibre (right). (Courtesy of [50])

The operating principle of a Fresnel sensors immersed in resin can be described as follows: when a guided light wave inside the fibre arrives at the interface between

the fibre output facet and the resin, most of the light is transmitted in the resin but a small fraction is reflected according to the Fresnel equations[12] [20]. The intensity of the reflected light is a measure of the refractive index of the material the sensor is immersed in.

2.4.3 Fresnel equations

The electric field of the incident electromagnetic wave (see Fig. 2.13) can be resolved in components parallel to the plane of incident ($\parallel$) and perpendicular to the plane of incident ($\perp$). With regard to the amplitude of the vector of the incident electric field A_i, the Fresnel equations describe the amplitude of the transmitted electric field A_t:

$$A_{t,\parallel} = \frac{2n_1 \cos\Theta_i}{n_2 \cos\Theta_i + n_1 \cos\Theta_t} A_{i,\parallel} \,, \tag{2.17}$$

$$A_{t,\perp} = \frac{2n_1 \cos\Theta_i}{n_1 \cos\Theta_i + n_2 \cos\Theta_t} A_{i,\perp} \,, \tag{2.18}$$

and the reflected electric field A_r:

$$A_{r,\parallel} = -\frac{n_1 \cos\Theta_t - n_2 \cos\Theta_i}{n_2 \cos\Theta_i + n_1 \cos\Theta_t} A_{i,\parallel} \,, \tag{2.19}$$

$$A_{r,\perp} = \frac{n_1 \cos\Theta_i - n_2 \cos\Theta_t}{n_1 \cos\Theta_i + n_2 \cos\Theta_t} A_{i,\perp} \,. \tag{2.20}$$

The equations are valid under the assumption of a flat boundary surface, and non-magnetic, perfectly transparent materials. This assumption is valid for cleaved optical fibres and epoxy resin. In this work, only the reflected light is evaluated, for that reason only the equations for the case of reflected light will be presented. Under the assumptions of normal incident light ($\Theta_i \approx 0$ in Fig. 2.13), Eq. 2.19 and Eq. 2.20 can be simplified to:

$$A_{r,\parallel} = -\frac{n_1 - n_2}{n_1 + n_2} A_{i,\parallel} \,, \tag{2.21}$$

$$A_{r,\perp} = \frac{n_1 - n_2}{n_1 + n_2} A_{i,\perp} \,. \tag{2.22}$$

[12] First deduced in 1823 by August-Jean Fresnel (1788-1827)

The ratio of reflected to incident light is described by the reflectivity R:

$$R = \frac{|A_r|^2}{|A_i|^2} = \frac{I_r}{I_i}\,, \tag{2.23}$$

with the reflected (I_r) and incident light intensity I_i. For normal incident light, the distinction between parallel and perpendicular components disappears and Eq. 2.21, Eq. 2.22 and Eq. 2.23 can be written as:

$$R = \left(\frac{n_1 - n_2}{n_1 + n_2}\right)^2 . \tag{2.24}$$

The reflectance depends strongly on the fluid in which the Fresnel sensor is immersed in. The more the refractive indices of both materials equal each other, the lower the reflectance, and the greater the transmitted amount in the fluid[13]. This fact has to be considered, when performing refractive index measurements with Fresnel sensors, see Sec. 2.4.5.

2.4.4 Lorentz-Lorenz equation

The versatility of Fresnel sensors is based on the fact, that the refractive index is linked to other material properties through the Lorentz-Lorenz equation[14] [20]:

$$\alpha_p = \frac{3}{4\pi N} \cdot \frac{n^2 - 1}{n^2 + 2}\,, \tag{2.25}$$

with the mean polarisability α_p and the number of molecules per unit volume N. An alternative form of the Lorentz-Lorenz equation is:

$$A = \frac{4\pi}{3} N_m \alpha_p\,, \tag{2.26}$$

with the molar refractivity A and the Avogadro constant N_m. By substituting N_m in Eq. 2.26 with the molar volume given by:

$$\frac{N_m}{N} = \frac{M}{\rho}\,, \tag{2.27}$$

[13] Example: Measurements with an optical fibre ($n_{eff} = 1.4679$) in air ($n_{air} = 1.003$) yield a reflectance of 3.59 %, compared to measurements in resin ($n_{resin} = 1.584$) that yield only 0.14 %.

[14] Discovered independently and roughly at the same time by H.A. Lorentz (1880) and L. Lorenz (1881).

with the molecular mass M and the density ρ, and by inserting Eq. 2.25 into the resulting equation, one obtains:

$$A = \frac{M}{\rho} \cdot \frac{n^2 - 1}{n^2 + 2}. \tag{2.28}$$

This form of the Lorentz-Lorenz equation is a function of density ρ. It illustrates well the temperature dependence of the refractive index — also called Thermo-Optic Coefficient (TOC) — since the density of many materials is temperature-dependent, including polymers. The Lorentz-Lorenz equation is valid not only for gases and liquids [20], but shows also reasonably good validity for polymers [91]. This opens the possibility to quantify resin properties that are related to density by using refractive index measurements with Fresnel sensors.

Motivated by the Lorentz-Lorenz equation, Afromowitz [5] was one of the first to investigate the cure sensing capabilities of Fresnel sensors. His isothermal curing experiments with EPON™ Resin 828 (EPON 828) suggested a linear relationship between degree of cure and Fresnel sensors signals (there: intensity) for lower temperatures. Afromowitz's findings were confirmed by several authors [32, 34, 92]. Later, Lam and Afromowitz [92] specified for the same material that the relation becomes non-linear around the gel point under elevated temperatures. On the other hand, experiments with RTM 6 resin suggest a linear relationship even for elevated temperatures [143, 160].

Cusano et al. [32] quantified the degree of cure based on the refractive index for isothermal curing by linearising the Fresnel equation (Eq. 2.24) and under the assumption of small intensity changes. Antonucci et al. [12] and Robert and Dusserre [143] deduced the degree of cure during non-isothermal curing by using linear functions of the relative change in reflected light intensity.

The literature review suggests, that the correlation of Fresnel sensor signal and degree of cure is can be assumed to be linear for the vast part of the curing reaction. Deviations at elevated temperatures might be resin specific and have to be investigated individually. Empirical descriptions of the relation between degree of cure and refractive index have been shown for the isothermal case. For the non-isothermal case, first steps have been taken by relating the reflected intensity to the degree of cure.

2.4.5 Refractive index measurement with Fresnel sensors

In order to determine the resin refractive index n with the Fresnel equations, the incident intensity I_i, reflected intensity I_r and the effective fibre refractive index

n_f have to be known[15]. The literature research showed, that the most common approach is to measure, both, the incident (I_i) and reflected light intensity I_r, and to use literature values for the fibre refractive index n_f.

In this work a different approach is taken, since the applied commercial FBG interrogator did not measure the incident light intensity I_i. For that reason, a reference measurement is performed with a fluid of known refractive index (for simplicity: air) prior to every refractive index measurement. This referencing procedure allows to determine the resin refractive index through the following expression, which is derived from Eq. 2.23 and Eq. 2.24:

$$n = n_f \cdot \frac{1 \pm \left(\sqrt{\frac{I_r}{I_{r,air}}} \cdot \frac{n_{f,air} - n_{air}}{n_{f,air} + n_{air}} \right)}{1 \mp \left(\sqrt{\frac{I_r}{I_{r,air}}} \cdot \frac{n_{f,air} - n_{air}}{n_{f,air} + n_{air}} \right)}, \tag{2.29}$$

where I_r and $I_{r,air}$ are the reflected intensities in the fibre-resin and fibre-air interface, respectively, and n_{air} is the air refractive index. Since the environmental conditions between reference and actual measurement can differ, the fibre refractive index during reference measurement $n_{f,air}$ has to be considered.

It is worth noting, that the measured intensities I have to be corrected by the *zero intensity* I_0 induced by the dark current of the photo diodes. The zero intensity can be determined by turning off the laser source and by measuring the received intensity[16]. The obtained value for I_0 has to be deducted from all intensities I by:

$$I_r = I - I_0 \,. \tag{2.30}$$

From Eq. 2.29 one can see, that two cases have to be differentiated. For $n > n_f$, the root of equation Eq. 2.24 takes positive values, thus Eq. 2.29 becomes:

$$n = n_f \cdot \frac{1 + \left(\sqrt{\frac{I_r}{I_{r,air}}} \cdot \frac{n_{f,air} - n_{air}}{n_{f,air} + n_{air}} \right)}{1 - \left(\sqrt{\frac{I_r}{I_{r,air}}} \cdot \frac{n_{f,air} - n_{air}}{n_{f,air} + n_{air}} \right)} \,. \tag{2.31}$$

[15] Differing from Fig. 2.13, n is used to denote the resin refractive index, and n_f to denote the effective fibre refractive index from now on.

[16] During Fresnel measurements, the device was run at 18 % laser power. For zero intensity measurements the power was reduced to 0 %.

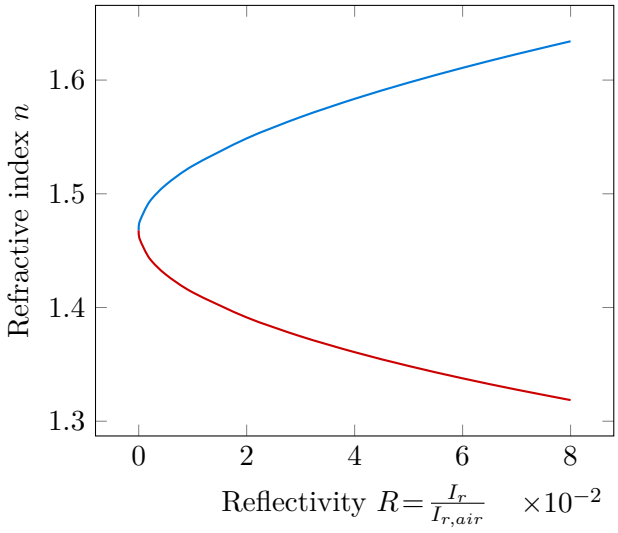

Figure 2.15: Refractive index calculated from generic reflectivity input. Case differentiation for $n > n_f = 1.4679$ (-) and $n < n_f$ (-).

In contrast if $n < n_f$, the root of equation Eq. 2.24 takes negative values, thus Eq. 2.29 becomes:

$$n = n_f \cdot \frac{1 - \left(\sqrt{\frac{I_r}{I_{r,air}}} \cdot \frac{n_{f,air} - n_{air}}{n_{f,air} + n_{air}}\right)}{1 + \left(\sqrt{\frac{I_r}{I_{r,air}}} \cdot \frac{n_{f,air} - n_{air}}{n_{f,air} + n_{air}}\right)}, \tag{2.32}$$

Fig. 2.15 shows the resulting refractive index generated from a generic input in Eq. 2.31 for $n > n_f$ and in Eq. 2.31 for $n < n_f$. The presented measurement approach assumes, that the incident light intensity I_i remains constant in the time span between reference and actual measurement. The validity of this assumption has to be examined. Moreover, precautions have to be made that assure that no light loss occurs in the light path during measurements. This can be done for example, by using bent-insensitive optical fibres and by avoiding any fibre motion.

When determining the fibre refractive index n_f and the reference refractive index n_{air}, the wavelength- and temperature dependence shown in Sec. 2.4.1 and Sec. 2.4.3 has to be factored in.

The TOC of fused silica is $dn/dT = 8.7 \times 10^{-6}\,\mathrm{K}^{-1}$ [165] and the expected temperature changes ΔT during the resin curing experiments will exceed 200 K. Given that the resin refractive index increases in the range of 3×10^{-2} during curing, the TOC of fused silica has a measurable effect on the results. Therefore, it has to be accounted for by:

$$n_f = n_{eff,0} \cdot \frac{dn}{dT} \cdot (T_0 - T)\,, \tag{2.33}$$

with the ambient temperature T_0, the effective fibre refractive index at ambient temperature $n_{eff,0}$ and the actual sensor temperature T.

The reference refractive index of air n_{air} and its dependence on temperature, wavelength, pressure, etc. has been described by several authors in the past. Tab. 2.1 gives an overview of these contributions and compares their scope. The equation

Table 2.1: Comparison of air refractive index models.

	Edlén [46]	Owens [136]	Peck [139]	Ciddor [26]	Mathar [115]
Year	1966	1967	1972	1996	2007
Wavelength (µm)	0.2...2.1	0.2...0.7	0.2...1.7	0.3...1.7	1.3...24
Temperature (°C)	15	-23...47	15	-40...100	10...25
H_2O content (%)	–	0...100	–	0...100	5...60
CO_2 content (ppm)	330	–	330	arbitrary	370
Uncertainty	–	3×10^{-6}	0.2×10^{-8}	3×10^{-8}	3×10^{-8}
Pressure (kPa)	101	0...405	101	80...120	50...102

published by Ciddor [26] stands out due its validity in a large wavelength window and temperature range. It represents the best fitting option for refractive index measurements under resin curing conditions. A sensitivity study on the model revealed that the air refractive index reduces by 10^{-3} when exposed to typical temperatures occurring during LCM processing. This change is relevant and shows that the actual temperature during the air refractive index measurements has to be accounted for. The vacuum applied during the measurements also affects the air refractive index. However, the sensitivity study revealed that it has only a minor effect on the air refractive index (10^{-5}) and can be neglected.

2.5 Summary

This chapter reviewed the current knowledge in composite manufacturing processes, in particular LCM processes, to identify gaps in the literature regarding process monitoring with embedded FOS.

It was found, that there is no unanimous opinion about the full extend of all process parameter since the monitoring requirements are specific to each process. However, the parameters pressure and temperature are most commonly monitored. This is because these parameters govern and trigger the main effects during processing, e.g. curing or flow, and a range of mould-mounted sensor solutions are available.

It is easily understood, that process parameters are not constant during processing and local variations inside the laminate may occur. Consequently, an inherent interest exist to measure parameters not only at the mould surface but inside the composite laminate [73].

The challenge is to provide an embedded sensor that is minimally invasive while measuring the parameters accurately. This is, because foreign bodies could influence the filling pattern during manufacturing or discriminate the structural integrity of the final part [111].

It was found, that the major process parameters are temperature, pressure, degree of cure and viscosity [73, 101, 137]. However, fewer sensing options are available for the latter two. The degree of cure has been previously measured with electrical sensors. However, available electrical sensors are bulky or require metallic wiring that is prone for electromagnetic interference in noisy manufacturing environment [55]. Optical sensors can overcome the short comings of electrical sensors. Especially fibre optic Fresnel sensors have the potential to provide a variable, convenient and cost effective sensor solution.

Several authors showed, that isothermal refractive index measurements in resin correlate well with the degree of cure values obtained by thermal analysis [5, 92]. However, very few attempts have been made to describe the sensor output analytically [32] or for non-isothermal conditions [12]. For the application in composite process monitoring, a thorough investigation of the relation between refractive index and degree of cure under isothermal and non-isothermal is necessary.

Viscosity is a cure-dependent rheological quantity that characterises the ability to deform matter. Applying deformation in an embedded environment is challenging. Comprehensibly, available literature on embedded viscosity sensors is scarce. Surface acoustic wave sensors using micro vibration have shown their potential for biosensors [51] and might be a solution for the future. Embedded dielectric sensors — with said disadvantages — have been used to correlate ionic conductivity with viscosity [90, 110]. Spectroscopic mould-mounted methods have shown the ability to relate relative peak changes in fluorescence or FT-IR spectra [101, 158] to viscosity. However, absolute measurements are not possible yet. Fresnel sensors could again provide an inexpensive solution, if the refractive index can be successfully related to viscosity.

Bearing in mind, that another fibre optic sensor (FBG) is capable of measuring mechanical strain and temperature, a combined sensor interrogation of FBG and Fresnel sensor would provide a powerful *dual-sensing* system for a variety of process parameters. *Dual-sensing* has been previously shown with laboratory equipment by Giordano et al. [56]. It was not shown, however, with an inexpensive, off-

the-shelf commercial fibre optic measurement system. Doing so, would open new possibilities for an all-optical-fibre sensing solutions for LCM process monitoring. In order to qualify the FBG interrogator for refractive index measurements with Fresnel sensors, it is necessary to calibrate the system for this application and to assure that the measurement uncertainty meets the specific requirements.

3 Calibration of the fibre optic measurement system for refractive index measurements and determination of measurement uncertainty

The applied fibre optic measurement system is designed to interrogate FBG sensors. Hypothetically, the same hardware can be used to interrogate other sensors for refractive index measurements, such as Fresnel reflectometer sensors. Thus, allowing *dual-sensing* applications with this system. The measurement system shown in Fig. 3.6 comprises several mechanical and electro-optical components that might alter the theoretical Fresnel sensor output shown in Fig. 2.15. During curing, the refractive index increases by several percent ($\Delta n_{cure} \approx 3 \times 10^{-2}$). So even small deviations can have an influence on the measurement result. Therefore, this chapter investigates the deviation between the actual measurement system output and an independent calibration reference. This is done in a wide refractive index range from 1.3 to 1.6. The range was chosen to cover resin curing which is typically occurring around 1.5, but also to allow measurements of fluids with lower refractive index such as curing agents or other fluids. Any deviations between actual measurement and calibration reference are eliminated subsequently by calibration. At last the uncertainty of the refractive index measurements is determined.

The structure of this chapter is the following: a short introduction on calibration in general is given in Sec. 3.1, followed by a description of the applied calibration procedure that uses a refractometer[1] as an independent evaluation instrument in Sec. 3.2. The calibration is performed with five high-purity, organic calibration fluids. Sec. 3.3 introduces the fluids and motivates their choice. The refractometer experiments and their results are presented in Sec. 3.4. The applied fibre optic

[1] A refractometer is a stationary refractive index measurement system that operates based on Snell's law.

measurement system is introduced in Sec. 3.5. Additionally, the assumption of constant incident intensity I_i is verified and the effective fibre refractive index n_f is determined. Then, the fibre optic refractive index measurements of the calibration fluids is performed in Sec. 3.6. After outliers have been eliminated the calibration results are presented in Sec. 3.7. At last a summary is given in Sec. 3.9. The results of this chapter have been previously published in Oelhafen et al. [130] and Oelhafen et al. [132]. Parts of the results have been gained in the master thesis by Mayr [116] under the supervision of the author.

3.1 Background on calibration

Measurement deviations consist of systematic deviations with a known and a unknown component, and random deviations. Both, random and unknown deviations, cannot be compensated and contribute to the measurement uncertainty. Known systematic deviations can be partly corrected. [40]

One way to do this is, to apply a correction function that matches the actually measured value with the true, unknown value. During the actual measurement the input variable (here: reflected intensity I_r) is determined and transferred into the uncorrected measurand (here: refractive index n) by a transfer function $f(I_r)$ (here: Eq. 2.29). The goal is to obtain the corrected refractive index n_{corr} by adjusting n with the correction function $g(n)$. This process is depicted in Fig. 3.1. The correction function is deduced by comparing the transferred value (here: n)

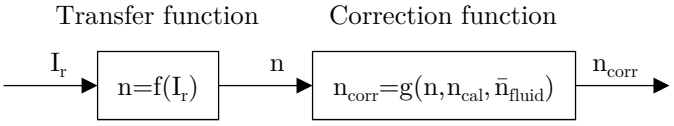

Figure 3.1: Flow chart describing the relation between transfer and correction function to obtain calibrated values.

with the true value (here: n_{cal}). This procedure assumes, that the true value of n_{cal} is sufficiently known.

In order to determine an accurate correction function, an adequate number of fluid refractive index measurements (n_{fluid}) in a calibration medium with known refractive index (n_{cal}) have to be performed. Repeated n_{fluid} measurements allow to single out and eliminate potential outliers, and allow to average the results by the arithmetic mean to obtain the mean fluid refractive index $\overline{n}_{fluid}$.

Common correction functions include: Linear approximation, polynomial interpolation and spline interpolation. Linear approximation, stand out due to their simplicity. If more than one calibration value exists, several linear approximations

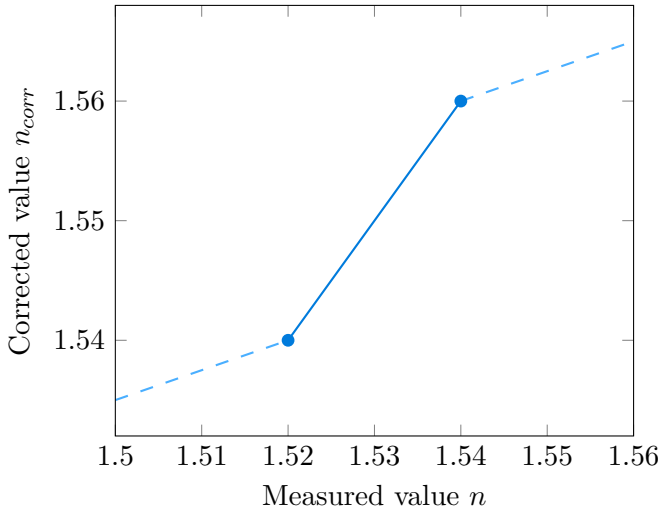

Figure 3.2: Exemplary linear approximation (-) in an interval between two calibration nodes (•). Adjacent linear approximations (- -) of other intervals are indicated.

can be performed between adjacent nodes. By doing so, the characteristic calibration curve is linearised and the obtained accuracy increases [77]. In-between two nodes the correction function approximates the calibrated values n_{corr} by a straight line as illustrated in Fig. 3.2. The correction function is described by:

$$n_{corr} = C_a \cdot (n + C_b)\,, \tag{3.1}$$

with the calibration constants C_a and C_b:

$$C_a = \frac{n_{cal}|_{s+1} - n_{cal}|_s}{\overline{n}_{fluid}|_{s+1} - \overline{n}_{fluid}|_s}\,, \tag{3.2}$$

$$C_b = \left(\frac{1}{C_a} \cdot n_{cal}|_{s+1}\right) - \overline{n}_{fluid}|_{s+1}\,. \tag{3.3}$$

Both calibration constants are evaluated between two adjacent nodes, denoted by $|_s$ and $|_{s+1}$. C_a represents the slope and C_b to the offset of the correction function.

The described method corrects refractive index values obtained from a single channel only. In the present case of a four-channel measurement system, the correction procedure has to be repeated for every channel.

3.2 Calibration procedure

The calibration procedure, shown in Fig. 3.3, relies on refractive index measurements of five high-purity, organic calibration fluids with two independent experiments in the refractive index range from 1.3 to 1.6. The experiments are performed

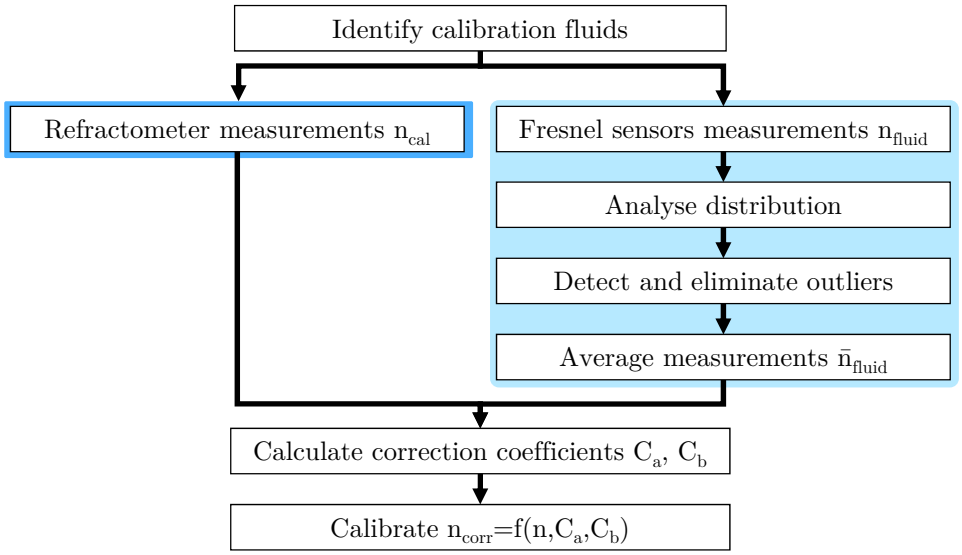

Figure 3.3: Flow chart of calibration procedure.

at approximately the same wavelength (1550 nm) and fluid temperature (24 °C). This is necessary because both parameters influence the refractive index, as has been shown in Sec. 2.4. The first experiment is performed with a specialised refractive index measurement system – a prism coupling refractometer – and yields the calibration refractive indices n_{cal}. These values act as a reference for the fluid refractive indices n_{fluid} obtained with Fresnel sensors in the same fluids. Measurements in each fluid are performed simultaneously with four Fresnel sensors and repeated 20 times. Thereafter, the samples which consist of 20 values from each channel and each fluid, are tested for normal distribution. Based on that, an adequate outlier test was performed and outliers were eliminated subsequently. The remaining values of each sample were averaged by the mean, so each sample is represented by its mean fluid refractive index $\overline{n}_{fluid}$. At last, the refractometer and Fresnel sensor values are used to determine the correction function coefficients of each channel and each fluid with Eq. 3.2 and Eq. 3.3.
Based on the obtained coefficients and the correction function given in Eq. 3.1, any refractive index value n can be calibrated in the refractive index range from 1.3 to 1.6.

3.3 Identification of calibration fluids

The transfer function (Eq. 2.29) that determines the refractive index based on the reflected intensity is non-linear, as can be seen from Fig. 2.15. That does not necessarily mean, that the correction function (Eq. 3.1) is non-linear too, because

it is independent of the transfer function. Theoretically, it is possible to perform the correction with one linear function described by two nodes (two calibration fluids). It cannot be ruled out, however, that the deviations are not constant over the refractive index range from 1.3 to 1.6. In order to get a clearer picture of the deviations, the refractive index range will be divided into four segments by five nodes, represented by five calibration fluids. Each segment is described by a separate correction function (Eq. 3.1) with a set of C_a and C_b values obtained from Eq. 3.2 and Eq. 3.3 [77].

The calibration fluids are required to be liquid, non-toxic, non-volatile and to be equally-spaced over the mentioned range. A literature review was conducted on available refractive index data of potential fluids in the wavelength range around 1550 nm and at ambient temperature. It was revealed, that little data is available in this range, and most sources cover the lower wavelength range in the visible spectrum (390 nm to 700 nm) since most commercial refractometer operate in this range. Based on the available data, five organic fluids were selected that cover the desired refractive index range. Fig. 3.4 visualises their distribution and Tab. 3.1 lists the fluids together with the respective refractive indices, wavelengths and temperature at which they were acquired.

The table shows that the available data was acquired under varying conditions. However, for a reliable calibration it is necessary to determine calibration values of all fluids under the same conditions. Thus, the available data is not useful as basis for a calibration.

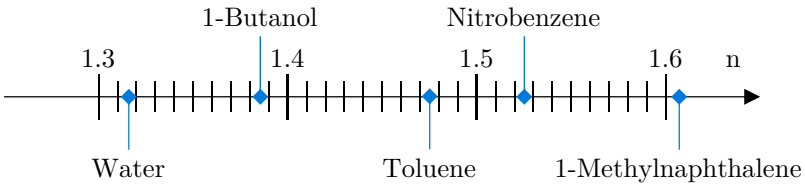

Figure 3.4: Distribution of selected calibration fluids in the refractive index range from 1.3 to 1.6.

Table 3.1: Selected calibration fluids in the refractive index range from 1.3 to 1.6.

	Index	Wavelength	Temp.	Source
Water	1.3167	1500 nm	20 °C	Kedenburg et al. [81]
1-Butanol	1.3858	1551 nm	27 °C	Moutzouris et al. [122]
Toluene	1.4737	1551 nm	27 °C	Moutzouris et al. [122]
Nitrobenzene	1.5247	1500 nm	20 °C	Kedenburg et al. [81]
1-Methylnaphthalene	1.6082	1310 nm	20 °C	Cusano et al. [34]

3.4 Calibration fluid refractive index measurements with prism coupling refractometer

The refractometer measurements were performed with a prism coupling refractometer (Model 2010/M, Metricon Corp., USA) in collaboration with Prof. Kostas Moutzouris of the University of West Attica, Greece. The refractometer comprises a diode laser source emitting radiation at 1551 nm and a gadolinium gallium garnet prism that is mounted on a rotating stage. A schematic of the refractometer is presented in Fig. 3.5.

The measurements were performed at 24.0 °C ± 0.5 °C by bringing few millilitres of the calibration fluid in direct contact with the prism and by directing the laser beam on the prism base at a given incident angle Θ_i. The laser beam is reflected at the prism-fluid interface onto a detector according to Snell's law (Eq. 2.15). By rotating the stage, the incident angle is increased until the reflected intensity I_r reaches a maximum. At that angle, total internal reflection occurs and the calibration fluid refractive index n_{cal} is calculated based on Eq. 2.16 and the known prism refractive index $n_p = 1.9340$. The resulting values are listed in Tab. 3.2. The refractometer measurements have an established refractive index uncertainty of $u_{CAL} = 2 \times 10^{-4}$.

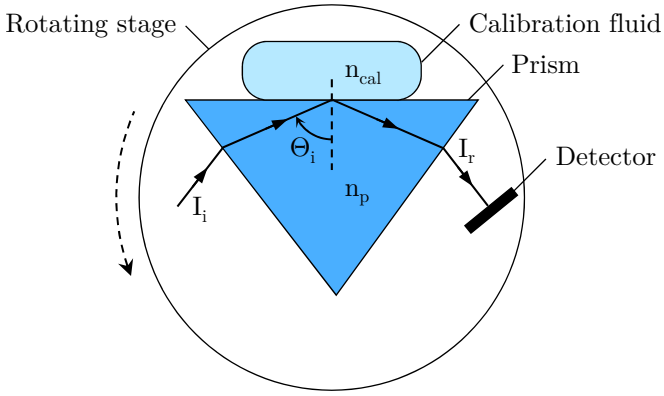

Figure 3.5: Prism coupling refractometer.

3.5 Fibre optic edge-filter FBG measurement system

A four-channel edge-filter-based fibre optic measurement system by fos4X GmbH was employed for the Fresnel sensor interrogation. A schematic of the system is shown in Fig. 3.6. It is equipped with an Amplified Spontaneous Emission (ASE) light source. The emitted spectrum (see Fig. 3.7) has a centre wavelength

Table 3.2: Refractive index values of five calibration fluids obtain with prism coupling refractometer.

Fluid	n_{cal}
Water	1.3159
1-Butanol	1.3869
Toluene	1.4753
Nitrobenzene	1.5224
1-Methylnaphthalene	1.5817

$\lambda_c = 1550\,\text{nm}$ which is used for FBG interrogation and a spectral bandwidth of approximately 50 nm. The optical signals in each channel are split into two paths. The signal in one path is measured directly with a photodiode, the other signal is edge-filtered before being measured by a photodiode of the same type. Both signals are amplified and then digitalized with a 16-bit analog-to-digital converter.

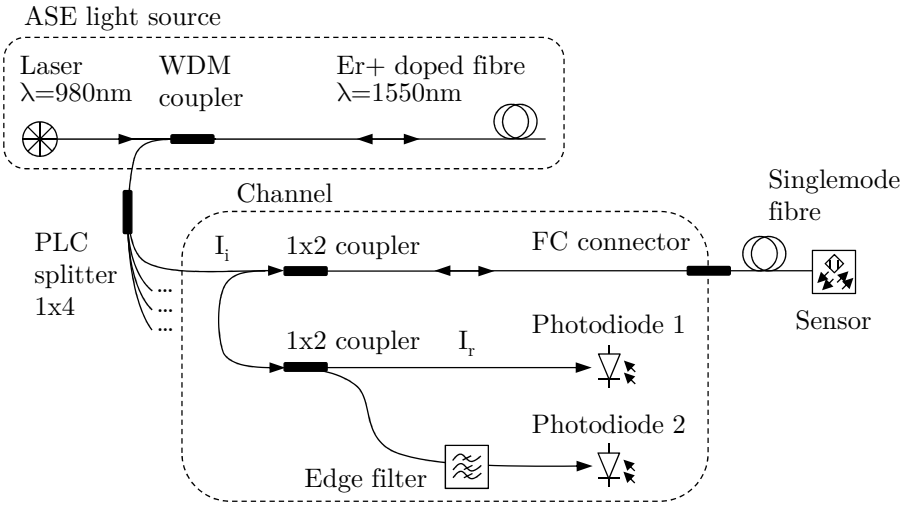

Figure 3.6: Schematic of four-channel edge-filtered FBG measurement system by fos4X GmbH. An ASE light source, consisting of a pump laser ($\lambda = 980\,\text{nm}$) that excites an erbium-doped fibre, generates broadband light ($\lambda_c = 1550\,\text{nm}$) that is guided out by a Wavelength-Division Multiplexing (WDM) coupler onto a 1x4 Planar Lightwave Circuit (PLC) splitter to four identical channels that each illuminates one sensor. The reflected light of a sensor is split by a 1x2 coupler into two paths. Once more the light is split by a 1x2 coupler into two paths. One path leads to a photodiode 1 and the other path is edge-filtered before it arrives at photodiode 2.

3.5.1 Investigation on the light source stability

The stability of the ASE light source was assessed by measuring fluctuations of the reflected intensity I_r of one channel after the light source had been switched on. Additionally, the incident laser power of that channel was measured with an

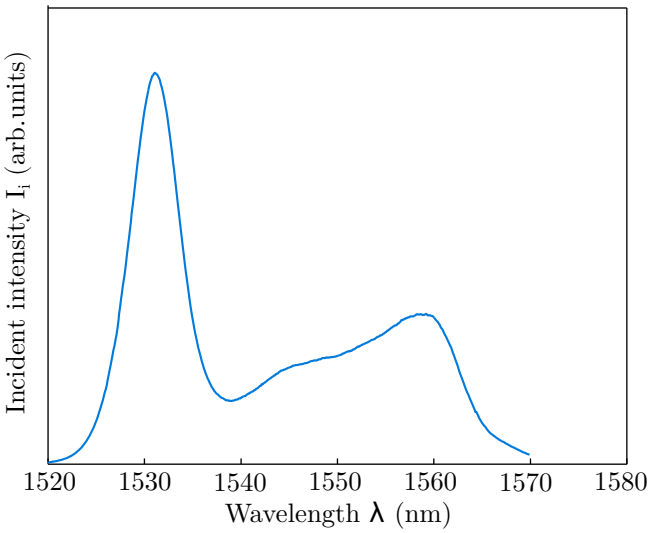

Figure 3.7: Exemplary emitted spectrum of the ASE light source measured at one channel, after [108].

external power meter (Thorlabs PM100USB). The measured intensity and power is plotted over time in Fig. 3.8. When the fibre optic system was switched on at $t = 0\,\text{min}$ the incident laser power and thus the reflected intensity took initial values. The magnitude of these values depends on the default laser power which can be adjusted between 0 % and 100 %. Through out all measurements in this work the laser power was set constant at 18 %.
After the device was switched on, both, the reflected intensity and the laser power increased for approximately 60 min, when both curves steadied. The remaining fluctuations were well below 1 arb. unit and can be neglected[2]. The initially increasing laser power is due to temperature gradients in the cold device that influence the thermal management of the light source. The laser power stabilises when the dissipated heat from the light source has heated the device to a constant temperature slightly above ambient temperature.

During the heating phase the signal drifts by ($< 2\,\text{arb. unit}$). This is generally low and it is concluded, that the assumption of constant incident light intensity is valid ($I_i = const.$). However, it is advised to switch on the system at least 1 h prior to Fresnel sensor measurements to avoid any influences.

[2]The analog-to-digital converters in the fos4Test system have a resolution of 16 bit which results in $2^{16} = 65\,536$ quantisation levels of the measurement signal. The quantisation levels are given in arbitrary units (arb. unit).

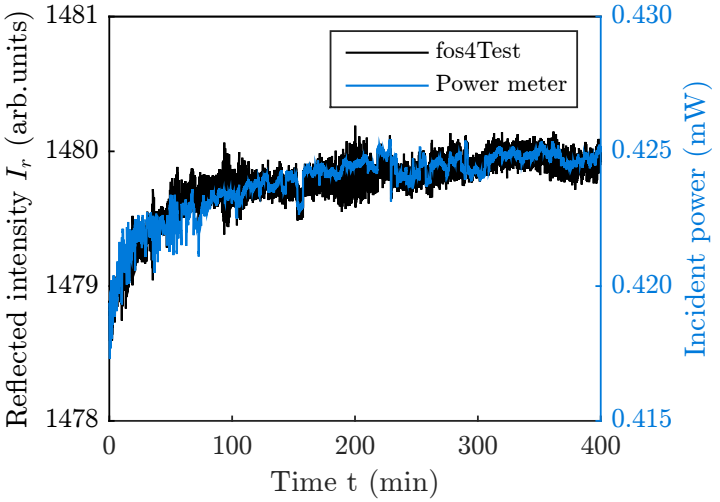

Figure 3.8: Synchronous measurement of incident and reflected light at one channel for 400 min after the fibre optic measurement system was switched on. The incident laser power was measured with an external power meter.

3.5.2 Determination of the effective fibre refractive index

Light propagation in an optical fibre is depended on the effective refractive index n_{eff} as was described in Sec. 2.4.1. Since n_{eff} of the applied Corning SMF28e singlemode fibres was not known, it was deduced by inscribing and interrogating a Fibre Bragg Grating (FBG) in the optical fibre. When light travels through a fibre containing an FBG, a certain amount of the incident light is reflected back from the FBG due to coherent scattering at the periodic refractive index variations. The strongest reflection causes a distinct peak in the reflection spectrum and occurs around the characteristic Bragg wavelength λ_B. By knowing the FBG grating period Λ, the effective fibre refractive index n_{eff} can be deduced according to the following equation [71]:

$$\lambda_B = 2n_{eff}\Lambda\,. \tag{3.4}$$

The effective fibre refractive index was determined during pre-trials by inscribing an FBG in several optical fibres. This was done in collaboration with the University of Applied Sciences Munich according to the method described by Juelich and Roths [78]. The Bragg wavelength $\lambda_B = 1549.5\,\text{nm}$ was chosen to match the centre wavelength of the fibre optic measurement system ($\lambda_B \approx \lambda_c$) and the grating period was $\Lambda = 535.2\,\text{nm}$. The arithmetic mean of the effective refractive indices was determined to $n_{eff} = 1.4473 \pm 0.0003$ at ambient temperature $T_0 = 23\,°\text{C}$.

3.6 Calibration fluid refractive index measurement with Fresnel sensors

This chapter describes the experimental setup (Sec. 3.6.1) and procedure (Sec. 3.6.2) that yields the refractive indices of the five calibration fluids measured with Fresnel sensors. The obtained results (Sec. 3.6.3) are analysed for outliers and subsequently averaged by the mean (Sec. 3.6.4).

3.6.1 Experimental setup

The goal of the experimental setup is to obtain refractive index values as accurate as possible. Therefore, any external influences have to be minimised and the temperature of the calibration fluid has to be maintained constant at 24 °C. The calibration setup shown in Fig. 3.9 consisted of a test tube filled with 2 ml calibration fluid that was immersed into a temperature-controlled water basin. The basin

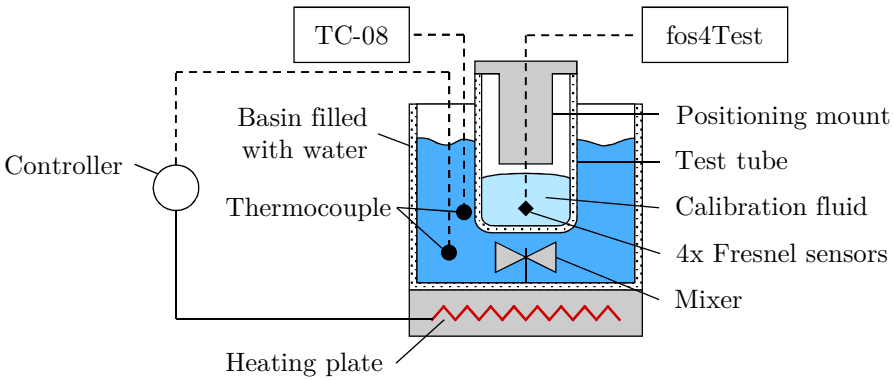

Figure 3.9: Setup for calibration of fibre optic measurement system.

was equipped with an automatic magnetic mixer for homogeneous temperature distribution. The large thermal inertia of the water basin ensured stable temperatures of 24.0 °C ± 0.2 °C inside the test tube. This was assured by pre-trials, that investigated the temperature distribution in the water basin and inside the test tube with 3-point calibrated thermocouples. The setup is designed to immerse four Fresnel sensors 5 mm deep into the calibration fluid at the same time. This is done to measure simultaneously with all four channels in each calibration repetition. In order to assure reproducible and exact sensor positioning in the fluid, the sensors were attached to a specific positioning mount that was placed on top of the test tube. The mount was equipped with four cannulas that guided the optical fibres. The optical fibres were guided from the positioning mount to the measurement system by a sturdy wire to inhibit motion or kinking to assure no light loss

during measurement. The test tube temperature was tracked with a thermocouple interrogated by a temperature measurement system (Pico Technology TC-08, UK). In order to prevent contamination of the calibration fluids, the thermocouple was placed outside of the test tube in the water basin.

3.6.2 Experimental procedure

The work flow of the experimental procedure performed in this paragraph is described in detail in Fig. 3.10. Prior to any measurements, the fibre optic measurement system was preheated for more than 1 h, in order to stabilise the light source. Fresnel sensors were prepared by removing the buffer from the optical fibres and subsequently cleaving the fibres to obtain planar tip surfaces. The sensor quality was assessed by measuring the reflected intensity in air $I_{r,air}$ at 18 % laser power. In case $I_{r,air} < 40\,000$ arb. unit, which is lower than 60 % of the photodiode threshold, the sensor was rejected and the cleaving operation was repeated.

In every calibration fluid, the experiments were simultaneously performed with 4 Fresnel sensors and repeated 20 times. 20 repetitions were performed since it is the suggested amount to perform statistical analysis [40]. In order to correct the influence of the dark current, the zero intensity I_0 was determined once for every fibre/fluid during the first repetition. This was done by measuring the reflected intensity while the laser was turned off. Prior to each fluid measurement, the reflected intensity in air $I_{r,air}$ was measured as a reference to obtain the fluid refractive index. During the $I_{r,air}$ measurement, data was recorded for 1 min and subsequently averaged by the arithmetic mean to equalise any signal fluctuations. At the same time, the air temperature T_{air} was used to calculate the reference fibre refractive index $n_{f,air}$ with Eq. 2.33, and the air refractive index n_{air} based on the equation suggested by Ciddor [26][3].

While air and fibre indices were determined, the calibration fluid inside the immersed test tube equilibrated thermally for at least 5 min. Then, the positioning mount with four Fresnel sensors was immersed in the calibration fluid. The reflected intensity in the fluid I_r was recorded for 1 min and subsequently averaged by the arithmetic mean. At the same time, the water basin temperature T_{fluid} was used to calculate the fibre refractive indices n_f of the Fresnel sensors with Eq. 2.33, to account for any temperature difference between ambient and basin temperature.

At last, the fluid refractive index n was calculated with Eq. 2.29 based on the obtained values for I_r, $I_{r,air}$, I_0, n_f, $n_{f,air}$ and n_{air}. In order to prevent contaminating the fluid, it was exchanged after every fifth repetition and the test tube was

[3] Assumption: 25 % relative humidity, 450 ppm CO_2-content and 101.3 kPa air pressure.

cleaned. For every new calibration fluid, a new test tube and a new set of 4 optical fibres was used.

3.6.3 Experimental results

The data of all Fresnel sensor measurements is shown in Fig. 3.11. The results obtained in each fluid are represented by a separate plot together with the respective refractometer value n_{cal}. Each plot shows the four samples (20 values) obtained from each of the four channels[4]. As expected the Fresnel sensor values exhibited an offset from the refractometer values and showed scattering. Some data points lied unexpectedly far from the majority of sample points. These points might be considered outliers and are assumed not to be part of the population. However, before the data is processed further, outliers have to be eliminated from the sample. Whether a data point is an outlier or not can be decided by statistical rules that depend on the specific sample distribution. Therefore, the distributions have to be analysed. Apart from potential outliers, the magnitude of the scattering was roughly the same in each sample, and scattering occurred around roughly the same (mean) value. This indicates that measurements taken from different channels are alike, with one exception: during measurements in butanol, the values of channel 3 exhibited a constant offset that differed significantly from the other channels (roughly by 0.015). Since the other fluid measurements show no abnormalities in the third channel, it is assumed that the deviation is not affect by the channel hardware. The raw data revealed, that the reflected reference intensity $I_{r,air}$ in this fibre was significantly lower compared to all other fibres. This could be caused by bad cleave quality due to varying material properties that lead to different fracture behaviour, or due to application errors during cleaving. The human factor can be ruled out, however, since the standardised and rigorously executed cleaving procedure was always performed by the same operator. Instead, it is supposed that the fibre refractive index n_f, which was assumed constant for all fibres, differed in this case. Since n_f is a proportional factor in Eq. 2.29 a refractive index change would explain the constant shift of the refractive index. However, the precise cause of this event remains unknown.

3.6.4 Analysis of distributions and outliers

Outliers are extreme values of a distribution of test data. These values have a big influence on statistical parameters such as the mean and can bias the outcome

[4]The same optical fibre was used for each measurement in a sample. Afterwards it was exchanged.

Table 3.3: Probability values p of Shapiro-Wilk test for each sample (in %).

Fluids	Ch. 1	Ch. 2	Ch. 3	Ch. 4
Water	0	2	0	0
Butanol	17	58	1	60
Toluene	5	0	1	0
Nitrobenzene	85	18	19	1
1-Methylnaphthalene	0	0	0	0

of the test. Therefore, further evaluation of the data demands that the sample point distribution is analysed. A standard procedure is to test samples for normal distribution because many statistical tests assume normal distribution [105]. In this work, the Shapiro-Wilk test, also known as *W-test*, was used because it is an established method for samples sizes below 20. Based on the W-test statistic, this test evaluates the hypothesis that a sample was taken from a normally distributed population. The equations for the W-test statistic and the resulting probability value p are derived in the literature [145, 149]. If p is below a certain level of significance α_{hyp} the hypothesis is rejected. In this work, the is rejected if $\alpha_{hyp} < 5\,\%$. This value is a common threshold value.

Resulting probability values p for the 20 samples are presented in Tab. 3.3. The results suggest that the hypothesis is rejected for 13 out of 20 samples. That means that normal distribution cannot be assumed in most cases and standard outlier tests cannot be performed. A possibility to detect an outlier for a wide range of distributions, including non-normal distributions, is provided by Chebyshev's inequality [170]:

$$P[|X - \mu| \geq k\sigma] \leq \frac{1}{k^2}\,. \tag{3.5}$$

It states: the probability P that a value X is further away from the mean μ than k times the standard deviation σ is below $1/k^2$. As a rule of thumb: the threshold for outliers is $k = 4$ [105]. Thus, the likelihood of an outlier outside 4σ is 93.8 %. However, this method is only applicable for samples with one outlier [105]. If several outliers occur in one sample a step-wise approach tests the observations in each step for outliers. One distinguishes forward and backward elimination. In this work, forward elimination was used, because it is considered more robust, if the maximum amount of potentially occurring outliers k in the sample s is known [24]. In this case, all values $X - \mu > 2\sigma$ are counted to the amount of potential outliers k. Based on that number, a subsample $s - k$ is formed which includes only the values with the lowest distance from the mean μ, and no outliers. Based on the subsample mean μ_{sub} and standard deviation σ_{sub}, each potential outlier X is

tested if $X - \mu_{sub} \geq 4\sigma_{sub}$. In case $X - \mu_{sub} < 4\sigma_{sub}$, X is not an outlier and the subsample is expanded by that value. Then, μ_{sub} and σ_{sub} are recalculated and the procedure is repeated until an outlier is identified. In that case, this outlier and all other potential outliers are eliminated from the sample.

Based on this procedure all samples were analysed and the eliminated outliers are listed in Tab. 3.4 divided by channel and fluid. In total 12 % off all values were detected as outliers. One can observe, that in channel 1 and in all 1-Methylnaphthalene samples more outliers were detected by tendency. The reason for that is unknown, however. An overview of the outlier-eliminated samples is given in Appendix A.1.

Table 3.4: Number of outliers detected in each sample.

Fluids	Ch. 1	Ch. 2	Ch. 3	Ch. 4	$\sum$
Water	3		1	4	8
Butanol	4	1	3	3	11
Toluene	4	1	1	2	8
Nitrobenzene	3	1			4
1-Methylnaphthalene	3	6	5	4	18
$\sum$	17	9	10	13	49

The calibration procedure described in Sec. 3.2 requires that the values of each sample are represented by one fluid refractive index. Therefore, the obtained values were averaged by the arithmetic mean to obtain the mean refractive indices $\overline{n}_{fluid}$. The offset Δn_{off} between the mean fluid refractive indices $\overline{n}_{fluid}$ and the respective refractometer values n_{cal} are illustrated in Fig. 3.12. The Fresnel sensor values were of the same magnitude, and were fairly close to the calibrated values. This indicates that the simplified Fresnel equation (Eq. 2.24) describes the fibre optic refractive index values fairly well, and that the fibre optic system shows no general deviations.

The strong deviation of channel 3 at $n_{butanol} \approx 1.39$ seemingly contradicts the previously made statement. Everything indicates that the deviation is attributed to material defects of the optical fibre and not of the measurement device, as has been elaborated previously. It is easily comprehensible that the two correction functions that are linked to this butanol sample are strongly influenced by that deviation. Using these biased values for calibration might corrupt future measurements. Since the butanol samples of channel 1, 2 and 4 lie close to calibration value $n_{cal,butanol}$, it is assumed that these values are close to the true value. For that reason, it was decided, to average their values and to use the result for channel 3 instead. The new butanol channel 3 value in is highlighted in Fig. 3.12 by (●).

After outliers had been eliminated, a final W-test for normal distribution revealed that all but three samples were normally distributed. It was decided to treat all samples as normal distributions in order to describe them by their mean and standard deviation. The mean fluid refractive indices $\overline{n}_{fluid}$ of each sample are depicted in Tab. 3.5 together with their respective standard deviations σ_n. It can be seen that σ_n is below 7×10^{-4} in all samples, including the corrupted butanol sample of channel 3. The standard deviation is a measure of the sample scattering and in Sec. 3.8 it is used to assess the measurement uncertainty.

When performing measurements with several channels simultaneously one question is whether results from different channels can be compared with each other or not. For that reason the scattering of the mean fluid refractive indices $\sigma_{\overline{n}}$ was analysed to provide a measure how much $\overline{n}_{fluid}$ values vary between channels. It was shown in all fluid measurements that $\sigma_{\overline{n}}$ was below 6×10^{-4}. Given that this is in the range of the measurement uncertainty (cf. Sec. 3.8) it is assumed that results from different channels can be compared with each other[5].

Table 3.5: Mean fluid refractive indices and standard deviation per channel and per fluid.

		Ch. 1	Ch. 2	Ch. 3	Ch. 4	$\sigma_{\overline{n}}$
Water	$\overline{n}_{fluid}$	1.315 56	1.315 72	1.315 24	1.315 58	0.000 20
	σ_n	0.000 06	0.000 47	0.000 16	0.000 16	
Butanol	$\overline{n}_{fluid}$	1.387 22	1.386 62	1.386 97[6]	1.387 08	0.000 31[7]
	σ_n	0.000 03	0.000 06	0.000 65	0.000 03	
Toluene	$\overline{n}_{fluid}$	1.472 56	1.473 41	1.472 22	1.472 51	0.000 51
	σ_n	0.000 22	0.000 16	0.000 31	0.000 17	
Nitrobenzene	$\overline{n}_{fluid}$	1.520 43	1.520 71	1.520 47	1.520 33	0.000 16
	σ_n	0.000 17	0.000 21	0.000 29	0.000 29	
1-Methylnaph.	$\overline{n}_{fluid}$	1.579 53	1.580 04	1.579 91	1.579 39	0.000 31
	σ_n	0.000 29	0.000 11	0.000 30	0.000 66	

3.7 Calibration results

The calibration constants of the correction functions were calculated based on Eq. 3.1, Eq. 3.2, Eq. 3.3, and with the obtained mean refractive indices $\overline{n}_{fluid}$ and the respective refractometer values n_{cal}. The resulting calibration constants C_a and

[5] This statement is limited by the fact that the irregular butanol sample of channel 3 was ignored.
[6] Arithmetic mean from channels 1, 2, and 4.
[7] Calculated excluding channel 3

C_b for each channel and interval are given in Tab. 3.6. The C_a values are close to

Table 3.6: Correction function coefficients C_a and C_b for four channels and four interval between 1.3159 and 1.5817.

Interval	Coeff.	Ch. 1	Ch. 2	Ch. 3	Ch. 4
1.3159 ... 1.3869	C_a	0.9908	1.0013	0.9898	0.9930
	C_b	0.0126	−0.0016	0.0142	0.0096
1.3869 ... 1.4753	C_a	1.0359	1.0186	1.0371	1.0347
	C_b	−0.0483	−0.0250	−0.0496	−0.0467
1.4753 ... 1.5224	C_a	0.9839	0.9958	0.9760	0.9851
	C_b	0.0269	0.0082	0.0393	0.0252
1.5224 ... 1.5817	C_a	1.0034	0.9996	0.9977	1.0040
	C_b	−0.0032	0.0023	0.0054	−0.0041

1. Since these values determine the slope of the correction function, this indicates that the difference between refractometer and Fresnel measurement is relatively small. The validity of this statement can be confirmed in Fig. 3.13. This image depicts the corrected refractive indices n_{corr} based on arbitrary fluid refractive index input n_{fluid} between 1.3159 and 1.5817 (exemplary for Ch. 3). For reference, the calibration refractive indices n_{cal} that determine the coefficients are also plotted. It can be seen that the linear approximations between the five nodes were fairly in-line. The effect of the calibration on the sensor output is illustrated in Fig. 3.14. The image presents theoretical refractive index values of a Fresnel sensor n_{theo} calculated with equation Eq. 2.29 based on generic reflectivity input $R = \frac{I_r}{I_{r,air}}$. The calibrated values resulting from applying the correction functions and coefficients of each interval are shown for comparison. The two distinct branches originating from the case differentiation introduced earlier (cf. Fig. 2.15).

The refractive index offset after calibration Δn_{cal} between the fluid n_{corr} and the theoretical values n_{theo} is shown in Fig. 3.15. Each interval is highlighted by a separate colour. The plot shows, that the magnitude of the offset was 10^{-3}. That is one order of magnitude smaller than the refractive index increase due to curing $\Delta n_{cure} \approx 10^{-2}$. This means that the calibration could be forgo if only relative refractive index changes are evaluated. If, however, absolute refractive indices are of interest, e.g. for cure monitoring, this offset is large enough to cause a difference of a few percent degree of cure. Additionally, one can see that the curves are not continuous at the transition from one interval to the other. This is due to the fact that the corrected refractive index is calculated from different sets of calibration coefficients. The observed refractive index step is in the order of 10^{-4}. It can be

neglected, since it is of the same order of magnitude as the measurement uncertainty (cf. Sec. 3.8).

3.8 Uncertainty of Fresnel sensor measurements

When reporting measurement results, it is necessary to provide a quantitative value of the quality of the result in order to assess the reliability of the measurement. The quality of the results may be influenced by deviations of the procedure, material, environment, operator, etc. The impact of these deviations on the quality is described by their respective standard uncertainties u_i. The combination of the occurring uncertainties yields the combined standard uncertainty. A list of uncertainty components and how they are determined is provided in Dietrich and Schulze [40].

The goal of this section is to investigate how accurate the refractive index can be determined with the four-channel edge-filtered FBG measurement system, and if the achieved accuracy meets the requirements for the application in resin cure monitoring. For this application the degree of cure has to be resolved with an accuracy of 5 % which resembles that of measurements performed with DSC. Given that the refractive index rises by approximately $\Delta n_{cure} = 3 \times 10^{-2}$ during curing, the system requires a minimal measurement uncertainty $u_{MS,min} < 1.5 \times 10^{-3}$.

Excursion: The recent history of expressing the measurement uncertainty

Until the 1970s there was no common understanding on how to express measurement uncertainty. This lack was address in a process by several international metrology institutions in the years following. In 1993 the International Organization for Standardization (ISO) presented the first version of the Guide to the Expression of Uncertainty in Measurement (GUM) [75]. This document provided for the first time general rules to gain confirmation on the uncertainty of measurement results. When these general rules were released, it was clear that they would not present a standard that helped to distinguish between acceptable and not acceptable measurement results, nor that these rules would provide precise instructions on how to measure uncertainty. The GUM authors emphasised that further standards had to be developed. In 2003 the VDA 5 guideline [162] was published, that provided detailed procedures how to evaluate measurement devices. This guideline adopted the recommendations by GUM and was later incorporated in the ISO 22514-7 standard [74]. In contrast to GUM, VDA 5 distinguishes between the uncertainty of the measurement system u_{MS} and the measurement process u_{MP}.

This differentiation is useful for the present case, since the goal is to assess the measurement system. According to VDA 5 the uncertainty of the measurement system u_{MS} was determined according to the following procedure:

1. analyse and determine uncertainty components.
2. determine uncertainties $u(x)_i$ either by:
   a) statistical analysis of a series of observations (type A), or by
   b) experience or other information (type B).
3. calculate standard uncertainty of measurement system u_{MS}.

Following the analysis in step 1, the relevant standard uncertainty components of this work are shown in Tab. 3.7. In step 2 the uncertainties are determined based on

Table 3.7: Standard uncertainty components of the measurement system.

Component	Description
u_{EVR}	Equipment variation occurring during repeated measurements.
u_{RE}	Uncertainty of the measurement device resolution.
u_{CAL}	Uncertainty of the calibration reference.
u_{BI}	Uncertainty of the offset from the calibration reference (bias).

one of two evaluation types suggested by GUM. The equipment variation $u_{EVR}(s)$ is determine by type A evaluation and is represented by the standard deviation σ_n of each sample (cf. Tab. 3.5). The maximum value per channel is referred to as $u_{EVR,max}$ and is listed in the first row of Tab. 3.8. Since the values of u_{EVR} and u_{RE} correlate, only the one with the greater value can be considered. The resolution $RE = 2^{-16} = 1.5 \times 10^{-5}$ is defined by the analog-to digital converters in the measurement system. For digital outputs a rectangular distribution can be assumed and the uncertainty of the resolution is determined to $u_{RE} = \frac{RE^2}{12} = 4.3 \times 10^{-6}$ by type B evaluation. Since $u_{EVR,max} \gg u_{RE}$, the uncertainty of the measurement device resolution is neglected. The uncertainty of the prism coupling refractometer $u_{CAL} = 2 \times 10^{-4}$ was also determined by type B evaluation based on the values provided in the refractometer specifications[8]. Since calibrating the fibre optic measurement system eliminated the offset between reference and actual measurement, the uncertainty stemming from the offset is $u_{BI} = 0$ and and can be

[8] `http://www.metricon.com/specifications`

ignored. In step 3 the combined standard uncertainty of the measurement system u_{MS} is determined for each sample based on the uncertainty components:

$$u_{MS} = \sqrt{u_{CAL}^2 + u_{BI}^2 + max\{u_{EVR,max}^2, u_{RE}^2\}}\,. \tag{3.6}$$

Tab. 3.8 shows the resulting combined standard uncertainty of the measurement system for each channel. Channel 1 showed the lowest combined standard uncer-

Table 3.8: Uncertainty components and resulting combined standard uncertainty of measurement system per channel. (x10^{-4})

Component	Ch. 1	Ch. 2	Ch. 3	Ch. 4
$u_{EVR,max}$	3.0	4.7	6.5	6.6
u_{CAL}	2.0	2.0	2.0	2.0
u_{MS}	3.6	5.2	6.8	6.9

tainty $u_{MS} = 3.6 \times 10^{-4}$ and channel 4 the largest ($u_{MS} = 6.9 \times 10^{-4}$). Thus, channel 4 governed the overall combined standard uncertainty of the measurement system. It is noted that this value rests well below the refractive index change of 3×10^{-2} experienced by a polymer during full cure [7].

These results indicate that the presented fibre optic measurement scheme, offers a user-friendly sensing option that does not require calibration after every cleave. The uncertainty in refractive index measurements is found to be slightly greater than the uncertainty achieved by Cusano et al. [34]. Yet it remains in the same order of magnitude, and — if required — it could be reduced by properly modifying the configuration, so as to directly measure the incident light intensity [154, 161].

3.9 Summary

Refractive indices of five calibration fluids in the refractive index range between 1.3 and 1.6 were measured with a four-channel fibre optic measurement system. Repeated measurements in each fluid showed little scattering which indicates good measurement precision. Moreover, measurements with different channels yielded similar results which suggests that measurements taken with different channels can be compared with each other.

For comparison, reference refractive index measurement of the same liquids were performed with a prism coupling refractometer. The results revealed an refractive index offset between the fibre optic system and the refractometer in the range of 10^{-3}. The specific cause for the offset could not be further specified. However, it

is assumed to be attributed to the influence of mechanical and electro-optical components of the measurement system. The offset was eliminated by calibrating the fibre optic measurement system based on linear approximation. The calibrated refractive index values diverted from the theoretical values in the range of 10^{-3}. This deviation is large enough to bias fibre optic cure monitoring. For absolute refractive index measurements it is therefore necessary to perform the calibration. However, if only relative changes are of interest a calibration can be forgo. At last, the uncertainty of the refractive index measurements was determined to 6.9×10^{-4} which is below the required minimal measurement uncertainty $u_{MS,min} = 1.5 \times 10^{-3}$. This proves that the fibre optic FBG measurement system provides adequate accuracy for fibre optic cure monitoring.

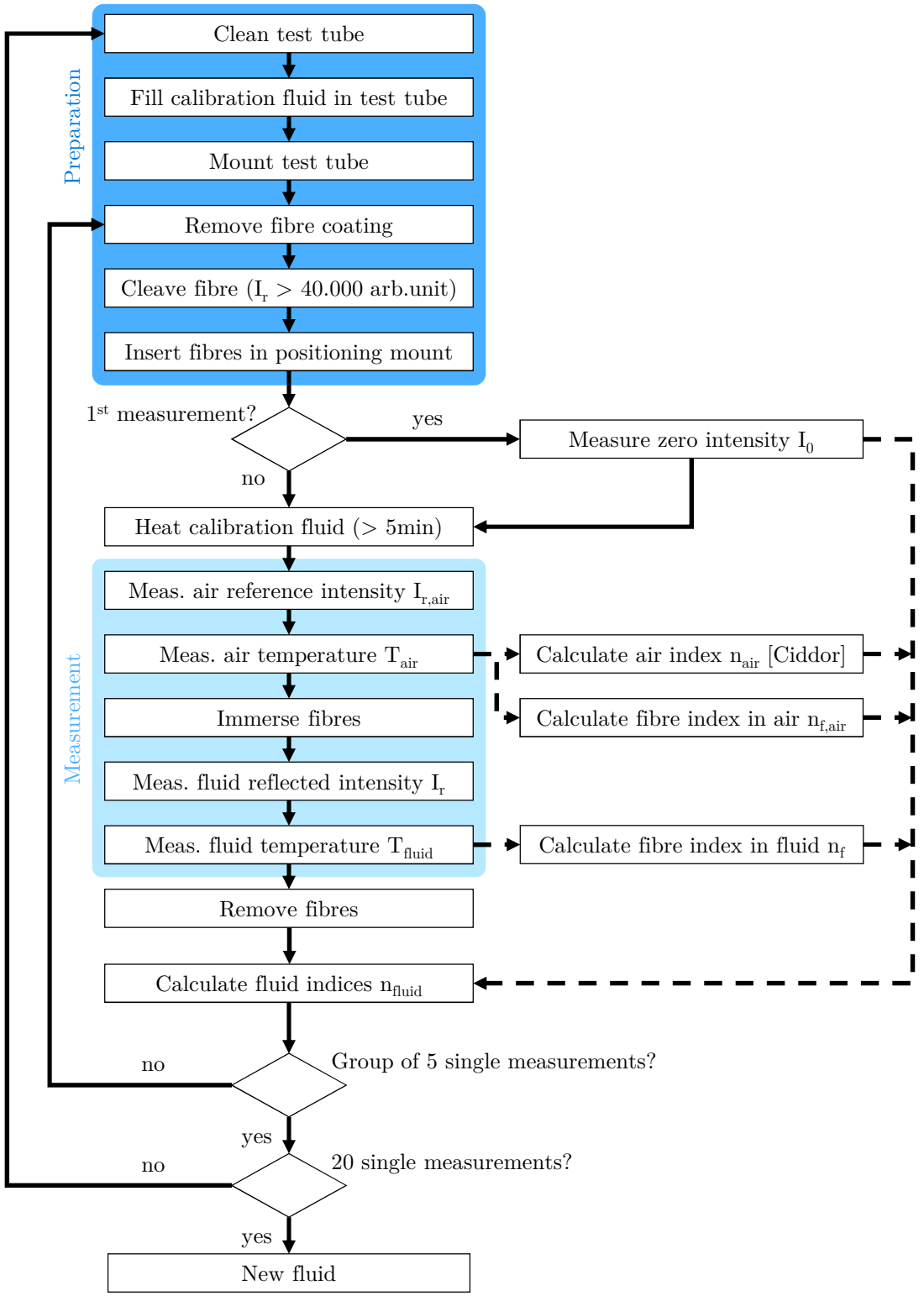

Figure 3.10: Flow chart of Fresnel sensor measurements as part of the calibration procedure.

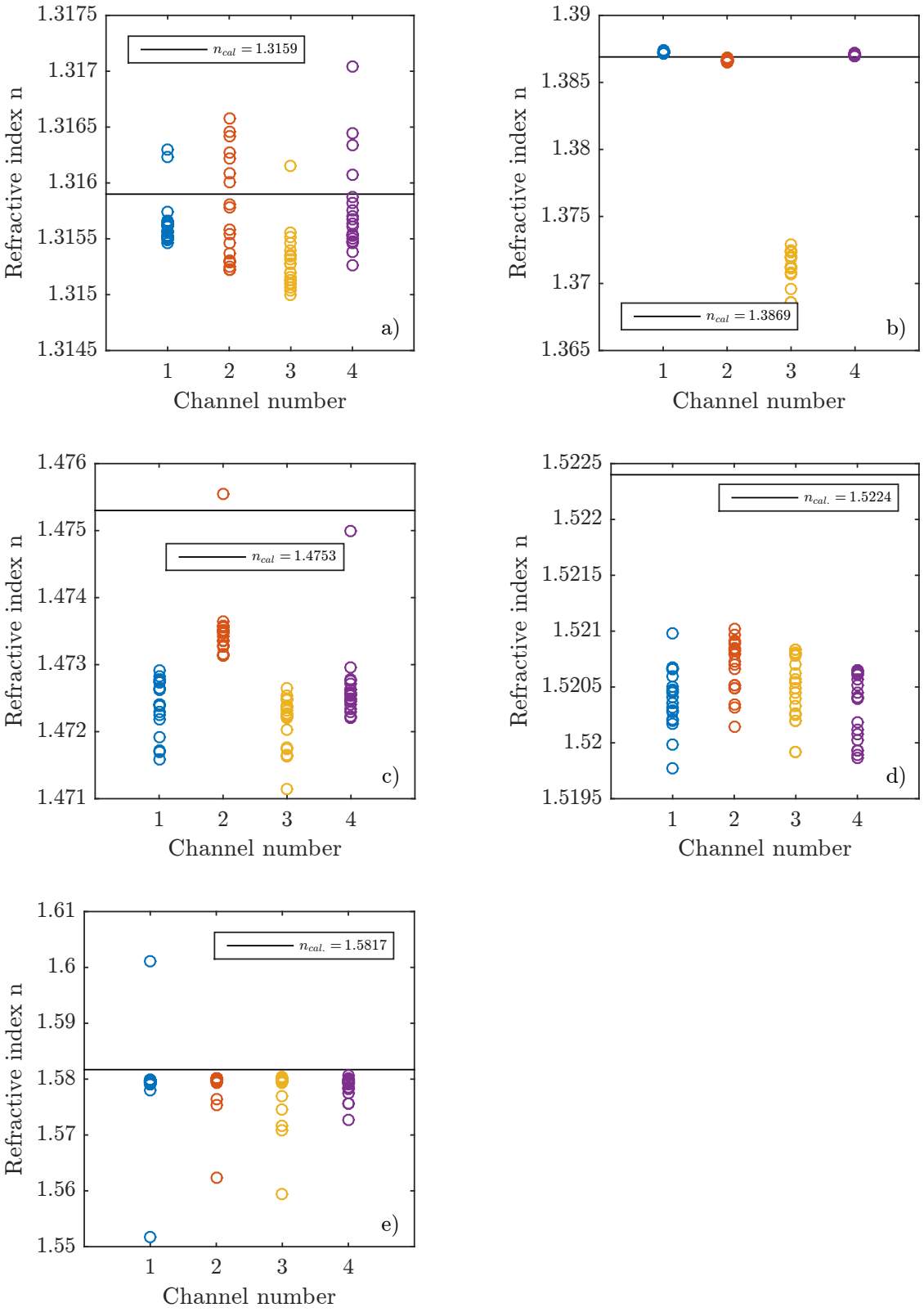

Figure 3.11: Refractive index measurements of water (a), butanol (b), toluene (c), nitrobenzene (d), and 1-methylnaphthalene (e) measured with four Fresnel sensors resulting in four samples per plot. Each sample is measured with one channel and comprises 20 values (○). For reference, the calibration fluid refractive indices n_{cal} obtained with the prism coupling refractometer are shown (-).

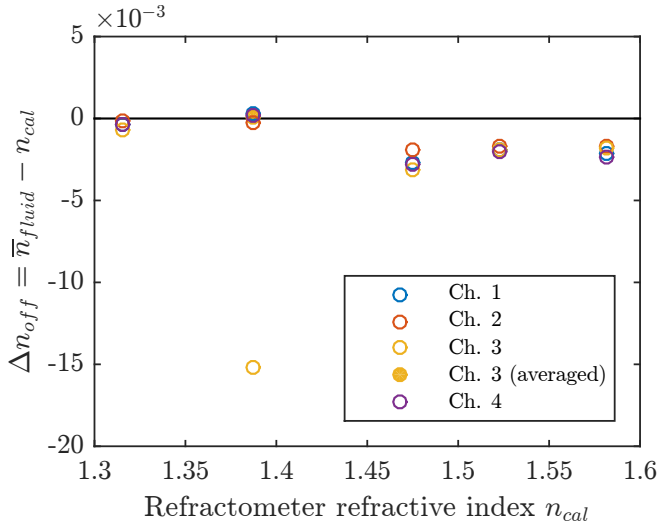

Figure 3.12: Offset Δn_{off} (○) between the mean refractive indices $\overline{n}_{fluid}$ and the respective refractometer values n_{cal}. Additionally, the offset of the shifted mean refractive index of channel 3 of the butanol sample is shown (●).

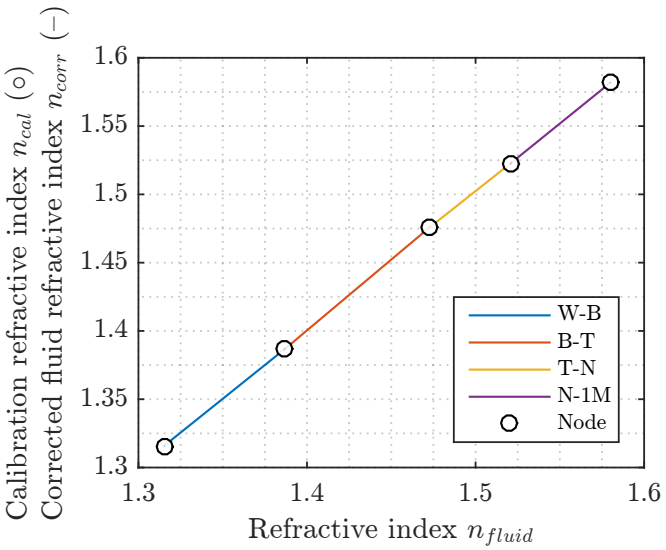

Figure 3.13: Corrected fluid refractive indices n_{corr} calculated based on four correction functions (–) and arbitrary fluid refractive index input $n_{fluid} = 1.3159 \ldots 1.5817$. Each correction functions is valid between two nodes (○). The nodes represent calibration refractive indices n_{cal} of water (W), butanol (B), toluene (T), nitrobenzene (N) and 1-methylnaphthalene (1M). The presented data shows four correction functions of channel 3.

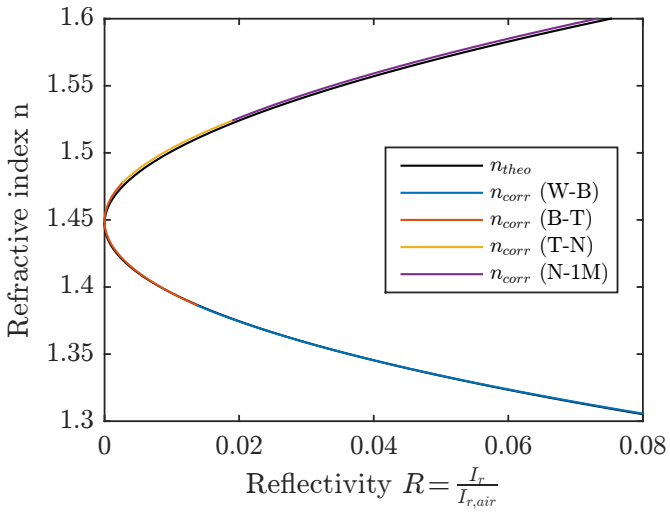

Figure 3.14: Comparison between theoretical Fresnel equation output n_{theo} and calibration output n_{corr}. The calibration was performed with corrections functions between the reference refractive index values of water (W), butanol (B), toluene (T), nitrobenzene (N) and 1-methylnaphthalene (1M). All curves are generated from generic reflectivity R input and a fibre refractive index $n_f = 1.4473$ in the refractive index range from 1.3 to 1.6.

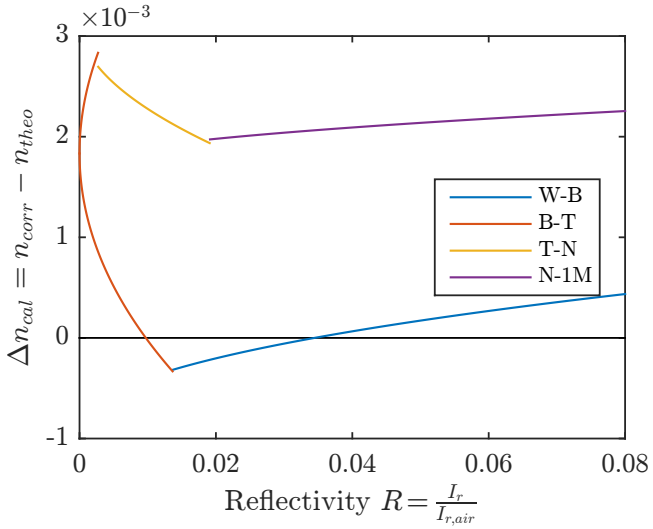

Figure 3.15: Refractive index offset Δn_{cal} between theoretical (n_{theo}) and calibrated refractive index values n_{corr}. The calibration was performed with corrections functions between the reference refractive index values of water (W), butanol (B), toluene (T), nitrobenzene (N) and 1-methylnaphthalene (1M). All curves are generated from generic reflectivity R input and a fibre refractive index $n_f = 1.4473$ in the refractive index range from 1.3 to 1.6.

4 Cure measurement with Fresnel sensors

The literature review on fibre optic cure monitoring with Fresnel sensors in Sec. 2.4 showed that few attempts have been made to describe the relationship between resin degree of cure and its refractive index during isothermal curing. Literature is even more scarce regarding non-isothermal cure monitoring. Several publication indicated a correlation of the raw Fresnel sensor signal (reflected intensity) and the degree of cure. However, it is advantageous to use the resin refractive index because it is a material property that allows assumptions on the actual material state. The literature review revealed also that previous research focused mainly on the investigation of the resin systems EPON 828 and RTM 6. To the best knowledge of the author, no data is available on EPS 600 until today.

The aim of this chapter is to provide a model function that describes the degree of cure of EPS 600 resin, under isothermal and non-isothermal curing conditions, based on the resin refractive index measured with fibre optic Fresnel sensors and the curing temperature.

The structure of this chapter is the following: Sec. 4.1 describes the method that is used to obtain a fibre optic degree of cure model. Since temperature control is such an important factor during resin curing and especially when correlating results of two measurement systems, Sec. 4.2 focuses on the temperature distribution of the applied heat source and the ideal sensor position. Sec. 3.6 and Sec. 4.4 describe in detail how the refractive indices and the degree of cure are obtained under comparable isothermal and non-isothermal conditions. The correlation of the refractive indices and the degree of cure is shown in Sec. 4.5. Based on the correlation a fibre optic cure model function is introduced in Sec. 4.6 and validated in Sec. 4.7. At last, a summary of the chapter is given in Sec. 4.8.

4.1 Methodical approach

Since the relation between the degree of cure and the refractive index of curing EPS 600 resin is unknown, the modelling approach relies on a correlation between

those two. This implies that two measurement systems have to be utilised in separate experiments in order to determine both measurands. The systems applied are a DSC for the degree of cure and a fibre optic measurement system for the refractive index. The work flow that describes how the model function was obtained is depicted in Fig. 4.1.

For an accurate correlation it is paramount that the experimental conditions are identical during both experiments — in particular the temperature. Since the desired model shall be valid for all conditions, the same isothermal and non-isothermal experiments are performed with both measurement systems. During the

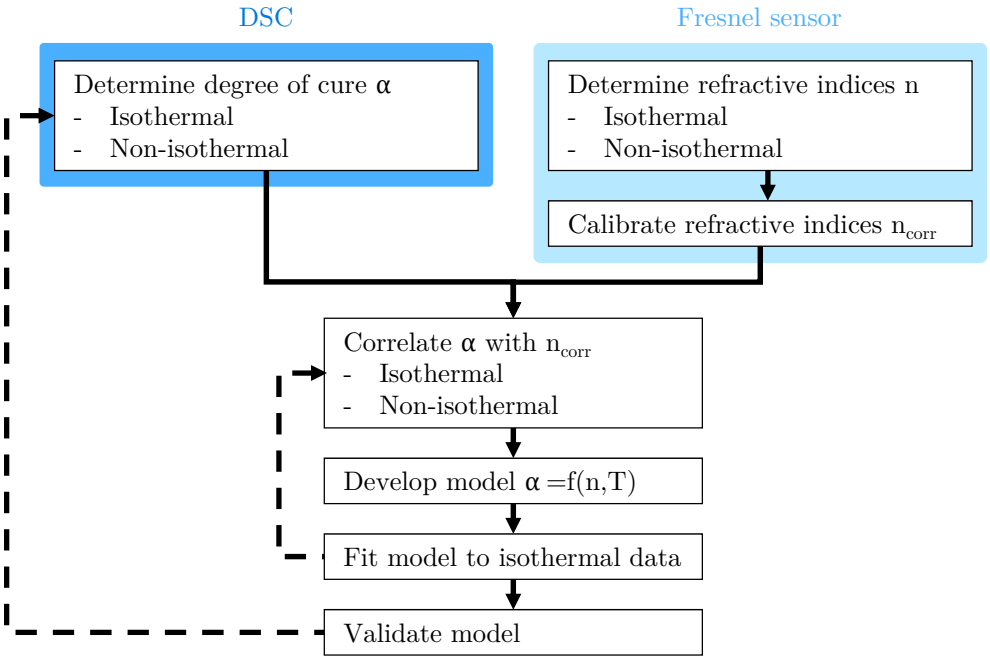

Figure 4.1: Work flow for obtaining degree of cure model.

isothermal experiments resin samples were cured at constant temperature until the cure reaction stopped. The experiments were repeated at different temperatures to investigate the temperature-dependent cure behaviour. This was followed by non-isothermal experiments were resin samples were cured while being exposed to constantly increasing temperature.

The degree of cure was calculated with Eq. 2.3 based on the released heat from the samples during the experiments ΔQ and the previously determined total released heat ΔQ_{tot}. The refractive indices was calculated based on Eq. 2.31 and subsequently calibrated with correction function Eq. 3.1 and the respective coefficients. In the next step, the measurement results from both measurement systems were correlated to obtain an isothermal and a non-isothermal correlation of the degree of cure and the refractive index. Based on the correlations, a model function

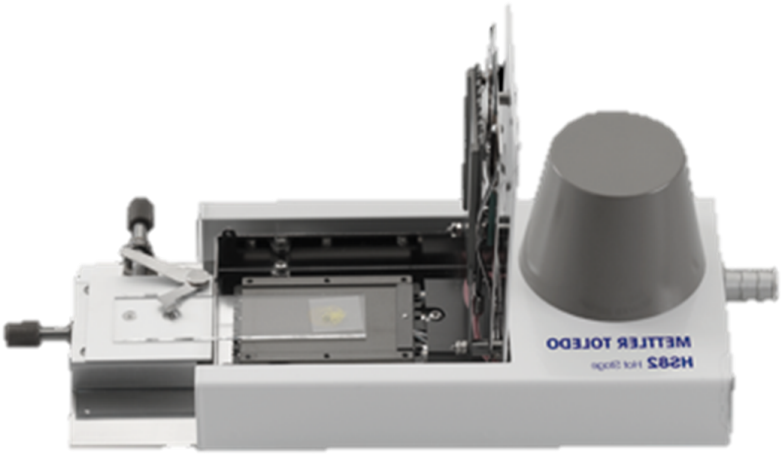

Figure 4.2: HS82 Mettler Toledo microscopy furnace with opened heating chamber and inserted object plate.

$\alpha = f(n, T)$ was developed that describes the degree of cure as a function of the refractive index and the current curing temperature. At last, the model function was fitted to the isothermal correlation and the validated by comparing the model output to the isothermal and non-isothermal DSC data.

4.2 Temperature distribution in furnace

It was previously shown that temperature is an important process parameter during resin curing. Temperature affects not only the curing process, but also the refractive index, as is evident from the Lorentz-Lorenz equation introduced in Sec. 2.4.4. Therefore, temperature control is paramount when comparing cure-dependent parameters from two different measurement systems.

The DSC has an internal heating and cooling stage that assures stable thermal conditions during the heat flow measurements. For the refractive index measurements this was not the case. Therefore, a microscopy furnace (Mettler-Toledo HS82, Switzerland) was used as an external heat source. The furnace shown in Fig. 4.2 is equipped with a flat rectangular heating chamber that introduces heat from the top and bottom with two Peltier elements. The heating chamber is designed to hold a microscopic object plate which is ejectable through a slit at the side. The operator has the option to observe the samples in the chamber with two glass-covered holes in the heating elements. The device uses an integrated Pt100 resistance thermometer for thermal control. Since the Pt100 is not installed in the chamber, the display temperature might divert from the actual furnace temperature. Therefore, internal temperature measurements were performed to identify regions in the furnace that provide accurate and stable temperature conditions.

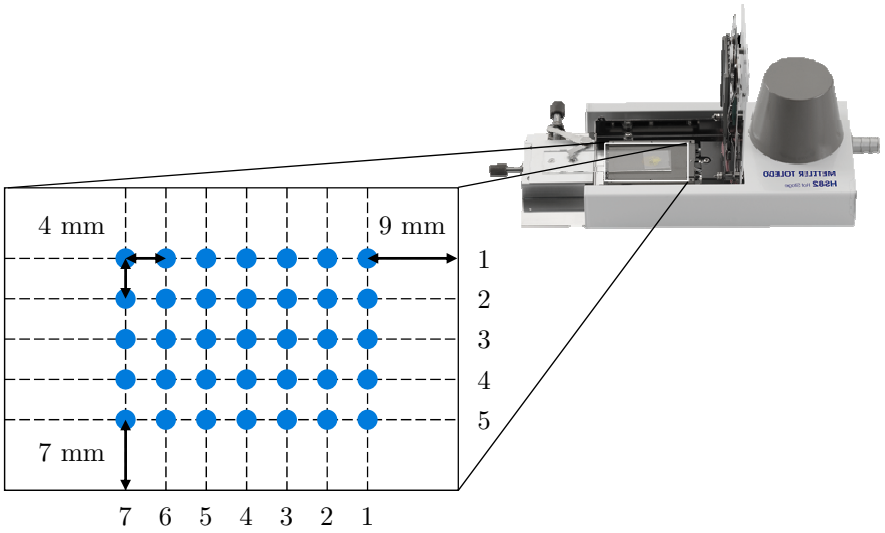

Figure 4.3: Thermocouple locations in heating chamber for mapping of temperature distribution.

For this purpose, five calibrated type-K thermocouples were fixed onto a microscope object plate[1] in a straight line and connected to a temperature measurement system (Pico Technology TC-08, UK). Then, the object plate was inserted into the furnace and heated to the desired isothermal temperature. In order to cover the whole furnace area and to reduce the amount of thermocouples needed, this routine was repeated seven times while the thermocouples were shifted horizontally on the object plate in each repetition. The location of the resulting 35 measurement locations is shown in Fig. 4.3. On each position, the temperature was recorded for 5 min, to obtain average values and to detect occurring fluctuations. The temperature distribution was recorded at 120 °C, 140 °C, 160 °C and 180 °C to cover a wider curing temperature range.

The results revealed that the temperatures diverted between 2 °C to 4 °C from the respective nominal value. The distribution of the mean temperature at 180 °C is shown in Fig. 4.4 on the left. This distribution is presented because it represents the curing temperature of EPS 600, thus it is considered the most relevant. The highest temperatures were recorded at the side of the opening slit. The lowest temperatures occurred near the centre where an observation window for the microscope can be found. The coloured plot indicates that temperatures changed over the length of the chamber but stay relatively constant over its width. This is useful since it allows to position the Fresnel sensors in parallel while they are exposed to the same local temperature. The ideal location for the Fresnel measurements can be

[1] An object plate was used because the actual resin experiments will be performed on one, and its thermal inertia might impact the temperature distribution.

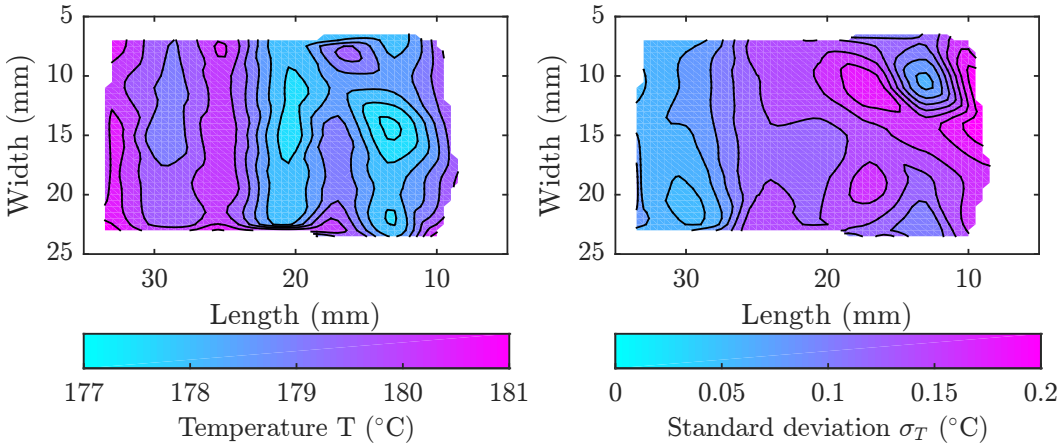

Figure 4.4: Temperature distribution (left) and temperature standard deviation σ_T (right) in HS82 microscopy furnace at nominal 180 °C.

found at length 25 mm where the nominal temperature of 180 °C is met in a small band of ±1.5 mm. The choice of this location was underpinned by a review of the other temperature distributions. It revealed an offset from the respective nominal temperature of only ±1 °C at this position.

Apart from meeting the nominal temperature, low temperature fluctuation are important for precise curing. The fluctuations during the isothermal measurement are expressed by the temperature standard deviation and are shown in Fig. 4.4 on the right. The measured fluctuations were generally below 0.2 °C and at 25 mm width at around 0.1 °C. This shows that the furnace temperature can be held very stable.

4.3 Resin refractive index measurements with Fresnel sensors

The isothermal measurements covered several repetitions at different temperature levels, see Tab. 4.1. During each repetition four Fresnel sensors were applied simultaneously. Non-isothermal measurement, however, were performed at a heating rate of 1 K/ min between 30 °C and 200 °C. The selected temperatures and heating rates represent typical values which occur during processing of aerospace premixed epoxy resins such as EPS 600. Fresnel sensors were prepared by stripping and cleaving the fibre. The sensors were then positioned on a microscope object plate within ±1.5 mm of the optimal position, see Fig. 4.5. In order to guarantee comparable conditions the sensors were aligned parallel to each other. During the non-isothermal measurements an additional type-K thermocouple was placed

Table 4.1: Number of isothermal refractive index measurement repetitions.

Temperature	Repetitions
120 °C	19
160 °C	3
175 °C	3
180 °C	20
185 °C	3

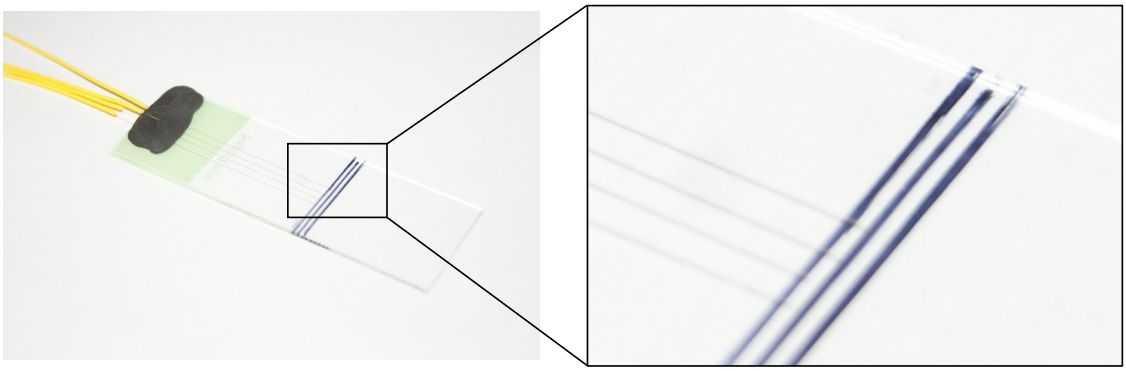

Figure 4.5: Four cleaved optical fibres (grey) fixed with sticky tape (black) on a microscope object plate (transparent). Enlarged: parallel alignment and positioning of the Fresnel sensors. Black bounds are marking the ±1.5 mm tolerance for the optimal furnace position.

next to the Fresnel sensors onto the object plate in order to synchronously record the local temperature. After that, the object plate together with the sensors was placed in the furnace, see Fig. 4.6. There, the zero intensity I_0 was determined and the setup was heated-up to measurement temperature subsequently. After dwelling for 4 min, a constant temperature distribution inside the furnace was reached. At this point, the air reference refractive index was determined with each sensor by averaging the recorded indices over 60 s. Then, the furnace was opened to wet the sensors with approx. 120 mg resin. At last, a glass cover plate was placed on the sensors to prevent direct contact between the resin and the furnace top. The furnace was closed 90 s later. Based on the recorded intensities and temperature it was possible to calculate the resin refractive index with the equations provided in Sec. 2.4.5. After the measurements were finished, the obtained refractive indices were calibrated with the correction function (Eq. 3.1) and the respective coefficients provided in Tab. 3.6.

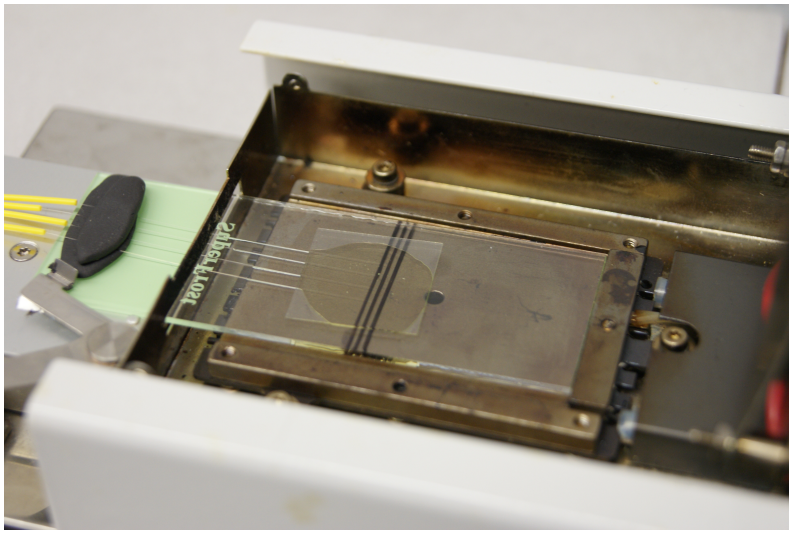

Figure 4.6: Inside view of the opened, preheated furnace where the inserted microscope object plate and four Fresnel sensors can be seen. The sensors are wetted with resin and covered with a glass cover plate.

4.3.1 Isothermal results

Fig. 4.7 shows the refractive index results during isothermal curing at 120 °C, 160 °C, 175 °C, 180 °C and 185 °C. At the end of cure the recordings were stopped after a pre-set time. Depicted are mean values obtained from several synchronous isothermal repetitions. The mean of each isotherm is computed by averaging all repetitions at each time step. It was observed, that the initial refractive index $n(t = 0, T)$ was dependent on the curing temperature and that it decreased with rising temperature. During resin curing, the refractive index increased exponentially. This occurred faster at elevated temperatures because the curing reaction progressed faster. Towards the end of cure the refractive index increase slowed down and eventually levelled out. This behaviour is explained with the Lorentz-Lorenz equation (Eq. 2.25). During curing the ratio of molar refractivity A and molecular mass M were considered constant which means that the refractive index gain was mainly attributed to volume or density change [33, 92, 124]. At the beginning of the experiment, the degree of cure was the same for all isothermal temperatures due to the strict experimental procedure. Therefore, the initial refractive index difference between the isotherms was only governed by the temperature dependence of the resin density. With progressing curing, the resin density increased [33] and therefore led to a cure-induced refractive index rise Δn_{cure} in the range between 2.8×10^{-2} and 4×10^{-2}. This matches the values of other resins reported in earlier studies [7]. Moreover, it was observed that the index rise was steeper at elevated temperatures. By the end of the reaction the cross-linking, and thus, the density

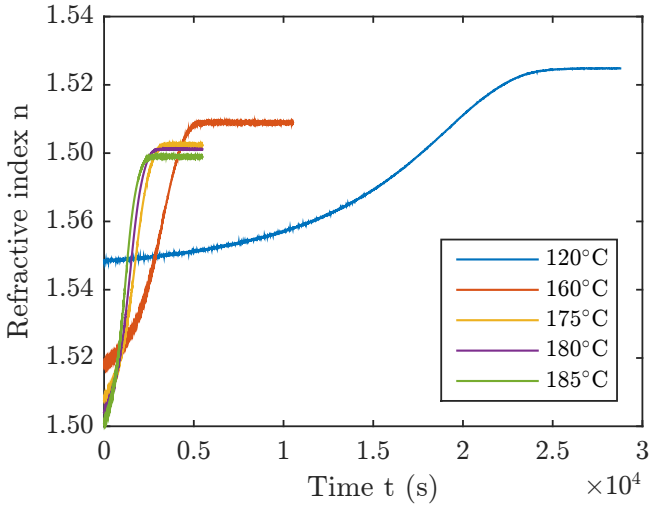

Figure 4.7: Mean refractive index during isothermal curing at 120 °C, 160 °C, 175 °C, 180 °C and 185 °C until the end of cure.

change slowed down. Consequently, the refractive index curve levelled out. Any further diffusion-controlled cross-linking could not be captured. The measurement precision was evaluated by the refractive index standard deviation σ_n which was computed from each time step. It was found that the standard deviation of all isotherms increased during curing, but remained in the range of 10^{-4}. This is sufficient because it is two orders of magnitude below the refractive index change observed during full cure ($\Delta n_{cure} > 10^{-2}$).

4.3.2 Non-isothermal results

Fig. 4.8 shows the evolution of the refractive index during curing at constantly increasing temperature from 30 °C to 200 °C at a heating rate of 1 K/ min. Depicted is the mean curve obtained from four separate measurements. Until approx. 140 °C the refractive index decreased almost perfectly linear. This was attributed to the decreasing resin density during temperature ramp-up. In the linear section, the slope of this curve was 3.8×10^{-4} and represents the resin TOC. This value compares well to the results obtained in quasi-isothermal measurements of the resin TOC reported by Oelhafen et al. [132]. Beginning at approx. 140 °C the curing reaction accelerated and the curve left the linear trend. At 165 °C the refractive index increased again when the resin density had risen enough to compensate for the effect of the resin TOC. At around 190 °C the curing reaction came to an end and the refractive index levelled out.

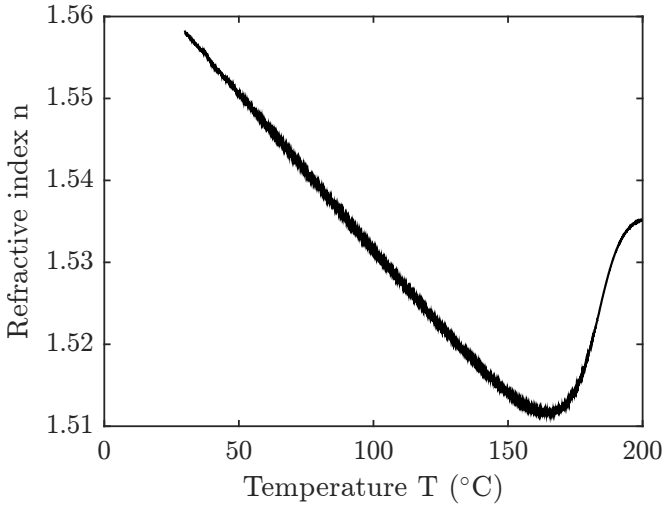

Figure 4.8: Mean refractive index measured with Fresnel sensors during non-isothermal curing from 30 °C to 200 °C at 1 K/ min heating rate.

4.4 Degree of cure measurement with DSC

In this work a TA Q200 DSC (TA Instruments, USA) was used for the thermal analysis of the EPS 600 resin. Prior to the actual experiments, the DSC was calibrated by a standardised procedure with sapphire and indium samples. In order to determine the degree of cure with Eq. 2.3 it was necessary to first measure the total released heat of the resin (ΔQ_{tot}). This was done by placing between 13 mg to 15 mg of resin in an aluminium sample pan and heating the sample from −30 °C to 300 °C at a heating rate of 1 K/ min while recording the released heat. The actual isothermal and non-isothermal measurements of the released heat of the resin samples (ΔQ) followed in separate experiments. These measurements were performed under the same thermal conditions as the refractive index measurements. At last, the degree of cure was calculated based on ΔQ and the previously determined ΔQ_{tot}.

4.4.1 Isothermal results

In Fig. 4.9 the isothermal degree of cure results are plotted over time. A typical s-shaped curing behaviour was observed which resulted from an increased reaction rate at the beginning of the curing cycle and a decreased reaction rate towards the end. It could be seen that greater curing temperatures led to greater reaction rates — expressed by steep slopes — and greater final degrees of cure. This can be explained by enhanced molecular motion at elevated temperatures and delayed vitrification which allows for stronger cross-linking before the polymer freezes. The

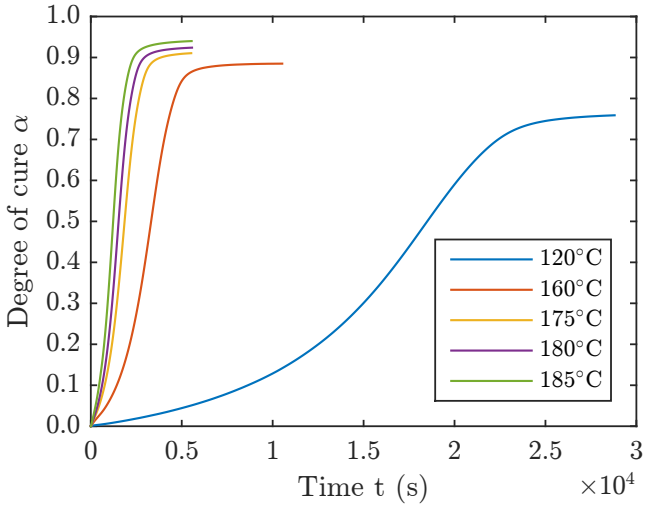

Figure 4.9: Degree of cure during isothermal curing at 120 °C, 160 °C, 175 °C, 180 °C and 185 °C obtained with DSC.

degree of cure was evaluated until no further increase in degree of cure was detectable.

4.4.2 Non-isothermal results

The degree of cure determined during the non-isothermal DSC measurements at a heating rate of 1 K/ min between 0 °C and 250 °C is depicted in Fig. 4.10. Again, an s-shaped curing behaviour was observed. At the beginning the degree of cure did not rise until approximately 120 °C when the reaction gradually took up speed leading to an exponentially growing degree of cure. At around 180 °C the curing rate reached its maximum and around 240 °C the heat flow released from the sample ceased when the maximum degree of cure was reached. The observed curing behaviour is favourable for processing since it enables resin flow until close to the recommended curing temperature window at 180 °C ± 5 °C.

4.5 Correlation of degree of cure and refractive index

The foundation for finding an adequate model is to correlate refractive index and the degree of cure values obtained under isothermal and non-isothermal conditions.

4.5.1 Isothermal correlation

The results of the isothermal correlation of the degree of cure and the refractive index are depicted in Fig. 4.11. The plot shows that the correlations of all iso-

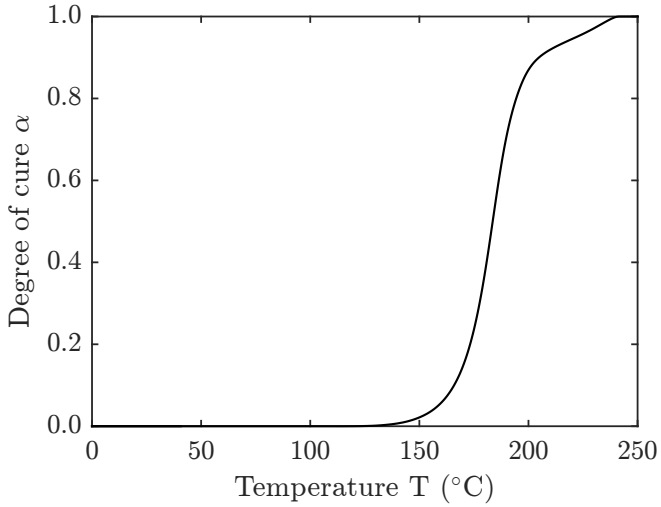

Figure 4.10: Degree of cure between 30 °C to 250 °C at a heating rate of 1 K/ min.

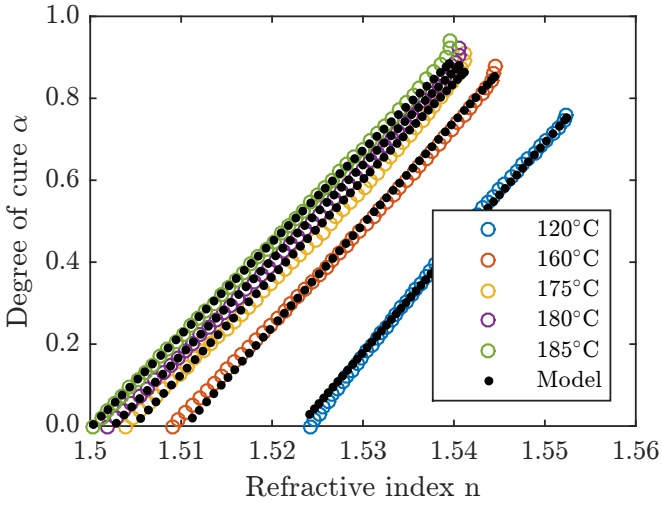

Figure 4.11: Correlation of degree of cure and refractive index measurements (∘) with superimposed refractive-index-based degree of cure model (·) during isothermal curing at 120 °C, 160 °C, 175 °C, 180 °C and 185 °C.

therms increased fairly linear during curing. It was observed that the correlation was temperature-dependent with a shift towards greater refractive indices for lower curing temperatures. That shift was attributed to the resin temperature dependence shown in Fig. 4.7. In order to find a functional description, the correlations were linearly fitted and the temperature dependence of their components was analysed (not shown). It was revealed that the observed refractive index shift can be described by a quadratic function of the temperature. The analysis showed also, that the linear slope was not the same for all isotherms. For decreasing temperatures the slope increased slightly. It was shown that the increase could also be described also by a quadratic function of the temperature. Similar to earlier studies [7, 92], the linear relationship did not hold until the end of cure. There, it

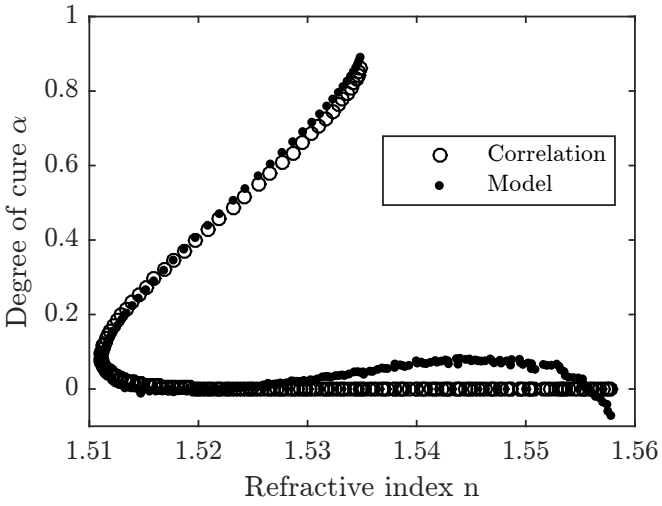

Figure 4.12: Correlation of degree of cure and refractive index measurements (∘) with superimposed refractive-index-based degree of cure model (·) during non-isothermal curing at 1 K/ min.

was observed that the degree of cure still increased by a couple percent while the refractive index remained constant.

4.5.2 Non-isothermal correlation

The correlation of degree of cure and refractive index measurements during curing under constantly increasing temperature from 30 °C to 200 °C at a heating rate of 1 K/ min is depicted in Fig. 4.12. Until approximately 140 °C the degree of cure remained unchanged while the refractive index decreased in the same time frame from 1.56 to 1.52 due to the resin TOC. Beginning at 1.52 , the degree of cure began to rise noticeably while the refractive index still decreased until 1.51. At this point the effect of the TOC was fully compensated by the cure-induced increase of the resin density which made the refractive index rise further. From then on the correlation showed a fairly linear increase until full cure was reached.

4.6 Refractive-refractive-index-based cure model development

The developed cure model was based on the Lorentz-Lorenz equation Eq. 2.25. The challenge was to relate density ρ to degree of cure α. Here, Cusano's approach [33] was followed which assumes that density is proportional to the degree of cure under isothermal conditions ($\rho \sim \alpha$). A measure for the degree of cure was obtained

Table 4.2: Cure model parameters.

Parameter	Value
a_1	0.0007
a_2	−0.3469
a_3	85.9382
b_1	−0.0002
b_2	0.1034
b_3	−37.4196
c_1	650.4987

by normalising the density to the initial density $\rho_0(T, \alpha = 0)$ and the maximum density $\rho_{max}(T, \alpha = \infty)$:

$$\frac{\rho - \rho_0(T)}{\rho_{max}(T) - \rho_0(T)} = \alpha\,. \tag{4.1}$$

In order to further simplify the equation, $\rho_0(T)$ and $\rho_{max}(T)$ were considered temperature-dependent parameters (K_1 and K_2). By solving Eq. 4.1 for ρ one obtains

$$\rho = \alpha \cdot K_1(T) + K_2(T)\,, \tag{4.2}$$

and by combining Eq. 2.28 and Eq. 4.2 and under the assumption $\frac{A}{M} = const.$ one obtains

$$\alpha = K_a(T) \cdot \left(\frac{n^2 - 1}{n^2 + 2}\right) + K_b(T)\,, \tag{4.3}$$

with the temperature-dependent parameters K_a and K_b. The correlations in Sec. 4.5 suggested, that both parameters can be described by quadratic functions of the temperature.

In order to expand the model to the non-isothermal domain an empirical term $ln(c_1 T)$ was introduced to compensate for high refractive indices at low temperatures and low degrees of cure ($\alpha < 0.1$). This term yielded the best results during an analysis of different functions. The resulting model is a function of the resin refractive index n, temperature T and seven fitting parameters:

$$\alpha(n, T) = (a_1 T^2 + a_2 T + a_3) \cdot \left(\frac{n^2 - 1}{n^2 + 2}\right) + (b_1 T^2 + b_2 T + b_3) + ln(c_1 T)\,. \tag{4.4}$$

The obtained function was fitted to the isothermal correlation values by a non-linear least-square MATLAB solver. A global solution was searched by using the MATLAB-integrated *MultiStart* algorithm. The acquired parameters are listed in Tab. 4.2.

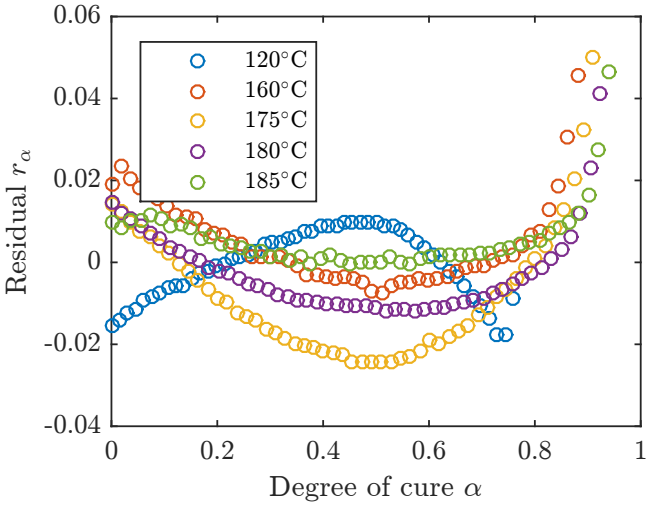

Figure 4.13: Residuals between the actual degree of cure and the model output during isothermal curing at various temperatures.

4.7 Cure model validation

The model equation (Eq. 4.4) was validated by comparing the model output with the correlation. The model output was generated by feeding the model with the refractive indices and temperatures used for the correlation, plus the model coefficients found in Tab. 4.2. The model output for the isothermal case is shown in Fig. 4.11 in comparison to the correlation. It can be seen that the model captured the shift attributed to the resin temperature dependence well and follows the linear trend of all isotherms. To further assess the goodness of fit, the residual r_α between the degree of cure and the model output is shown in Fig. 4.13. For an ideally fitting model, the residuals would be scattered around the 0 value along the degree of cure. This is not the case for the depicted values which indicate that model does not reproduce the degree of cure perfectly. However, the residuals remained generally below 0.02, except towards the end of cure ($\alpha > 0.86$), when they increased to $r_\alpha = 0.06$. Not surprisingly, the model reproduces what the correlation had shown previously. Towards the last few degrees of cure, the model underestimates the actual evolution of the degree of cure.

The model output for the non-isothermal case was generated by the same procedure. Fig. 4.12 shows the resulting model response in comparison to the correlation. At 0 degree of cure, great residuals were observed. These values correspond to the first stage of the heating ramp until approx. 140 °C where the refractive index dropped from 1.56 to 1.52 while the degree of cure remained at 0. To model this section is particularly challenging since two parameters (T, n) change while the dependent third parameter (α) remains practically unchanged. For that reason the

logarithmic term ($ln(c_1 \cdot T)$) is introduced in the model equation. This term is intended to compensate the otherwise overestimated degree of cure during the initial temperature-induced refractive index drop. The residual between model output and correlation was $r_\alpha < 0.1$, as can be seen in on the left hand side of Fig. 4.14 at $\alpha = 0$. This shows that the compensation was sufficient but not perfect. As soon

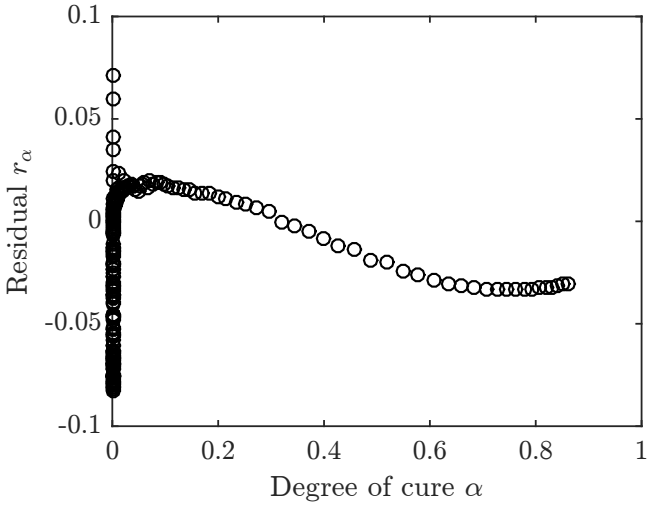

Figure 4.14: Residuals r_α between the actual degree of cure and the model output during non-isothermal curing.

as the polymerisation accelerated at $n \approx 1.52$ (140 °C), the model prediction was adequate. During curing the residual was found to be $r_\alpha < 0.035$.

In summary: the model followed the correlation generally well. The short comings of the model concern the underestimation of the final degree of cure by a few percent, and the overestimation of the degree of cure during the very early stages of non-isothermal curing, where practically no conversion takes place. This leads to the conclusion that this model allows to measure the degree of cure fibre optically with adequate accuracy under different thermal conditions. In distinction to previous publications [12, 143, 160] the presented work sets itself apart by providing an analytical model for Fresnel sensors that relies on the resin refractive index and which is valid for all isothermal and non-isothermal conditions relevant for composite process monitoring. Moreover, a residual analysis has been presented for the first time to assess the goodness of fit of the analytical model.

4.8 Summary

EPS 600 epoxy resin was cured under isothermal and non-isothermal conditions in two different experimental setups. In the first setup the resin refractive index was measured with fibre optic Fresnel sensors. In the second setup the degree of

cure was measured with DSC. The results of both experiments were correlated for the isothermal and the non-isothermal case. Based on the correlation an analytical model was developed that describes the degree of cure as a function of the current resin temperature and the resin refractive index. The validation showed that the model reproduced the degree of cure well. It underestimated the final degree of cure by a few percent, and overestimated the degree of cure during the very early stages of non-isothermal curing, where practically no conversion takes place. The goodness of fit of the model was evaluated with the residuals between model and correlation. It was found that the residuals were below 0.02 degree of cure apart from the previously mentioned regions. This shows that the introduced model has an adequate accuracy and is suitable to be applied for fibre optic cure monitoring during isothermal and non-isothermal curing conditions. The introduced model extends the state of the art by being based on the refractive index while being validated for all isothermal and non-isothermal conditions relevant for composite process monitoring.

5 Viscosity measurement with Fresnel sensors

Viscosity is one of the decisive process parameters in composite manufacturing because it controls resin flow and therefore influences preform infusion. The initial viscosity increase until 1 Pa·s is of particular interest because — as a rule of thumb — the resin flow stops at this point [138]. Measuring and subsequently adapting the resin viscosity (e.g. by change of temperature), can potentially increase the productivity in composite manufacturing processes. The literate review showed, that very few resin viscosity sensing solutions are available that might be suitable for integrated composite manufacturing process monitoring. In the past, fibre optic Fresnel sensors have proofed to be suitable to measure several parameters. Up until now, no fibre optic viscosity sensor has been reported for integrated composite manufacturing process monitoring.

The aim of this chapter is to provide a model function that describes the viscosity of EPS 600 resin in a range between 0 Pa·s to 1 Pa·s under isothermal and non-isothermal curing conditions as a function of the resin refractive index and the curing temperature.

The structure of this chapter is the following: in Sec. 5.1 the methodical approach is introduced that describes how the refractive-index-based viscosity model was developed. This is followed by the results of isothermal and non-isothermal viscosity measurements performed in a rheometer in Sec. 5.2. In order to provide a first indication of the model function, the obtained isothermal viscosity results are correlated with previously obtained refractive index values in Sec. 5.3. The selected viscosity model, the determination of the model parameters, and its combination with the previously introduced refractive-index-based degree of cure model is presented in Sec. 5.4. This is followed by fitting the refractive-index-based viscosity model to the isothermal correlation and assessing the goodness of fit by analysing the residuals. Finally, a summary of this chapter is given in Sec. 5.6. Part of the measurement results have been gained in the bachelor thesis by Dickes [39] under the supervision of the author.

5.1 Methodical approach

The literature review yielded no previous publications about the relation between the refractive index n and viscosity η of curing resins. However, it was found that the viscosity of curing resin has previously been described as a function of the degree of cure α and temperature T. The approach, illustrated in Fig. 5.1, is to combine this existing viscosity model $\eta = f(\alpha, T)$ and to combine it with the refractive-index-based degree of cure model $\alpha = f(n, T)$ introduced in chapter 4 in order to form a refractive-index-based viscosity model $\eta = f(n, T)$.

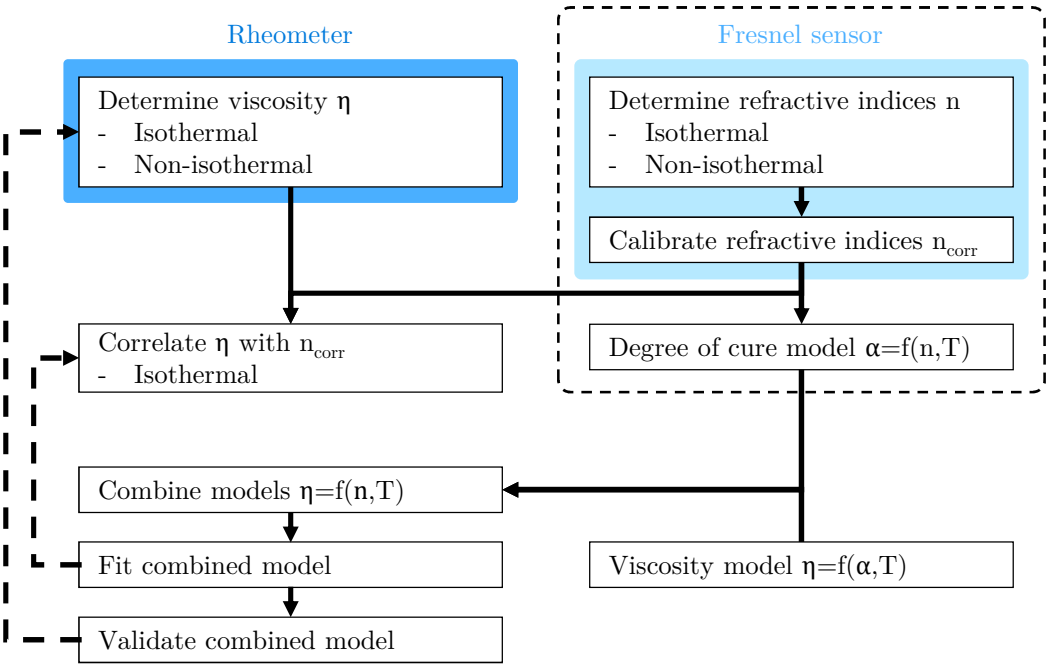

Figure 5.1: Work flow for obtaining viscosity model. Results obtained in chapter 4 are indicated by a dashed box.

At first, isothermal and non-isothermal viscosity measurements were performed in a rheometer. The thermal conditions were identical to the conditions during the refractive index measurements in chapter 4. This allows to correlate both data sets. Then, the model parameters of the refractive-index-based viscosity model were fitted to the isothermal correlation. At last, the refractive-index-based viscosity model output was validated against the previously determined isothermal and non-isothermal viscosity data.

5.2 Viscosity measurement with rheometer

The viscosity experiments were performed with a rotational Anton Paar MCR 302 rheometer. In this rheometer a fluid is placed in the gap between a rotating

and a stationary plane and subjected to sheering (cf. Sec. 2.3.2). Depending on the measurand of interest, the rotating plane is either rotated or oscillated. The applied rotating plane had a 25 mm diameter and was dismountable. For accurate temperature control, the rheometer was equipped with a H-PDT 200 heated bonnet.

The viscosity of the uncured and at 80 °C pre-heated liquid resin is between 0 Pa·s and 1 Pa·s. For that reason isothermal viscosity values were obtained with rotational measurements in a cone-plate configuration. The isothermal experiments were performed at 120 °C, 160 °C and 180 °C until the viscosity reached at least 1 Pa·s. The measurements were repeated several times to allow averaging of the results. A list of the isotherms and their respective repetitions is presented in Tab. 5.1. The non-isothermal viscosity values were recorded at a constant heating

Table 5.1: Number of isothermal viscosity measurement repetitions.

Temperature	Repetitions
120 °C	3
160 °C	3
180 °C	6

rate of 1 K/ min from 30 °C to 200 °C. During that heating ramp, the viscosity will increase strongly which would inhibit any rotation. Therefore, the non-isothermal samples were subjected to oscillation in a plate-plate configuration with a plate gap of 0.30 mm. This configuration was used because thermal expansion has a lower impact on gap distance and results in better measurement accuracy.

Rheometer parameter study

Rheometer measurements yield only reliable results if no shear-thinning occurs during the rotational measurements and if the oscillatory measurements are performed within limits of the LVE (cf. Sec. 2.3.2). For that reason a rotational shear rate sweep was carried out in a low viscosity state from $\dot{\gamma} = 360\,\mathrm{s}^{-1} \ldots 0.1\,\mathrm{s}^{-1}$ at 180 °C to investigate the dependence of the shear rate on the viscosity. The investigation yielded no shear rate-dependence until $\dot{\gamma} \approx 100\,\mathrm{s}^{-1}$. Thus, this value was used as the standard shear rate for the rotational measurements.

In order to find the right settings for the oscillatory measurements in a wide temperature range, amplitude and frequency sweeps were performed at various curing states and temperatures. It was found that the material had linear-viscoelastic behaviour until a deformation of $\gamma = 0.5\,\%$. The frequency sweeps, however, yielded no clear answer regarding the right choice of the angular frequency ω. Therefore, the suggestion made by the ASTM D4473 norm was followed and the angular fre-

quency was set below 1.5 Hz [2]. Based on these findings, the deformation $\gamma = 0.5\,\%$ and the angular frequency $\omega = 1\,\mathrm{Hz}$ were selected as standard settings for the oscillatory viscosity measurements of EPS 600.

Rheometer measurement procedure

The measurement procedure for the isothermal and the non-isothermal measurements was identical: prior to the experiments the whole rheometer setup was preheated at the desired temperature for 10 min. This ensured a constant temperature distribution and allowed thermal expansion of the rheometer shaft. It is noted, that preceding temperature measurements at different locations inside a 1.5 mm cone gap had shown that the assumption of constant temperature with in the gap can be made. Since each repetition was performed with a new plate, rheometer software routines were used to calibrate the rheometer prior to each repetition. This included the measurement of the inertia of all rotating parts for precise torque measurement and the adjustment of the zero point to set the cone gap accurately. The ensuing experiment steps were timed precisely to ensure that the resin samples have the same thermal history. At first, the Peltier bonnet was opened and a preportioned amount of approx. 120 mg resin was placed on the plate. Then, the gap was adjusted and potential surplus resin was removed with a cotton bud. Lastly, the bonnet was closed and the measurement was started. All measurements began with a short period of cone rotation at $1\,\mathrm{s}^{-1}$ to reduce entrapped gas bubbles and to homogenise the resin.

5.2.1 Isothermal results

The viscosity values obtained during isothermal resin curing at 120 °C, 160 °C and 180 °C are shown in Fig. 5.2 in the range from 0 Pa·s to 1 Pa·s. Illustrated is the mean value of all repetitions over time. Additionally the respective standard deviation σ_η is shown as a ribbon. At 160 °C and 180 °C the standard deviation is little and the ribbon is hardly visible. With progressing curing time the mean viscosity values of all curves increased exponentially. Elevated curing temperature led to faster curing reaction and to lower initial viscosity. At the recommended infusion temperature (120 °C) the viscosity remained at a low level for a prolonged time. It took several hours until the resin viscosity started to increase noticeably. At elevated temperatures the curing reaction progressed much faster which lead to an earlier viscosity increase, as can be seen in the 160 °C and 180 °C curves. At these temperatures the resin infusion is typically finished and the material is being cured. A fast viscosity increase at these temperatures is favourable for productivity be-

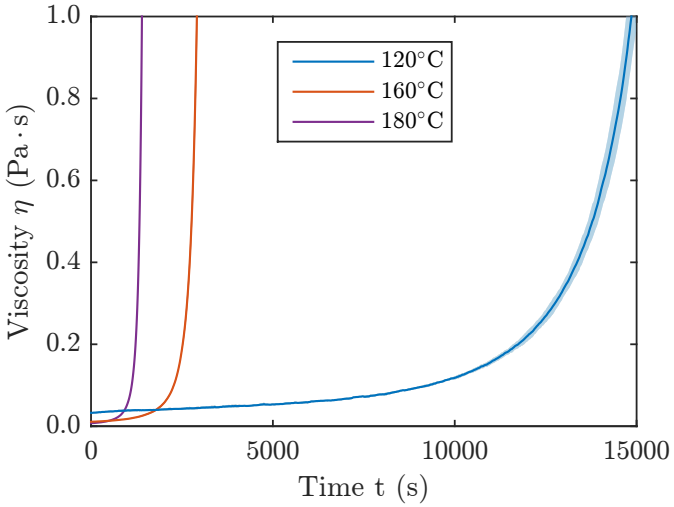

Figure 5.2: Mean viscosity (-) and standard deviation σ_η (ribbon) during isothermal resin curing at 120 °C, 160 °C and 180 °C until $\eta = 1\,\text{Pa·s}$. The data was obtained in a rotational 25 mm cone-plate rheometer configuration.

cause the final material properties are reached faster which reduces the cycle time. The scattering of the rheometer measurements was evaluated based on the standard deviations of the mean resin viscosity σ_η. The data shows, that σ_η increased exponentially with progressing curing. At $\eta = 1\,\text{Pa·s}$, the calculated standard deviations were $\sigma_{\eta,120} = 0.11\,\text{Pa·s}$, $\sigma_{\eta,160} = 0.10\,\text{Pa·s}$ and $\sigma_{\eta,180} = 0.08\,\text{Pa·s}$, corresponding to approx. 10 % of the mean viscosity. During the early curing stages the scattering is noticeably lower as can be seen from the initial viscosity values $\eta(t = 0, T)$. The results suggest that the rheometer provided viscosity values with a good precision.

5.2.2 Non-isothermal results

The non-isothermal viscosity results are depicted in Fig. 5.3. The plot shows the complex viscosity values in the range between 0 Pa·s and 1 Pa·s obtained during non-isothermal, oscillatory resin curing at a heating rate of 1 K/ min from 30 °C to 200 °C. Until approx. 120 °C the resin viscosity decreased. This was due to increasing temperature that lowered the resin density. Gradually, the network formation compensated this effect and the viscosity levelled out at approx. 0.03 Pa·s. At around 170 °C the polymerisation accelerated and the viscosity increased exponentially. At this point during infusion the resin flow comes to a halt. The presented viscosity curve represents a typical viscosity curve of cross-linking resins subjected to increasing temperatures. The processing window, between 120 °C to 180 °C, can be clearly identified as the region with the lowest viscosities.

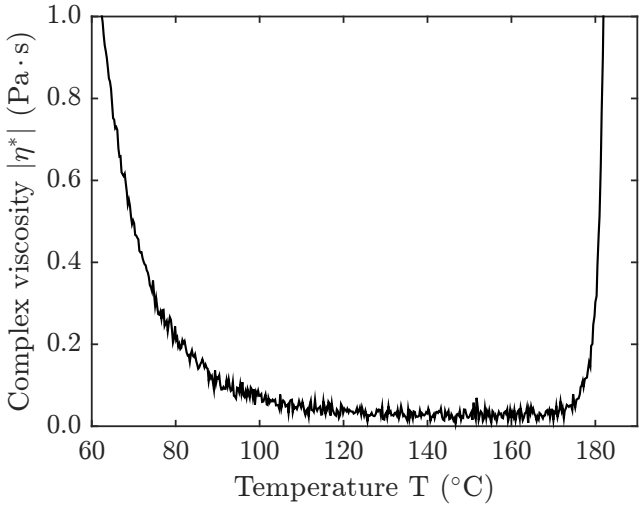

Figure 5.3: Complex viscosity during curing from 30 °C to 200 °C at 1 K/ min heating rate. Depicted is an excerpt of the date showing only the viscosity below (1 Pa·s). The data was obtained in a rotational 25 mm plate-plate rheometer configuration.

5.3 Isothermal correlation of viscosity and refractive index

The isothermal correlations of mean viscosity and refractive index measurements is used to visualise the relation between both parameters, and to fit the parameters of the refractive-index-based viscosity model in a later stage.

Fig. 5.4 shows the correlations obtained during isothermal curing at 120 °C, 160 °C and 180 °C between 0 Pa·s and 1 Pa·s. All isotherms show an exponential viscosity increase with rising refractive index. However, the correlations of the respective isotherms did not match. Instead, at lower temperatures they were shifted towards greater refractive indices. The same temperature-dependent shift was observed in the isothermal correlation of degree of cure and refractive index shown in Fig. 4.11. Further, it was observed that the correlations covered a narrower refractive index range at lower temperatures. This is not surprising since the refractive index gain is also lower at these temperatures, as can be seen in Fig. 4.7.

5.4 Refractive-index-based viscosity model development

The literature review showed that no refractive index based viscosity models have been published previously. However, a wide range of viscosity models have been developed in the past to describe the effect of curing and temperature on the

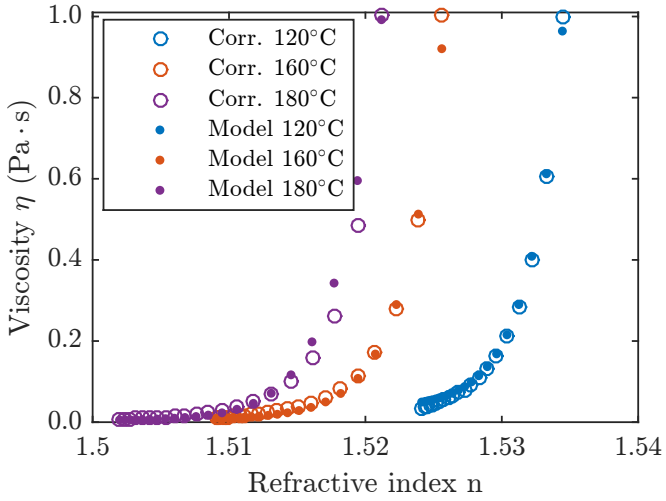

Figure 5.4: Correlation of viscosity and refractive index measurements (∘) with superimposed refractive-index-based viscosity model (·) during isothermal curing at 120 °C, 160 °C and 180 °C.

development of viscosity. A good literature overview is provided in Halley and Mackay [64].

In this work, the approach is to combine an existing viscosity model with the refractive-index-based degree of cure model introduced in chapter 4. For this purpose, a modified version of the empirical Castro-Macosko gelation model by Khoun et al. [85] was used:

$$\eta(\alpha, T) = \underbrace{\left(A_1 e^{\frac{E_1}{RT}}\right)}_{\eta_1(T)} + \underbrace{\left(A_2 e^{\frac{E_2}{RT}}\right)}_{\eta_2(T)} \cdot \left(\frac{\alpha_{gel}}{\alpha_{gel}-\alpha}\right)^{\left(d_1\alpha^2+d_2\alpha+d_3\right)} . \tag{5.1}$$

The model consists of the two viscosity terms $\eta_1(T)$ and $\eta_2(T)$ that account for non-isothermal and isothermal behaviour, respectively, and a term at the end that accounts for the degree of cure. In this case, the degree of cure α is represented by the previously introduced refractive-index-based degree of cure model (Eq. 4.4). The constants A and E were obtained from the non-isothermal and isothermal viscosity measurements, respectively, by expressing the viscosity as a linear relationship of the inverse of the temperature in Arrhenius plots. Fig. 5.5 shows three Arrhenius plots of the viscosity during non-isothermal curing between 30 °C to 200 °C at heating rates between 1 K/ min, 2 K/ min and 3 K/ min. The applied heating rates cover the specified range defined by aerospace specifications for RTM 6 which is a premixed epoxy resins similar to EPS 600. The viscosity obtained during the three heating rates match until approx. 160 °C which suggests that the heating rate has no influence on the viscosity development. The 1 K/ min curve exhibits an earlier

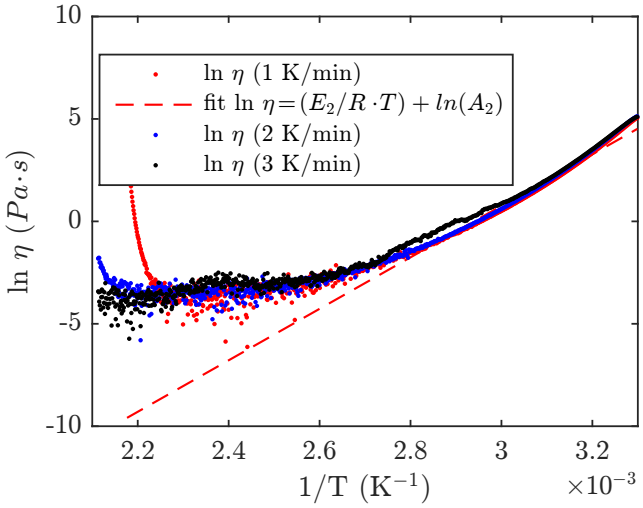

Figure 5.5: Arrhenius plot of the viscosity measured during non-isothermal curing at different heating rates. A linear fit (- -) of the values obtained at 1 K/ min is shown additionally.

viscosity increase because the resin was exposed to elevated temperatures for long time due to to lower heating rate. This gave the curing reaction more time to accelerate. No significant viscosity increase is recorded during the 2 K/ min and 3 K/ min heating ramp before the final temperatures are reached. Therefore, the A_1 and E_1 values were obtained from a linear fit of the 1 K/ min curve.

Fig. 5.6 shows the Arrhenius plot of the initial viscosity during isothermal curing at 80 °C, 115 °C, 120 °C, 125 °C and 180 °C. The selected temperatures span the

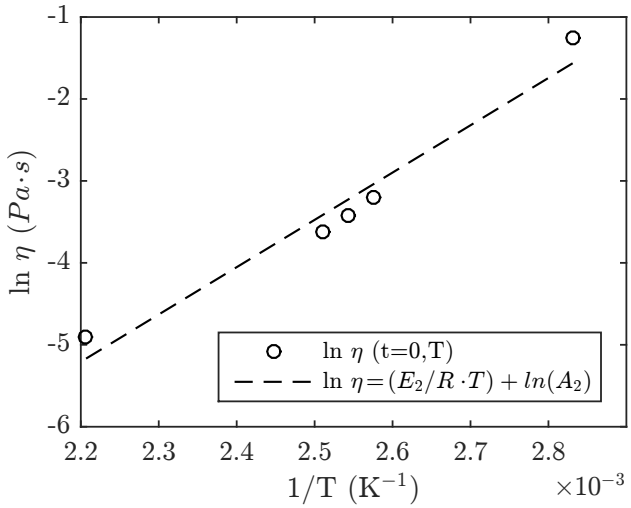

Figure 5.6: Arrhenius plot of the initial viscosities $\eta = f(t = 0, T)$ (∘) measured at different isothermal temperatures. Additionally the linear fit (- -) between the inital viscosities is shown.

whole temperature range occurring during EPS 600 processing. A linear fit between

the obtained values yield A_2 and E_2 which are listed in Tab. 5.2 together with the values for A_1 and E_1.

Further model parameters include the degree of cure at the gel point $\alpha_{gel} \approx 0.7$ which was estimated at the intersection of the storage and loss modulus according to Winter [166] based on different isothermal oscillatory measurements in the rheometer. The other parameters are the universal gas constant R and fitting parameters d_1, d_2 and d_3.

The refractive-index-based viscosity model is composed of the modified Castro-Macosko viscosity model (Eq. 5.1) and the refractive-index-based degree of cure model (Eq. 4.4) and its parameters from Tab. 4.2. The missing fitting parameters d_1, d_2 and d_3 of the refractive-index-based viscosity model were fitted to the isothermal correlation shown in Fig. 5.4 by a non-linear least-square MATLAB solver. A global solution was searched by using the MATLAB-integrated *MultiStart* algorithm. The acquired values for d_1, d_2 and d_3 are listed in Tab. 5.2.

Table 5.2: Parameters for refractive-index-based viscosity model.

Parameter	Value
A_1	9.02×10^{-17}
A_2	1.67×10^{-8}
E_1	1.04×10^{5}
E_2	4.80×10^{4}
R	8.31
α_{gel}	0.70
d_1	−32.44
d_2	19.40
d_3	3.01

5.5 Viscosity model validation

The refractive-index-based viscosity model was validated with isothermal and non-isothermal rheometer viscosity data. In the isothermal case, model output was generated based on isothermal refractive indices and their respective temperatures obtained in Sec. 4.3.1, and the model parameters listed in Tab. 4.2 and Tab. 5.2. The generated model output is shown in Fig. 5.4. It is plotted against the refractive index in comparison the isothermal correlation of viscosity and refractive index. It was observed that the modelled values followed the correlation well. The goodness of fit was evaluated by the residuals between the rheometer viscosity value of the correlation and the viscosity model output $r_\eta = \eta - \eta_{model}$ as shown in

Fig. 5.7. Until $\eta \approx 0.6\,\mathrm{Pa{\cdot}s}$ the residuals at 120 °C and 160 °C were particularly low

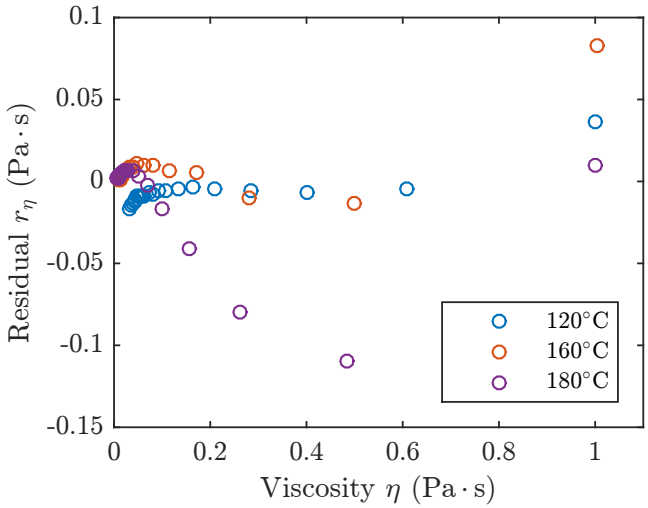

Figure 5.7: Residuals r_η between the actual viscosity and the model output during isothermal curing at various temperatures.

($r_\eta < 0.02\,\mathrm{Pa{\cdot}s}$). This behaviour around the resin infusion temperature (120 °C) is favourable since precise viscosity measurement is useful during the resin infusion phase. In the same period, the residuals at 180 °C increased faster. Overall, the maximum occurring residual was below 0.11 Pa·s in the observed viscosity range. This value was similar to the observed standard deviation during the rheometer viscosity measurements. This led to the conclusion that the model describes viscosity reliable in the range from 0 Pa·s to 1 Pa·s.

The model response under non-isothermal curing conditions was assessed by analysing the model output as a function of temperature. Model output was generated based on non-isothermal refractive indices and their respective temperatures obtained in Sec. 4.3.2. Fig. 5.8 shows the viscosity model output as a function of temperature in comparison to the complex viscosity measured in a rheometer. The plot shows a section of the data obtained during non-isothermal curing from 30 °C to 200 °C at a heating rate of 1 K/ min. At the beginning of the heating ramp a distinct offset between the model output and the rheometer data was observed. There, the model overestimated the actual viscosity. This offset was caused by inaccuracies of the refractive-index-based degree of cure model in this specific temperature range (cf. Sec. 4.5.2). However, the offset diminished constantly until approx. 120 °C. From then on the model output followed the viscosity data fairly well and captured even the steep viscosity increase beginning at 170 °C reliably. Although the model response is not perfect, the plot suggests that it describes the viscosity accurately in the relevant temperature range for resin infusion between 120 °C and 180 °C.

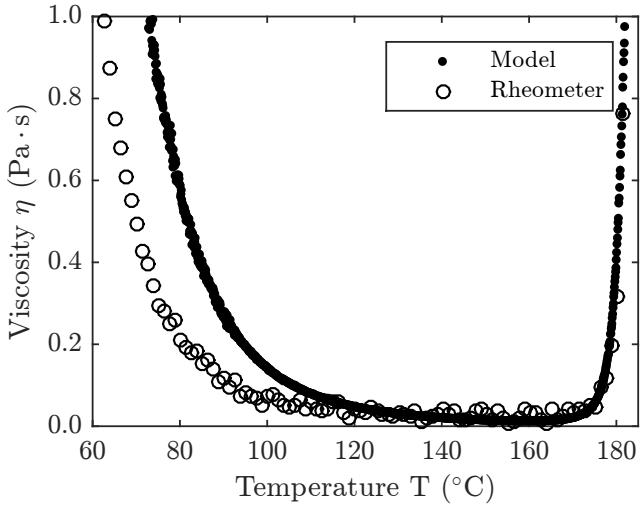

Figure 5.8: Complex viscosity (∘) measured during non-isothermal curing at a heating rate of 1 K/ min with superimposed refractive-index-based viscosity model output (·).

Moreover, the goodness of fit was assessed by the residuals between the non-isothermal viscosity values and the viscosity model output $r_\eta = \eta - \eta_{model}$. Fig. 5.9 shows the residuals with a focus on the infusion temperature range. In this tem-

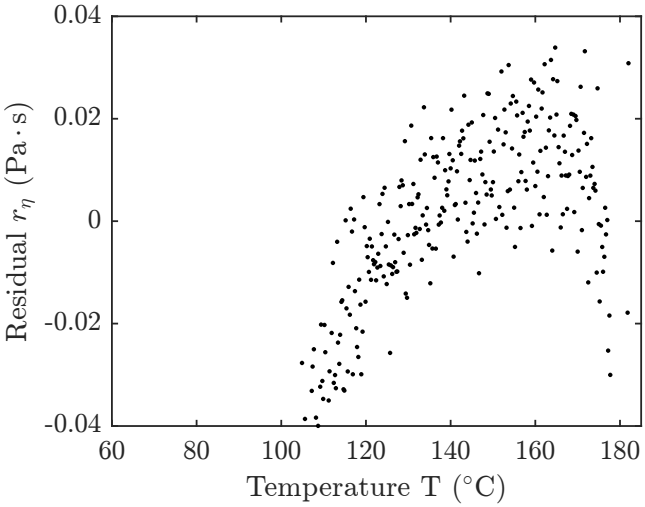

Figure 5.9: Residuals r_η between the actual viscosity and the model output during non-isothermal curing. Depicted is an extract of the data with a focus on the resin infusion temperature range between 120 °C and 180 °C.

perature range the residuals scattered randomly and the majority of the residuals were $r_\eta < 0.02\,\mathrm{Pa{\cdot}s}$. This confirms the assumption that the model describes viscosity during non-isothermal curing with particularly good accuracy in the infusion temperature range. The greater deviations below 120 °C are acceptable because viscosity changes in this temperature range are less relevant for the process.

As a side note: when comparing both curves in Fig. 5.8, it is obvious that the viscosity curve measured fibre optically was smoother than the curve obtained by the rheometer. This was due to the fact, that the fibre optic curve was modelled based only on refractive index and temperature. In contrast to the rotational rheometry, the fibre optic measurement was unaffected by potential mechanical influences. This represents an advantage of the fibre optic viscosity sensor.

5.6 Summary

A refractive-index-based viscosity model was developed by combining an established viscosity model with the refractive-index-based degree of cure model introduced in a previous chapter. The parameters of this new refractive-index-based viscosity model were fitted to the isothermal correlation of viscosity and refractive index in the viscosity range between 0 Pa·s to 1 Pa·s. The goodness of fit was evaluated based on the residuals between isothermal and non-isothermal viscosity measurements in comparison to the model output. It was found, that the model described the viscosity particularly well in the temperature range that is most important for resin infusion (120 °C to 180 °C). In that range the maximum residuals for the isothermal case were $r_\eta = 0.11$ Pa·s which is in the range of the rheometer variance. For the non-isothermal case the residuals were $r_\eta = 0.02$ Pa·s which is even lower. During non-isothermal curing, greater residuals were determined below 120 °C. This was attributed to the inaccuracy of the refractive-index-based degree of cure model in this range. Since this range is not of particular interest during resin processing the deviations were acceptable.

6 Application of fibre optic sensors during composite manufacturing

Fibre optic FBG measurement systems have previously been used for temperature or strain monitoring during composite manufacturing in the past. Using other fibre optic sensor types, such as Fresnel sensors, with the same measurement system creates a powerful and inexpensive monitoring solution for composite manufacturing. In the previous chapters it was shown, that such a system is suitable to measure the resin refractive index with Fresnel sensors and to deduce the resin degree of cure and viscosity. The obtained results suggested, that the investigated system meets all prerequisites for *dual-sensing* of FBG and Fresnel sensors during LCM processing.

With this sensor combination several *dual-sensing* scenarios are conceivable. Due to the bigger costs of the FBGs[1] it is favourable, however, to use a scenario in which they are reused. One potential scenario is to measure the mould temperature with FBG temperature sensors and to measure resin properties, such as degree of cure and viscosity, with component-integrated Fresnel sensors. A modification of this approach is to use moulds made of composite material and to integrate the said FBG temperature sensor into the laminate during mould manufacturing. Thus, both sensor types are integrated in a laminate, yet only the inexpensive component-integrated Fresnel sensors cannot be reused after manufacturing. The cost-intensive FBG temperature sensor remains in the mould wall and can be reused.

In order to showcase *dual-sensing* during composite manufacturing with a commercial fibre optic FBG measurement system it is necessary to provide an adequate interface for the mould-integrated fibre optic sensor. When integrating fibre optic sensors into laminates the biggest challenge is to establish a robust egress of the optical fibre that withstands the harsh environment during composite manufacturing and the service life. Lateral egress at the composite edge is obvious but impractical since composite structures have to be machined at the edges after demoulding. Vertical egress, however, seems to be promising but requires a more sophisticated interfaces that guides the fibre through all overlying layers. Due to the demanding

[1] Costs per FBG: > 30€

requirements, there are currently no commercial fibre optic mould interfaces for mould-integrated fibre optic sensors on the market, to the best knowledge of the author. Thus, the second aim of this chapter is to design an interface for integrated fibre optic sensor with the specific application in composite moulds of wind turbine blades.

The structure of this chapter is the following: an introduction to temperature measurements with FBG sensors is given in Sec. 6.1 and a new sensor design based on a Carbon Fibre Reinforced Plastic (CFRP)-reinforced tube is introduced. In order to access mould-integrated fibre optic sensors the design of a new interface for composite moulds is introduced in Sec. 6.2. In Sec. 6.3 the newly developed FBG temperature sensor and interface are integrated in the laminate of a composite mould. The focus of this section is the mould design and the location of the integrated temperature sensors. In Sec. 6.4, the sensor-equipped composite mould is used to showcase fibre optic *dual-sensing* during composite manufacturing by simultaneously recording the mould temperature, resin degree of cure and resin viscosity with the same measurement system. In Sec. 6.5 the chapter is closed by summarising the achieved results.

6.1 Temperature measurement with FBG temperature sensors

The reflected centre wavelength of a Bragg grating λ_B is depended on the effective fibre refractive index n_{eff} and the grating period Λ according to Eq. 3.4. The versatility of FBG sensors arises from the temperature and strain dependence of both, n_{eff} and Λ. The total differential of Eq. 3.4 can be written as [135]:

$$\Delta\lambda_B = 2\left[\Lambda\frac{\partial n_{eff}}{\partial l} + n_{eff}\frac{\partial\Lambda}{\partial l}\right]\Delta l + 2\left[\Lambda\frac{\partial n_{eff}}{\partial T} + n_{eff}\frac{\partial\Lambda}{\partial T}\right]\Delta T\,, \tag{6.1}$$

with the grating length l. The first term accounts for strain effects that lead to a shift of the Bragg wavelength. The second term describes the effect of temperature on the Bragg wavelength shift due to changes of the grating spacing and the refractive index. It can be rewritten as [135]:

$$\Delta\lambda_B = \lambda_B(\alpha_\Lambda + \alpha_n)\Delta T\,, \tag{6.2}$$

with the thermal expansion coefficient $\alpha_\Lambda = (1/\Lambda)(\partial\Lambda/\partial T)$, and the thermo-optic coefficient $\alpha_n = (1/n)(\partial n/\partial T)$. For GeO_2-doped silica fibres $\alpha_\Lambda \approx 0.55 \times 10^{-6}\,\mathrm{K}^{-1}$

[135] and $\alpha_n \approx 8.7 \times 10^{-6}\,\mathrm{K}^{-1}$ [165]. Waxler and Cleek [165] noted, however, that other researchers have found differing values for the TOC in the range between $8.5 \times 10^{-6}\,\mathrm{K}^{-1}$ to $10.8 \times 10^{-6}\,\mathrm{K}^{-1}$. It is noteworthy that the thermo-optic effect is one order of magnitude greater than the thermal expansion coefficient. This highlights that thermal expansion of the optical fibre plays a minor role during temperature measurements with FBG sensors.

Under the assumption that an FBG is not subjected to strain, the temperature changes ΔT can be deduced based on the measured Bragg wavelength shift $\Delta\lambda_B$ with Eq. 6.2. This equation is commonly simplified by combining α_Λ and α_n to the temperature coefficient k_T [107]:

$$\Delta\lambda_B = \lambda_B\, k_T\, \Delta T\,. \tag{6.3}$$

An established method to measure temperature with an FBG is to house the FBG in a tube as shown in Fig. 6.1. An adhesive is used to position the optical

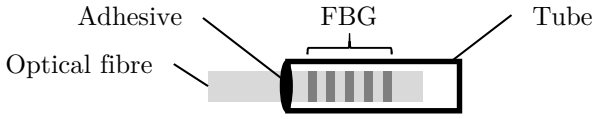

Figure 6.1: Schematic of an FBG temperature sensor.

fibre concentrically in the tube. Any force applied to the tube is deflected from the FBG thus it is only subjected to temperature. Several authors have proposed sensor designs based on different tube materials such as glass [65, 102, 107] or metal [121]. Both tube materials clearly have their advantage but also have disadvantages when applied in uneven structures as sometimes is the case in composite structures. Glass tubes for example are relatively flexible and adapt to the preform geometry. When overloaded, however, the brittle material behaviour can cause abrupt tube failure. Metal in contrast is more ductile and thus more tolerant to overloading. However, the material is much stiffer than its glass counterpart due to its greater Young's modulus which can impede sensor application in uneven geometries. A new sensor design was proposed by Oelhafen et al. [131] based on a CFRP-reinforced glass tube which combines properties of metal and glass and provides a flexible, yet fail-safe alternative. This sensor design was applied in the present work. The following paragraphs describe the design and manufacturing of the CFRP-reinforced glass tube and the sensor calibration.

FBG temperature sensor with composite body

The requirements for the laminate-integrated sensor are high radial stiffness to

withstand rough handling, while offering flexibility to allow free sensor application in curved structures, e. g. moulds for wind turbine blades. In order to meet these requirements, the isotropic material properties of FRP are exploited by producing FRP-reinforced glass tubes in a winding process. This process winds reinforcing fibres around a glass tube at a given winding angle. A large winding angle (relative to the tube axis) provides radial stiffness and axial flexibility due to the fibre orientation. In this work, a special pull-winding process developed by Fraunhofer - Institut für Produktionstechnologie, Germany, was used to produce CFRP-reinforced glass tubes. There, a reinforcement carbon fibre yarn (1K Toho Tenax HT40) was pulled through an epoxy resin bath (Hexion H235/L235) and subsequently wound on a polyimide-coated glass tube with 510 μm outer diameter. A 135 μm thin non-overlapping layer of carbon fibre was applied at a winding angle of 30°. Greater winding angles would yield even more favourable mechanical properties but could not be produced reliably. Two microscopy cross sections of the obtained sensor tube are shown in Fig. 6.2. The resulting CFRP-reinforced tube has a 400 μm inner diameter and a 780 μm outer diameter.

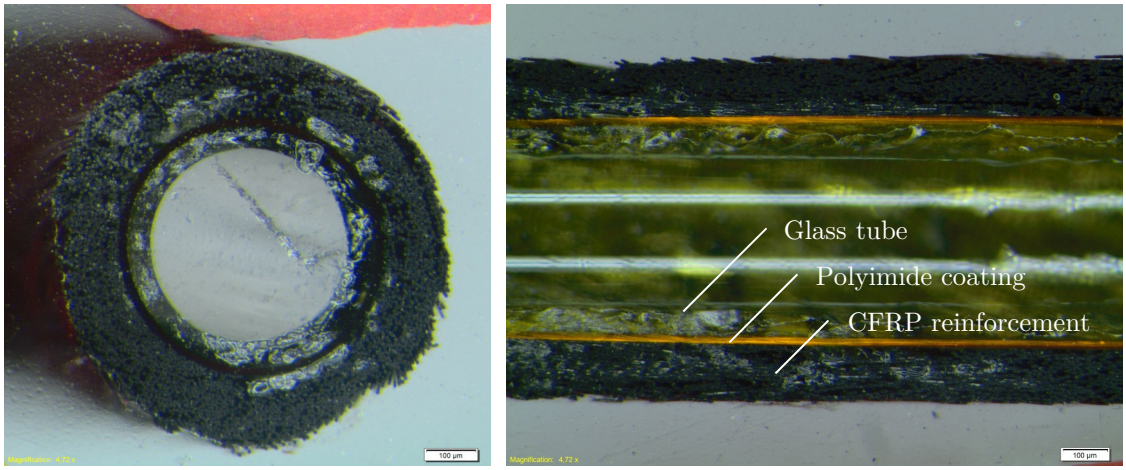

Figure 6.2: Microscopy cross sections of the CFRP-reinforced sensor tube in radial direction (left) and axial direction (right).

The mechanical behaviour of the glass, metal and CFRP-reinforced tubes were investigated previously in 3-point-bending and compression tests [131]. The results showed that the CFRP-reinforced tube exhibits intermediate stiffness combined with gradual degradation when overloaded which is favourable for integration in FRP laminates.

Based on the sensor design introduced in Fig. 6.1 an FBG temperature sensor was produced with the CFRP-reinforced tube, see Fig. 6.3. With this new design the upsides of glass and metal tubes were combined while reducing their previously mentioned downsides.

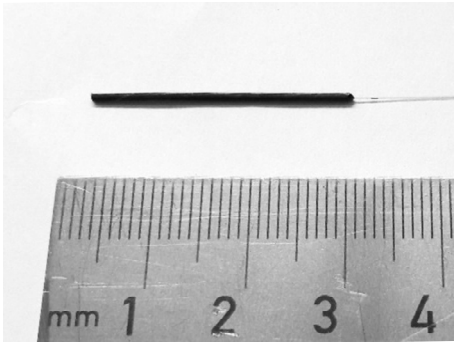

Figure 6.3: Fibre optic temperature sensor consisting of an FBG housed in a CFRP-reinforced tube. For scale the sensor is placed next to a ruler.

Calibration of FBG temperature sensor

The temperature sensitivity of FBG temperature sensors is defined by their temperature coefficient k_T (cf. Eq. 6.3). It is obtained under controlled thermal conditions by exposing the sensor to different temperatures while recording the corresponding wavelength shift. Subsequently, k_T is obtained from a linear fit of the recorded data. In this case, the sensitivity was determined after the sensor was integrated in the laminate (see Sec. 6.3). Since the internal laminate temperature is not known an additional type-K thermocouple was integrated in close proximity to the FBG for accurate reference temperature measurement. Then, the laminate was heated to three distinct temperature levels (26 °C, 125 °C and 185 °C) which cover the temperature range experienced during processing of EPS 600 resin. At each level the temperature was held for several minutes to assure constant thermal conditions. The measured wavelength and temperature values were averaged by the arithmetic mean to compensate potential signal fluctuations. Fig. 6.4 shows the obtained mean wavelength and temperature values. Based on a linear fit of these values the temperature coefficient was determined to $k_T = 11.3 \times 10^{-6}\,\mathrm{K}^{-1}$ with Eq. 6.3. A comparison between the temperature measured with the integrated FBG and the reference sensor during a typical composite manufacturing cycle is shown in Fig. 6.5. The zero point on the time scale is set to match the start of the infiltration in Sec. 6.4. The deviations between both signals is 7 °C at 120 °C and below 2 °C at 180 °C. The exhibited deviations are relatively large compared to previous reports were the temperature uncertainty of FBG temperature sensors was reported to be as low as ±0.1 K with laboratory equipment [83].

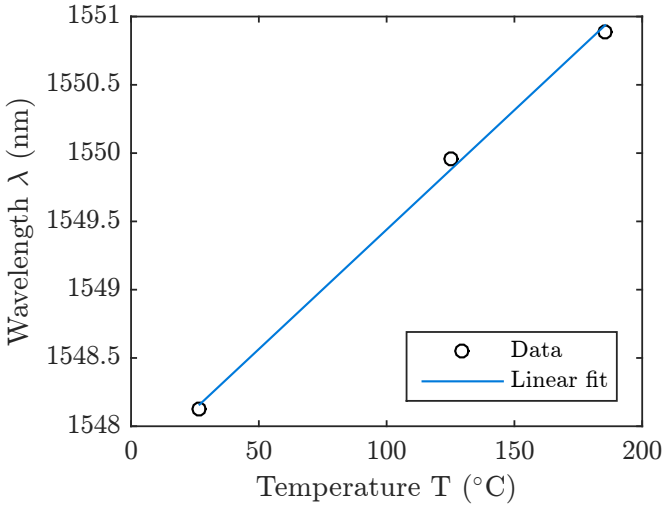

Figure 6.4: Correlation of wavelength measured with an FBG and temperature measured with a type-K thermocouple (o) at three distinct temperatures. In addition, the linear fit ($R^2 = 0.997$) between the data points is shown (–).

6.2 Mould interface for fibre optic sensor

Ever since fibre optic sensors are integrated in FRP laminates, a major obstacle is to connect the integrated sensor with the exterior measurement system. In order to address this problem, different sensor interfaces have been published previously [18, 27, 52, 60] and several patents have been granted [99, 151]. The proposed interfaces can be differentiated into interfaces that exit the laminate perpendicular to it and those where the interface exits the laminate at the edge. Most of the published interfaces are custom build to interrogate integrated sensors in *smart* structures as presented in the work by Friebele, E. J. et al. [52]. Only few interfaces actually provide a sturdy connector for optical fibres [60]. Since the requirements differ in each application and the market for laminate-integrated sensors is still small no commercial solutions are available. This is particularly the case for composite moulds.

Many composite moulds are equipped with integrated heating circuits. In case of modern wind turbine blade moulds up to 80 individual heating circuits are installed that need to be controlled individually based on temperature sensor information. Applying quasi-distributed fibre optic temperature sensors, e.g. FBGs, is a promising approach to minimise the amount of integrated individual sensors. In order to access mould-integrated fibre optic sensors, customised interfaces are necessary. The interface requirements were developed in collaboration with a German blade manufacturer and arise from the mould fabrication process and the harsh environment during blade manufacturing. The most important requirements are:

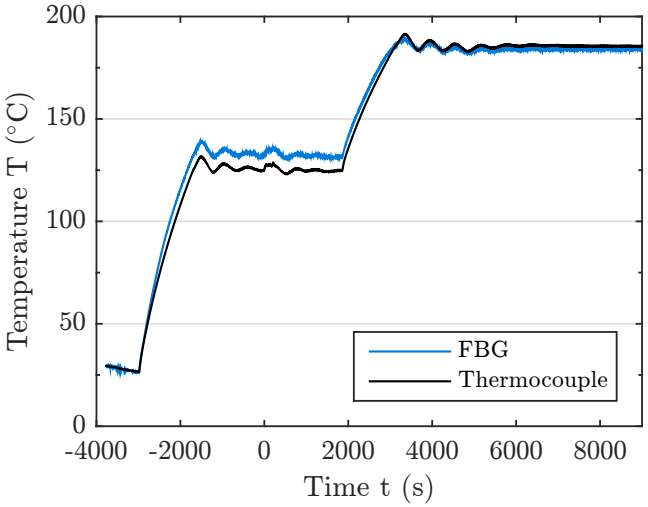

Figure 6.5: Mould temperature measured during composite manufacturing cycle with integrated FBG temperature sensor (–) and type-K thermocouple (–). The time $t = 0\,\mathrm{s}$ marks the start of the infiltration when the component was manufactured in Sec. 6.4.

- temperature resistance up to 150 °C,
- signal attenuation below 1 dB (insertion loss),
- resin tightness under vacuum atmosphere (approx. 5 mbar),
- applicable in VARI process,
- rigid design to withstand manufacturing environment, and
- integrated connector.

Based on the requirements, a fibre optic interface for composite moulds was designed over the course of a term project [120]. The presented interface allows to access an integrated optical fibre perpendicular to the laminate surface by connecting an external optical fibre to the interface. Fig. 6.6 shows the two halves of an interface during interface fabrication. The right half accommodates an off-the-shelf Lucent Connector (LC) coupler while the left half acts as a cover. The optical fibre containing the sensors is guided through the interface foot and is connected to the LC coupler. Both halves are mated and sealed with temperature resistant cyanoacrylate to provide a tight connection.

When a sensor and its respective interface is deployed during FRP manufacturing both components are positioned on the same laminate ply. The interface foot is designed to orient the interface perpendicular to the ply and to absorb loads directed at the interface. Additional plies can be placed over the interface by slitting the plies in order to allow the interface to slide through. The stretched interface

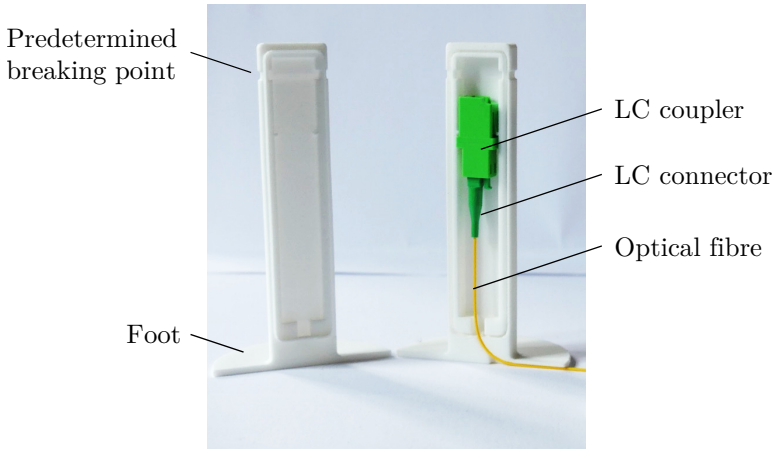

Figure 6.6: Mould interface for fibre optic sensors consisting of two mateable halves and a integrated Lucent Connector (LC) coupler. The figure shows the two halves of the interface prior to mating.

design serves two purposes: firstly, it allows to access sensors in thick laminates and secondly, it provides some distance between the fibre optical components and potential integrated heating elements in the mould. This reduces the heat load on these components which allows to use standard components with a temperature limit of 80 °C. Since the interface is tightly sealed, no precautions have to be made during resin infusion. After curing and demoulding the LC connector inside the interface can be accessed by breaking open the interface at the predetermined breaking point as shown in Fig. 6.7.

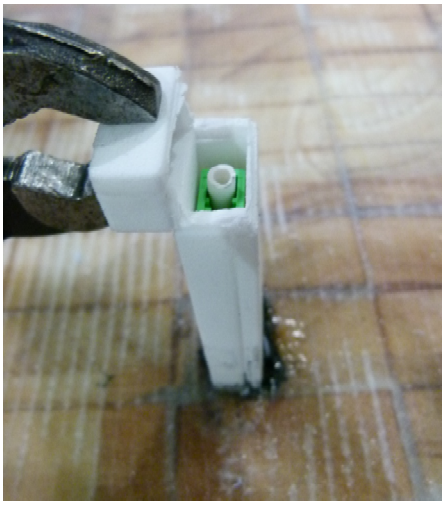

Figure 6.7: Fibre optic mould interface after laminate integration and mould manufacturing. The LC coupler is accessed by opening the predetermined breaking point of the interface.

In order to assure that the technical requirements are met several tests were performed. The seal tightness was tested in a vacuum chamber by exposing the

interface to a vacuum atmosphere with pressures below 5 mbar for over 10 min. Still in the vacuum chamber, the interface was submersed in water. If the seal was not tight, water would leak into the cavity of the interface. Water is an ideal medium for this test because its viscosity is a magnitude lower than that of heated resin[2]. Several repetitions revealed no ingress of water which proofed the tightness of the introduced interface. The signal attenuation due to redirecting the optical fibre in the interface was measured with a fibre optical power meter (Joinwit Ltd., China). It was shown, that the power loss was between 1.1 dB to 1.3 dB which is slightly above the required value. For the present application this value is still acceptable. If, however, the power loss for a given application is critical, the signal attenuation can be lowered by redesigning the interface and increasing the bend radius inside the interface. The temperature resistivity is assured by using a PA 12 polymer blend for the 3D printing process. PA 12 has a melting temperature beyond 180 °C. If necessary, the temperature resistivity of the interface can be further increased by switching to high-performance polymers such as PEEK and by using high-temperature LC connectors and couplers. The manufacturing costs would likely triple, however.

6.3 Mould design and sensor integration

In order to showcase fibre optic *dual-sensing* during composite manufacturing of flat composite components, a 800 mm x 500 mm flat composite mould is designed and manufactured. *Dual-sensing* shall be accomplished by measuring resin properties with component-integrated Fresnel sensors during manufacturing while monitoring the mould temperature with a mould-integrated fibre optic FBG temperature sensor at the same time.

The layup of the composite mould is based on a design typically used for wind turbine blade moulds. It consists of an initial layer of glass fibre fleece, that represents the mould surface and acts as a sacrificial layer for repair work. The fleece layer is followed by several layers of glass and carbon fibre Non-Crimp Fabric (NCF) around a 25mm thick balsa wood core. A sectional view of the different layers is displayed in Fig. 6.10. The application of balsa wood in the centre creates a sandwich structure that provides additional stiffness and thermal insulation to the mould. This is advantageous for dimensional accuracy of the produced components and thermal management.

[2] $\eta_{water}(T = 20\,°\mathrm{C}) \approx 0.001\,\mathrm{Pa{\cdot}s}$
$\eta_{resin}(T = 180\,°\mathrm{C}) \approx 0.01\,\mathrm{Pa{\cdot}s}$

The mould was manufactured in two separate infiltration steps: in the first step, the glass fibre fleece and the carbon fibre biaxial NCF were stacked on a flat mould. During the stacking process the fibre optic FBG temperature sensor together with its mould interface and a reference type-K thermocouple were placed in between the carbon layers in the centre of the preform. Then, a VARI infusion setup (cf. Fig. 2.1) was placed over the stack and the preform was infiltrated with the 2-component epoxy resin Araldite® LY 8615/ Aradur® 8615 from Huntsman. This resin system is designed for mould applications because glass transition temperatures (T_g) beyond 180 °C can be reached with the appropriate curing cycle. For good dimensional accuracy it is important that the curing temperature of the composite components is below the T_g of the composite mould. The maximum mechanical properties are reached at curing temperatures beyond 150 °C. However, these temperatures would destroy the optical LC connectors which have a temperature limit of 80 °C due to the applied adhesives that centres the optical fibre in the ferrule. Therefore, the mould was cured in an oven at 50 °C over night. The obtained component was rigid enough for further processing but did not have the final mechanical properties. After demoulding, the component had a smooth surface where it was in touch with the mould. This side will later act as the actual mould surface. The surface on the other side was covered by the VARI setup and is rough. That rough side was used to co-bond the remaining layers of the mould layup. In the second step, an electric heating wire (Huikshoven ELKM-A) was glued onto the rough side in a meandering pattern as shown in Fig. 6.8. Using a heating wire — instead of e.g.

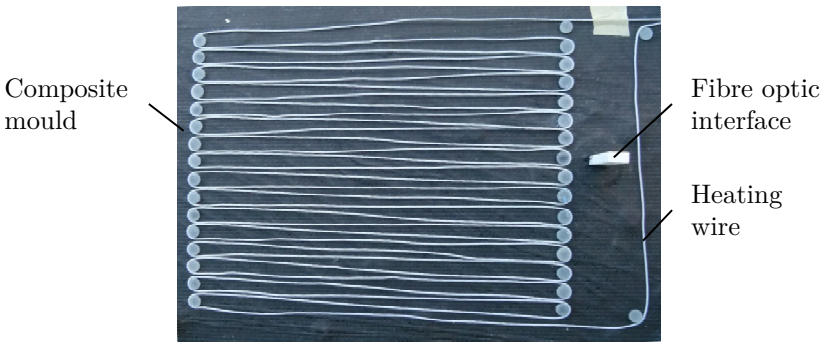

Figure 6.8: Integration of heating wire in a composite mould. The wire is glued to the surface of a previously cured composite panel.

heating cartridges — has the advantage that heat can be introduced evenly and very close to the mould surface. This is advantageous for homogeneous curing and precise temperature control. The specific properties of the applied heating wire can be found in the data sheet provided in the appendix A.4. The heating wire was only applied at the centre of the mould in an area of 500 mm x 400 mm where it

introduced 590 W (2950 W m^{-2}). In order to protect it from overheating, the wire was placed away from the fibre optic mould interface . The remaining layers of glass fibre NCF and balsa wood were placed on top of the heating wire. This layup allows straight heat introduction into the manufactured component and minimises heat transfer in the opposite direction due to the low thermal conductivity of the balsa wood core. Since the fibre optic interface and the sensor was placed between plies, the top plies and the balsa wood core had to be provided with a small hole that would allow the interface to fit through. After the layup was finished, it was cover with a VARI infusion setup. Subsequently the component was infiltrated and cured at 50 °C over night. In order to reach its final mechanical properties, the integrated heating wires were used to temper the mould at elevated temperatures. Using the integrated heating wires instead of an oven protected the delicate optical connectors. The resulting flat composite mould is depicted in Fig. 6.9. The mould

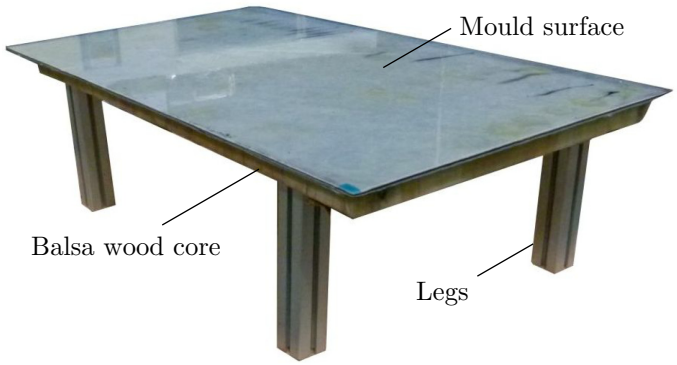

Figure 6.9: Isometric view of flat FRP mould resting on aluminium legs.

surface, which is used to produce flat composite components, is facing upwards in this image. The white colour of the surface stems from the glass fibre fleece in the first layer. Underneath the thick balsa wood core is visible through the covering glass fibre NCF layers which appear transparent.

6.4 Dual-sensing of process parameters with fibre optic sensors during composite manufacturing

In the previous section a flat composite mould was designed and manufactured. The mould was equipped with an integrated electric heating system, thermocouple temperature sensors for temperature control and a fibre optic FBG temperature sensor for temperature monitoring. The fibre optic temperature sensor is connected to an external measurement system by a mould-integrated interface.

In this section the mould is used to manufacture a flat composite component while performing fibre optic dual-sensing during a complete vacuum assisted resin infusion process. This is done by simultaneously interrogating the mould-integrated FBG temperature sensor and a component-integrated Fresnel sensor for cure and viscosity measurement. The experimental setup is shown in Fig. 6.10.

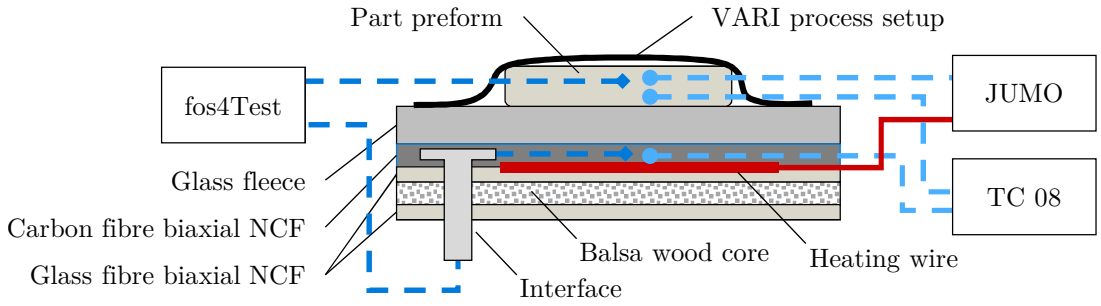

Figure 6.10: Sectional view of mould and preform during FRP manufacturing (not drawn to scale). The location of fibre optic sensors (--◆) and thermocouples (--●) is shown together with their respective measurement systems and the JUMO temperature controller.

The preform of the composite component comprised a quasi-isotropic layup of biaxial glass fibre NCF. The Fresnel sensor and two thermocouples were integrated between the central layers of the layup as shown in Fig. 6.11. One of the

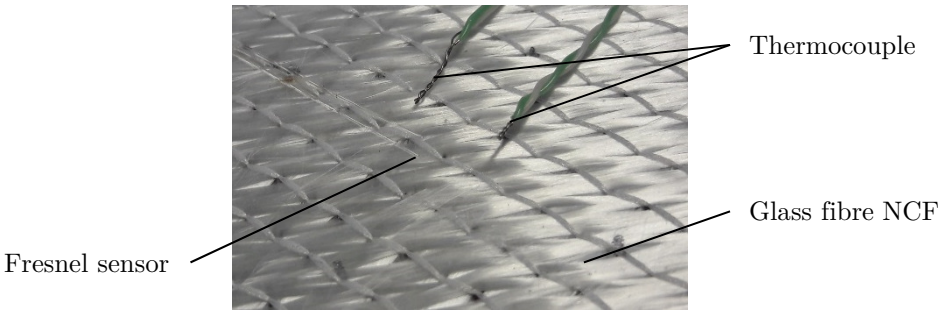

Figure 6.11: Integration of Fresnel sensor and thermocouples into glass fibre NCF layup.

thermocouples was connected to a controller (JUMO dtron 304, Germany) which controlled the heat introduction of the heating wires. The other thermocouple was connected to a temperature measurement system (Pico Technology TC-08, UK) to measure the component temperature synchronously with the refractive index obtained by the Fresnel sensor.

Experiment

After preforming was finished, the preform was covered with a VARI infusion setup. In the next step the vacuum bag was evacuated, and the mould was covered with an insulation layer. Then, the integrated heating wire was used to raised the mould

temperature until infusion temperature was reached (120 °C). The temperature rise was recorded with the mould-integrated FBG temperature sensor and is depicted in Fig. 6.5 between −3766 s and 0 s. Meanwhile, the resin was preheated at 80 °C in a separate oven. Shortly before resin infusion, the reference air refractive index was measured with the Fresnel sensor in order to calculate the resin refractive index accurately according to Eq. 2.29. Thereafter, resin was infused for approx. 30 min until it reached the resin outlet. This point marked the end of the infusion. After that the temperature was raised at a heating rate of 2.4 K/ min to 180 °C curing temperature. When this temperature was reached, the component was cured for approx. 1.5 h. Previous publications have shown, that during the glass transition the temperature dependence of the refractive index of resins changes drastically [124]. This effect has been previously recorded with Fresnel sensors in cured resins by performing a temperature cycle around the assumed T_g [3, 34, 56]. This resin characteristic is used in the present experimental setup to detect the T_g with integrated Fresnel sensors. Since the mould is not equipped with an integrated cooling system, its insulation was removed temporarily to cool down the mould to 150 °C. Then, the mould was reheated to 230 °C to pass the T_g which was estimated to be at 210 °C. Determining the T_g at the end of the curing cycle is a reliable measure to assess the final degree of cure. This is because the T_g rises even when the reaction is only diffusion controlled [8]. This is an advantage over standard characterisation methods, such as DSC, which cannot capture the last few degree of cure when no heat is released.

Results

The data of the mould-integrated FBG temperature sensor has been previously shown in Fig. 6.5. The results indicated that the mould temperature was successfully acquired with the fibre optic measurement system during the composite manufacturing process. The synchronously obtained data of the component-integrated Fresnel sensor and thermocouple are plotted over time in Fig. 6.12. The upper plot depicts the Fresnel sensor data and the lower plot the temperature obtained with a thermocouple. The Fresnel sensor data in the upper plot comprises the refractive index, the degree of cure and the viscosity of the EPS 600 resin. The refractive index was calculated from the equations presented in Sec. 2.4.5. The degree of cure and the viscosity were deduced from the refractive index and the thermocouple temperature with the refractive-index-based models introduced in chapter 4 and chapter 5. In addition, the plot shows viscosity data obtained with a rheometer as a comparison to the viscosity values obtained with the fibre optic sensor. The rheometer data was obtained under the same thermal conditions as the present

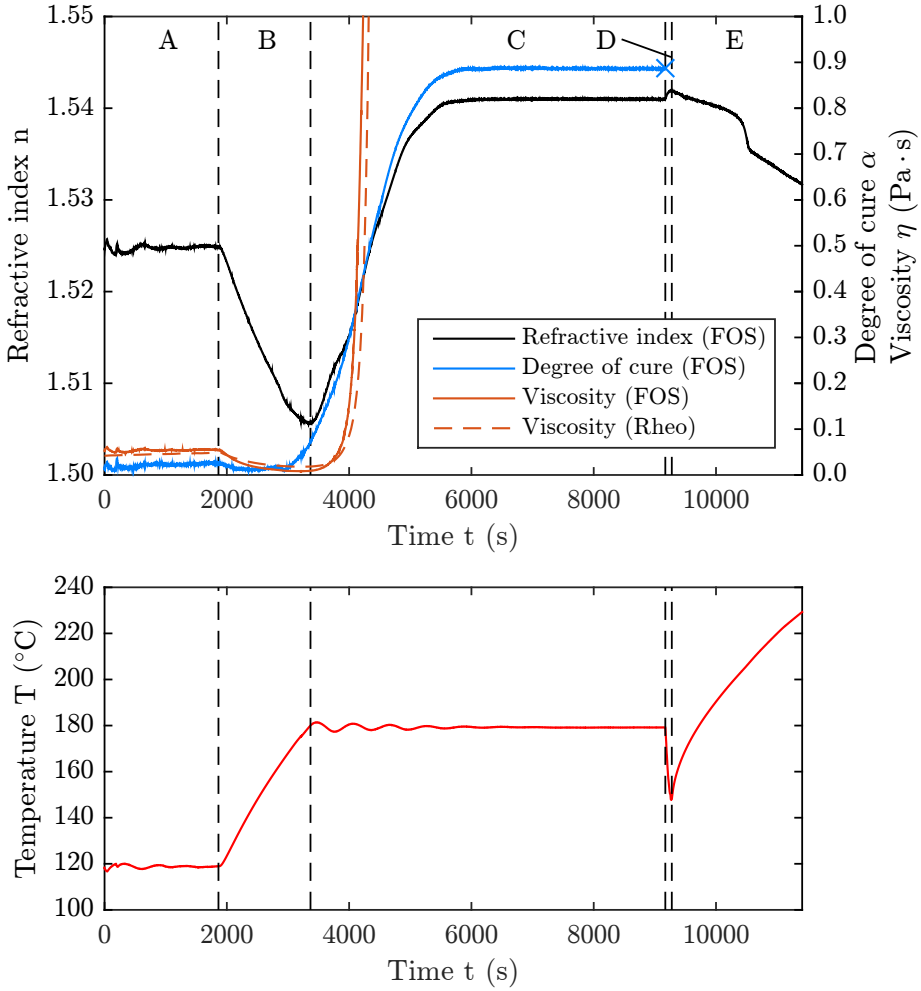

Figure 6.12: Viscosity, degree of cure and refractive index of EPS 600 resin measured with a Fresnel sensor and its temperature measured with a thermocouple during an aerospace curing cycle. The cycle comprises infusion at 120 °C, followed by a 2.4 K/ min heating ramp to 180 °C and subsequent curing. The cycle is followed up by a final temperature cycle between 150 °C and 230 °C to fibre optically detect the glass transition temperature. Additionally shown is the viscosity data obtained with a rheometer during a cycle with a 2 K/ min heating ramp.

experiment with the only difference that the heating rate was slightly lower with 2 K/ min (compared to 2.4 K/ min).

Both plots are separated in five segments of different thermal conditions (A to D). The segments are separated by vertical dashed lines. Segment A covers the isothermal infusion until $t_1 = 1860$ s. Segment B runs from t_1 until $t_2 = 3370$ s and defines the non-isothermal time span while the mould is heated from 120 °C to 180 °C. Segment C runs from t_2 until $t_3 = 9170$ s and covers the isothermal curing phase at 180 °C. Segment D and E cover the temperature cycle to detect the T_g. From t_3 until $t_4 = 9280$ s the mould is cooled down and subsequent reheating from t_4 until the end.

During isothermal infusion in A all sensor signals stayed practically constant. Any cure-induced parameter change was too small to distinguish from the signal noise.

However, as soon as the temperature was raised in B a steep refractive index decline by $\Delta n = 0.020$ was observed. The decline is attributed to the resin TOC and is very similar to the observations made in Fig. 4.8 during non-isothermal curing. In the same time span, the fibre optically measured degree of cure initially dropped to $\alpha \approx 0.02$ but subsequently recovered and rose to $\alpha = 0.07$. The initial drop is not plausible since the degree of cure should only rise. This behaviour is explained with the inaccuracy of the degree of cure model during the very early stages of cure as explained in Sec. 4.7. Since the drop is minor and at the beginning of cure it is considered negligible. The fibre optically measured viscosity declined initially in this segment due to thermal effects but levelled out by the end of the segment due to increasing cross-linking. This behaviour resembles the observations made during non-isothermal viscosity measurement in Fig. 5.3.

In C, the curing temperature of 180 °C is reached and all measurands underwent drastic changes. The refractive index increased steeply by $\Delta n = 0.035$ until the reaction slowed down and a plateau was reached at $n = 1.541$. At the beginning of C, the temperature control was not stable yet and oscillated by approx. ±2 °C which is obvious in the temperature plot between 3370 s to 6000 s. This led to slight temperature-induced refractive changes due to the TOC of the resin. The degree of cure curve was unaffected by the temperature variation and increased smoothly from $\alpha = 0.07$ to the final degree of cure. This is explained by the fact that the refractive-index-based degree of cure model compensates temperature variations. The viscosity increased exponentially at 180 °C and exceeded 1 Pa·s within a couple of minutes of the isothermal curing phase. When comparing the fibre optically measured viscosity with the rheometer values it can be seen that the obtained values are of the same magnitude and the effects (e.g. cure induced viscosity increase) are captured at the same time. Occurring differences are mainly attributed to the lower heating rate during the rheometer measurement which distort the comparison slightly. This provides another verification of the fibre optic viscosity sensor.

In segments D and E the resin was fully cured. Therefore, only the refractive index and its temperature-dependent behaviour was evaluated. During the fast cool down in D a slight refractive index rise was observed. When the temperature rose again in E the refractive index declined. At around $t = 10\,500$ s a sharp refractive index drop by $\Delta n = 0.03$ was observed in a 3 min time span. Since the temperature increased monotonously, and the resin had been fully cured before, this

refractive index drop is explained with the transition from the solid to the glassy state. In general, the glass transition of thermosetting polymers is accompanied by drastic material property changes, such as thermal expansion, density, heat capacity and modulus [109, 161]. The observed drop is attributed to a change in density which affects the resin refractive index according to the Lorentz-Lorenz equation (Eq. 2.28). Several researchers have monitored this effect in neat resin samples with Fresnel sensors during isothermal curing [3, 34, 56]. The T_g was assessed at the inflection point of the refractive index curve. This procedure is a standard used for T_g detection during thermal analysis. The obtained temperature was 206 °C and compares well to the $T_g = 203\,°C$ obtained in DSC measurements. This results shows the ability of Fresnel sensors to detect the T_g during composite processing. In future applications this value could be used to deduce the final degree of cure based on the empirical diBenedetto equation [167].

6.5 Summary

A new FBG temperature sensor with a composite body has been developed and integrated into the laminate of a composite mould to measure the mould temperature. This new sensor design provided more favourable mechanical properties compared to the state of the art tubes made of metal and glass. In order to access the integrated sensor a fibre optic interface was developed which is designed to be integrated in composite moulds. The sensor-equipped composite mould was designed to produce a flat composite component. The component itself was equipped with an integrated Fresnel sensor to measure several resin properties, such as refractive index, degree of cure and viscosity, during processing.

Data of the mould-integrated FBG temperature sensor and the component-integrated Fresnel sensor was acquired during a complete aerospace curing cycle of a composite component. This experiment demonstrated for the first time dual-sensing of two types of fibre optic sensors with a commercial FBG measurement system during composite manufacturing. This functionality allows to measure a wide range of process parameters with a single device. This may lead to lower monitoring costs and pave the way for new fibre optic sensor applications.

The component-integrated Fresnel sensors delivered refractive index, degree of cure and viscosity data from within the laminate during processing. Particularly viscosity had been measured previously with electrical sensors. The experiment demonstrated for the first time that this is also possible with fibre optic sensors. It is anticipated that fibre optic viscosity sensors allow new insights into composite manufacturing and process simulation validation.

Finally, the capability of Fresnel sensors was presented to detect the glass transition temperature at the end of cure. It was outlined that this opens new possibilities to determine the final degree of cure.

7 Conclusions and contributions

The aim of this work was to expand the capabilities of fibre optic process monitoring during composite manufacturing. To achieve this aim, a measurement method was established to interrogate fibre optic Fresnel sensors for refractive index measurements with a commercial fibre optic FBG measurement system. The measurement system was calibrated with Fresnel sensor to accurately measure the refractive index and to determine the measurement uncertainty.

The literature review showed that the resin degree of cure and viscosity are two important parameters during composite manufacturing. The available sensing options for laminate-integrated measurements were found to be limited or in the case of viscosity not available. Two new analytic models for Fresnel sensors were developed to measure the degree of cure and viscosity of epoxy resin, based on the resin refractive index and its temperature. Both models were validated under isothermal and non-isothermal conditions.

The new sensing capabilities were shown during composite manufacturing by measuring the degree of cure and viscosity with laminate-integrated Fresnel sensors. Additionally, an FBG temperature sensor integrated in the mould was interrogated simultaneously with the same measurement system to showcase the ability of *dual-sensing*. The following conclusions were drawn from the presented work, and the contributions to the knowledge and literature on fibre optic process monitoring were identified:

1. Commercial fibre optic FBG measurement systems possess the necessary hardware to interrogate Fresnel sensors for refractive index measurements. A measurement method was developed to determine the refractive index based on simplified Fresnel equations and the reflected intensity from a fibre optic Fresnel sensor. However, the accuracy and precision of the refractive index measurements with this method were unknown. Therefore, repeated Fresnel sensor refractive index measurements were performed in a refractive index range from 1.3 Pa·s to 1.6 Pa·s with five calibration fluids under controlled thermal conditions and in the wavelength range around 1550 nm. The same fluids were investigated under the same conditions with a precise reference measurement system — a prism coupling refractometer. The offset between

the fibre optic to the reference system was eliminated by calibration based on linear approximation.

Conclusion: Refractive index measurements with Fresnel sensors interrogated by a commercial fibre optic FBG measurement system are possible and provide new sensing options. It became clear that calibrating the measurement system is necessary for absolute refractive index measurements, due to the fact that the offset of the uncalibrated refractive indices can compromise fibre optic degree of cure measurements notably. The calibration covered a wide refractive index range which opens the possibility to apply this system not only during composite manufacturing but also in entirely different applications. The results suggested, however, that the calibration could be forgone for relative refractive index measurements.
Contribution: A refractive index measurement method and calibration method for a commercial fibre optic FBG measurement system was introduced.

2. It was unknown if the refractive index measurement uncertainty of the FBG measurement system is sufficient for process monitoring applications. Therefore, the measurement uncertainty was determined according to VDA 5 guideline [162]. The main contribution to the uncertainty was the variance of the refractive index measurements. These were obtained from repeated measurements in calibration fluids.

   Conclusion: The uncertainty of the refractive index measurements with the fibre optic FBG measurement system is comparable to results found in literature obtained with laboratory equipment [34]. The obtained measurement uncertainty is sufficiently low for fibre optic cure monitoring.
   Contribution: Determination of the refractive index measurement uncertainty of Fresnel sensors interrogated with a commercial FBG measurement system.

3. The literature review revealed a lack regarding sensor solutions for laminate-integrated measurements of the degree of cure and viscosity of resins. Fibre optic Fresnel sensor measurements of the resin refractive index possess the potential to close this gap. An analytical model was developed that describes the degree of cure as a function of the resin temperature and refractive index based on a correlation of DSC and Fresnel sensor measurements. The model was validated under isothermal and non-isothermal conditions. The developed refractive-index-based degree of cure model was then combined

with an established viscosity model [85] to obtain a refractive-index-based viscosity model. The parameters of this new viscosity model were fitted to the isothermal correlation of viscosity values obtained in a rheometer and the refractive index in a range between 0 Pa·s to 1 Pa·s. The validity of the viscosity model was shown for isothermal and non-isothermal curing conditions of an aerospace epoxy resin.

Conclusion: Degree of cure measurements with Fresnel sensors are possible during all relevant conditions of composite manufacturing with two minor limitations: Determination of the final degree of cure with fibre optic sensors remains challenging because the underlying correlation of the model has systematic inaccuracies. These stem from the limited ability of the DSC to capture the final increase of degree of cure during diffusion-controlled curing. Moreover, it remains challenging to model the first few degree of cure precisely during non-isothermal curing. This is due to the strong temperature dependence of the refractive index even in the uncured state. It was found, that the viscosity model fits particularly well in the temperature range that is most important for resin infusion: 120 °C to 180 °C. The limitations of the viscosity model at low temperatures during non-isothermal curing are mostly attributed to the underlying degree of cure model.
Contribution: A new analytic model was developed to determine the degree of cure of an aerospace epoxy resin during curing based on the refractive index measured with fibre optic Fresnel sensors. It extends the state of the art by being valid for all isothermal and non-isothermal conditions relevant for composite process monitoring. Additionally, an analytical viscosity model for Fresnel sensors was introduced for the first time. This model combined an established viscosity model [85] with the previously developed degree of cure model. The viscosity model was validated under isothermal and non-isothermal conditions for typical viscosities occurring during resin infusion until 1 Pa·s.

4. Fresnel sensor interrogation during composite manufacturing with a commercial FBG measurement system is a promising method for inexpensive process monitoring. In order to demonstrate the feasibility, a Fresnel sensor was integrated in the laminate of a composite part and the degree of cure and the viscosity was recorded. At the same time, an FBG temperature sensor was interrogated with the same measurement system to showcase the ability to perform *dual-sensing*. This sensor had been previously integrated in the lam-

inate of the composite mould, together with a newly developed fibre optic interface to access the integrated sensor.

Conclusion: Non-available interfaces for laminate-integrated fibre optic sensors remain the bottleneck for a more widespread application. Fibre optic Fresnel sensors are a valid alternative to measure the degree of cure during composite manufacturing. The ability to also measure the viscosity opens new possibilities for composite process development, process control and simulation validation. The ability to interrogate more then one sensor type with the same fibre optic measurement system opens new possibilities for a wider application of fibre optic sensors in the industry.

Contribution: A fibre optic interface for composite moulds was developed for the application in wind turbine blade moulds. Additionally, a Fresnel sensor was applied for the first time during composite manufacturing to measure the resin degree of cure and viscosity based on the resin refractive index and temperature. By also synchronously monitoring the mould temperature with a mould-integrated FBG temperature sensor, *dual-sensing* was demonstrated for the first time with a fibre optic measurement device during composite manufacturing.

8 Future work

The work described in this thesis offers several opportunities for future research. This includes: improvement of the refractive index measurement methodology, simplification of the calibration procedure, cure monitoring based only on fibre optic sensors and exploitation of thermo-optical properties of thermosetting resins to develop new sensors for process monitoring.

Continuous incident intensity measurement
Since the FBG measurement system is not designed to interrogate Fresnel sensors certain compromises had to be accepted to perform refractive index measurements. This includes reference measurements to compensate the unknown incident intensity emitted by the measurement system in order to acquire the refractive index. Performing air reference measurements requires an extra step that adds complexity to the refractive index measurement. Moreover, the measurement relies on the assumption of constant incident light intensity which is generally valid but represents an element of uncertainty. Thus, it is favourable to spare the extra measurement step.

Theoretically, it is possible to acquire the incident light intensity at one of the four channels of the system, since they are all connected to the same light source. Thus, the equation to obtain the refractive index simplifies to Eq. 2.24. The challenge is to determine the the splitting ratio of the various couplers precisely and to assure that the resolution of the external incident light intensity measurement equals that of the internal analog-to-digital converter. Alternatively, an internal solutions can be pursued in which the hardware is expanded by optical components to measure the incident light. This would require the collaboration of the hardware manufacturer, however.

Simplified calibration procedure
The calibration procedure presented in chapter 3 is elaborate and not practical for industrial application. A more simplified, standardisable procedure is necessary for an economic calibration. It is recommendable to replace the SMF-28e optical fibres applied in the experimental setup by a more robust alternative waveguide.

Also, fewer calibration nodes can be used if the target refractive index range can be narrowed down.

Fibre-optic-only cure monitoring

The analytical models for degree of cure and viscosity measurements rely on the resin temperature input. In this work the temperature input was provided by additional thermocouples. In future applications it is desirable to replace the metallic temperature sensor by a fibre optic alternative to fully exploit the potential of fibre optic sensors. This can be realised by two individual sensors or two sensors combined in one fibre. Giordano et al. [56] presented a combined solution that consisted of a Fresnel and FBG sensor in one optical fibre. Each sensor was interrogated with an individual wavelength spectrum (1310 nm and 1550 nm). By using just one wavelength the necessary hardware would be simplified and the commercial FBG measurement system could be employed. It remains unknown under which boundary conditions both sensor signals can be discriminated in the same wavelength range.

Exploitation of refractive index temperature-dependency

The TOC of the resin refractive index changes during the glass transition by a factor of 3 to 4 [124]. This characteristic has been used by Oelhafen et al. [132] to detect the glass transition with Fresnel sensors during quasi-isothermal curing of thermosetting resin. Similar behaviour can be observed after the material is fully cured. This is evident in segment E of Fig. 6.12 from the different slopes of the refractive index curve in the vicinity of the glass transition. The observed phenomena vary depending on if the material is currently curing (vitrification) or if the material is fully cured. The reason and underlying effects for this behaviour need further studying. It is assumed, however, that this optical characteristic of thermosetting resins could be used to develop new fibre optic sensors. Glass transition detection could be used e.g. during composite manufacturing to indicate that the mechanical properties have sufficiently progressed which could initiate the demoulding process. This would make the mould available again while the de-moulded part is fully cured in an auxiliary oven.

The necessary energy for the temperature modulation during isothermal curing could be introduced either locally, by an additional optical fibre, or by the mould temperature controller. Even slight temperature variations of the mould temperature can result in noticeable refractive index variations as is evident in segment C of Fig. 6.12. By purposely applying small, periodic temperature modulations, resin vitrification could be detected during isothermal curing.

A Appendix

A.1 Indices of five calibration fluids measured with FOS without outliers

In order to facilitate comparability, all sub-figures have a refractive index range of ±0.004. The butanol values in sub-figure (b) exhibit the smallest offset from the refractometer values and little scattering, except for the channel 3 sample that lies outside the depicted range.

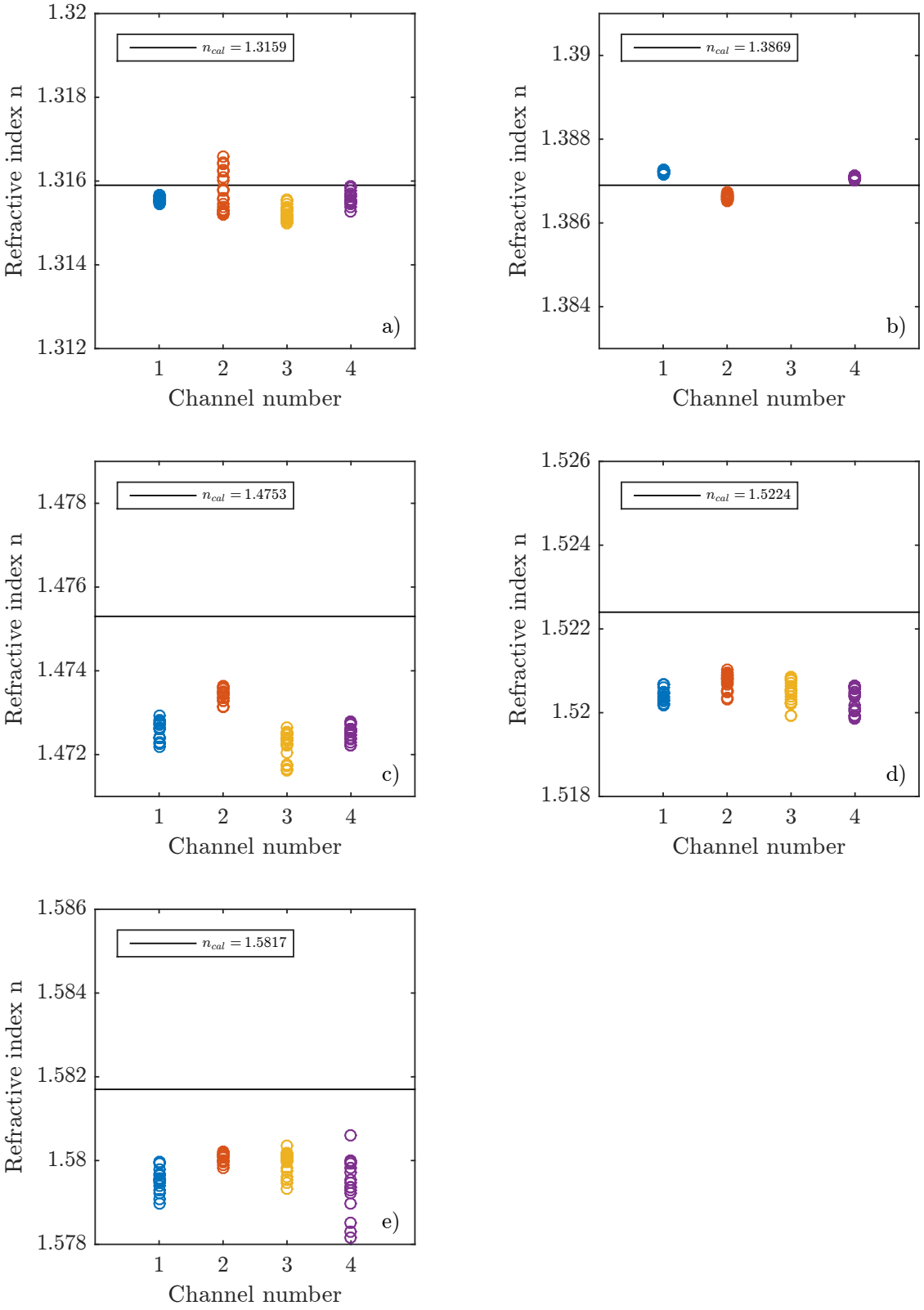

Figure A.1: Five plots showing 4 refractive index samples of water (a), butanol (b), toluene (c), nitrobenzene (d), and 1-methylnaphthalene (e) measured with Fresnel sensor. Each sample represents a channel. Outliers have been eliminated from the values (○) of each sample. For reference, the calibration refractive indices n_{cal} obtained with the prism coupling refractometer are shown (−).

A.2 Data sheet of EPS 600

HEXION
Responsible Chemistry

EPIKOTE™ System 600

Product Description

EPIKOTE™ Resin System 600 is at processing temperature (>50°C) a low viscous, polyfunctional, unmodified epoxy resin system based on methylenedianiline and aromatic amine.

Application Areas/Suggested Uses

EPIKOTE™ Resin System 600 is a 1-component, high-performance epoxy resin system with a long pot life. Two remarkable features are the good processing and mechanical properties of the cured resin. Moreover, it also provides outstanding chemical resistance. The water adsorption of the neat resin samples is in comparison with other standard materials remarkable low. The mechanical properties of EPIKOTE™ Resin System 600 are even better than mechanical properties of other systems with a comparable glass transition temperature.

Benefits

- High performance
- High fracture toughness
- Low water absorption / high chemical resistance
- Long pot life
- 1-K System

Sales Specifications

Property	Standard	Value	Unit	Test Method
Delivery Form		High viscous liquid		
Epoxy Value		19.5 ± 1.3	%	Pyridin / HCl Method
Gel Time		75 ± 15	minutes	DIN 16945
Viscosity at 50°C		4900 ± 1500	mPa.s	DIN 53019

Typical Properties

Property	Standard	Value	Unit	Test Method
Density at 20°C		1.085 ± 0.025	g/cm³	DIN 53217

Processing Data

Property	Unit	Value	Method / Standard
Viscosity			ISO 2884
50°C	mPa.s	4500 +/- 1500	
80°C	mPa.s	300 +/- 50	
120°C	mPa.s	50 +/- 20	
Refractive index at 25°C		1,584 +/- 0,002	DIN 51423-2
Gelation time			
120°C	hh:mm	04:20 +/- 00:20	DIN 16945
150°C	mm:ss	75:00 +/- 15:00	
180°C	mm:ss	23:00 +/- 05:00	

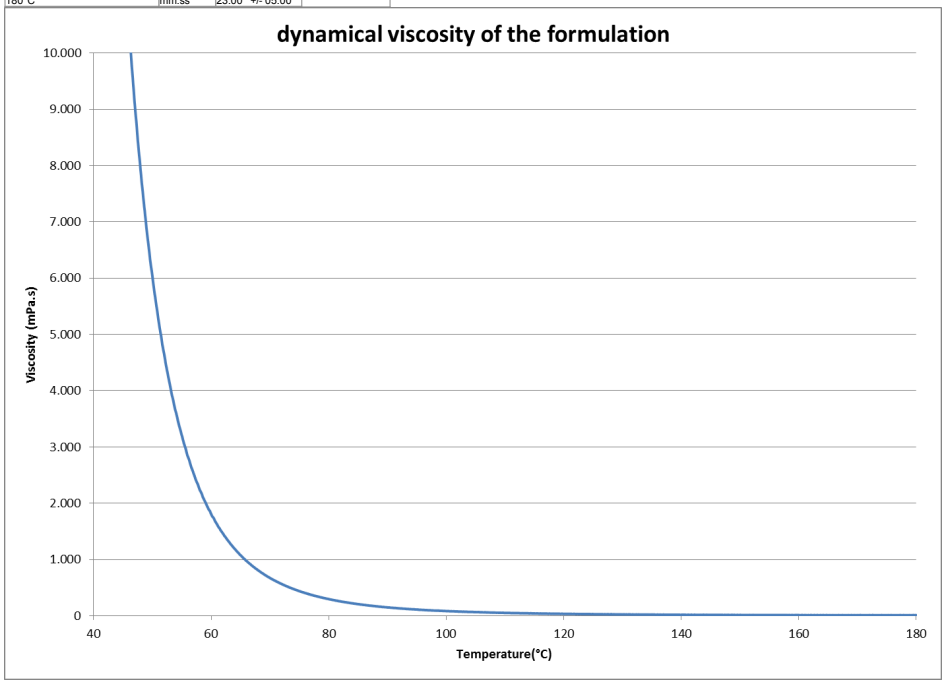

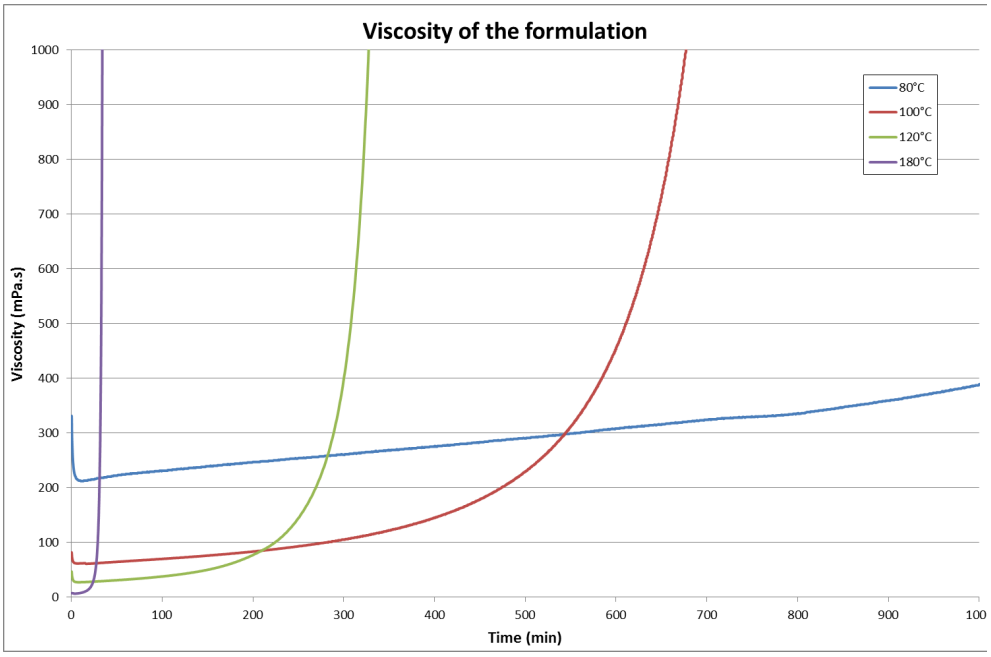

Exemplify curing cycle

2h 180°C

TYPICAL PROPERTIES OF THE CURED, NON-REINFORCED MATERIAL

Curing: 2h 180°C

Property	Unit	Value	Test Method
TG, **DSC** first run			DSC (10K/min)
Onset	°C	210 ± 3	DIN 53445
Midpoint	°C	212 ± 3	
DMA			DMA (2K/min)
Onset	°C	208 ± 5	DIN EN 61006
Peak max	°C	240 ± 3	
Tensile test @ RT			DIN EN ISO 527-1
Tensile strength	MPa	75 ± 10	

Tensile modulus	MPa	3075 ± 100	
Elongation at break	%	3 - 4	
Bending test @ RT			DIN EN ISO 178
Flexural strength	MPa	130 ± 10	
Flexural modulus	N/mm²	2950 ± 100	
Fracture performance (SENB) @ RT			ISO 13586
Fracture toughness K1C	MN/m3/2	0,70 ± 0,10	
Fracture energy G1C	J/m²	210 ± 20	
Density at 25°C	g/cm³	1,15 ± 0,01	DIN 51757

Chemical resistance (7d at RT)	**Weight increase %**	**Value** (1)	**Comments**
Methylethylcetone	---	-	Destroyed sample
Ethanol	23	+/-	
Toluene	0,1	+	
Dichloromethane	84	-	Flexible sample
Ethylacetate	58	-	Flexible sample
Skydrol	-0,5	+	
Hexane	-0,1	+	
Sodium hydroxide w=25%	0,2	+	
Sulphuric acid w=50%	24	+/-	
Sulphuric acid w=98%	---	-	Destroyed sample
Nitric acid w=65%	---	-	Destroyed sample

(1)

+ no changes;

+/- some changes of the mechanical properties are recognised;

- serious changes of the mechanical properties are recognised

Processing Details

Material preheating

For better mixing and impregnation results, preheating of the component is recommended

EPIKOTE™ Resin System 600	65 - 80°C

Safety, Storage & Handling

Please refer to the SDS for the most current Safety and Handling information.

EPIKOTE™ Resin System 600 should be stored at -18°C in its carefully sealed original containers. Under these conditions the shelf life is a minimum of 6 months from date of certification.

Heating larger quantities of EPIKOTE™ Resin System 600 and its formulations with other epoxy resins above 80°C has to be strictly avoided. Extreme care should be taken when working with accelerators.

When warming up, strictly avoid any local overheating, e.g. by use of improper heating equipment, like drum band heaters, immersion heaters, heating plates, hot air blowers, flames or electromagnetic radiation.

Contact Information

For further technical inquiries on the properties and performance of this matrix system in reinforced composites, please contact us at customer Service Center +1 888 443 9466 or at Hexion4information@hexion.com

A.3 Data sheet of RTM 6

Description
HexFlow® RTM 6 is a degassed, monocomponent resin specifically designed for resin transfer moulding (RTM) processes and to fulfil the requirements of the aerospace industry.

Nature
HexFlow® RTM 6 is a premixed epoxy system for service temperatures from -60°C up to 120°C (-75°F up to 248°F). At room temperature, it is a brown translucent paste but its viscosity decreases quickly by increasing the resin temperature.

Advantages
- Monocomponent system
- Already degassed. Ready for use
- High glass transition temperature
- Excellent hot/wet properties
- Easy to process (low injection pressure)
- Long injection window ≥150 min at recommended injection temp.
- Low moisture absorption
- Short, simple cure cycles

Transport classification
Product classification:
- HexFlow® RTM 6 Mono-Component: UN 3233 division 4.1 (type C)

Availability
HexFlow® RTM 6 resin is available with a wide range of Injectex®, HexForce® and multiaxial fabrics (carbon, glass, aramid, hybrid).

Storage

• Shelf Life	@ 23°C	15 days minimum
• Guaranteed Shelf Life	@ -18°C	6 months

Typical Resin Properties
Gel Time

Temperature (°C)	Time (min)
120	> 240
140	95
180	30
210	12 Water Pick-up (neat resin)

(14 days in water/70°C)

HexFlow® RTM 6

180°C mono-component epoxy system for
Resin Transfer Moulding and Infusion technologies

HEXCEL

Product Data Sheet

Viscosity Profile

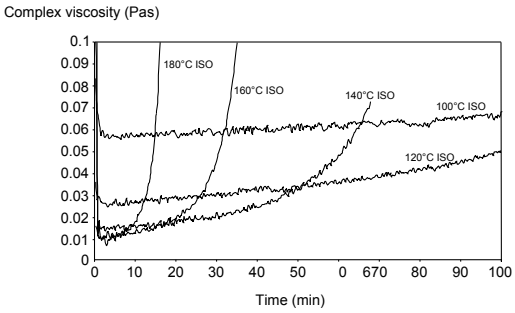

HexFlow® RTM 6 Isothermal viscosity

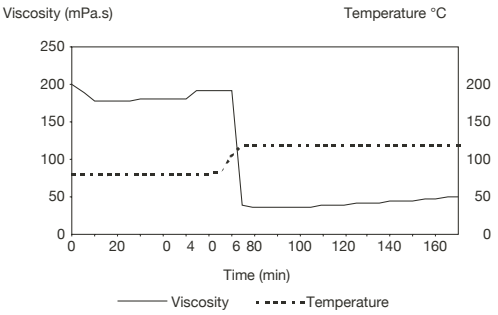

Viscosity for a standard injection cycle

Viscosity evolution versus storage time at 80°C

	Initial viscosity 120°C (mPa.s)	Viscosity after 2h at 120°C (mPa.s)
T0	33	59
T0 + 2h30 80°C	32	59
T0 + 5h00 80°C	33	63
T0 + 7h30 80°C	35	75
T0 + 10h00 80°C	38	89

T0: time to reach 80°C.

Water Pick-up (neat resin)

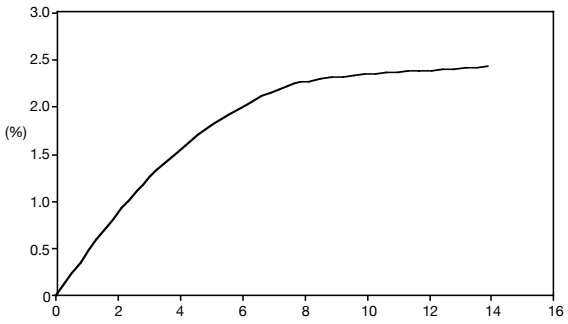

(14 days in water/70°C)

HexFlow® RTM 6

180°C mono-component epoxy system for
Resin Transfer Moulding and Infusion technologies

HEXCEL

Product Data Sheet

Neat Resin Properties

	Tensile	Flexure
Strength (MPa)	75	132
Modulus (MPa)	2890	3300
Strain (%)	3.4	
Standard specifications	ASTM D638	ASTM D790

Uncured resin density: 1.11 g/cm^3 at 25°C
Cured resin density: 1.14 g/cm^3 at 25°C
Fracture toughness
(G1C /ASTM D 5045): 89 J/m^2
Coefficient of Thermal Expansion: 52.7 e-6 /K

Properties on Composite Laminate

Composition of the laminate: Injectex® G0926: 5H Satin weave of 370g/m2, HR 6K
Epoxy powdered fabric
Fibre volume fraction: 57%
HexFlow® RTM 6 resin
Inject the resin under vacuum/low pressure (1 to 5 bar)
Cure cycle 120 min at 180°C - no postcure

Dry/RT Properties

	Tensile Warp	I.L.S. Warp	Compression Warp	In Plane Shear
Strength (MPa)	860	62	680	95
Modulus (GPa)	67	-	60	4.3
Standard specifications	EN 2597 B	EN 2563	EN 2850 A1	EN 6031

Values obtained for G0926 SD (AS4C J) E01 RTM6

Wet/70°C Properties

	Tensile Warp	I.L.S. Warp	Compression Warp	IPS
Strength (MPa)	895	44	370	78
Modulus (GPa)	65	-	63	3.5
Standard specifications	ISO 527-4 Type 3	EN 2563	EN 2850 A1	EN 6031

Values obtained for G0926 SD (AS4C J) E01 RTM6

HexFlow® RTM 6

180°C mono-component epoxy system for
Resin Transfer Moulding and Infusion technologies

HEXCEL

Product Data Sheet

Process Specification

Injection:

- Preheat resin at 80°C
- Preheat the mould at 120°C
- Inject the resin (80°C) under vacuum/low pressure (1 to 5 bars)

Please consult: HexFlow®RTM6/RTM6-2 Safety & Processing Recommendations for Injection & Infusion for more information

Standard Cure and Post-cure Cycle

Recommended cure cycle : 120 min at 180 °C - no postcure

Cure Cycle Possibilities

	Cycle N°1 (*)	Cycle N°2 (*)
Temperature 180 °C	 120 min	 90 min
DMA dry - Glass Transition - E' onset value - E" peak - Tan delta peak	 202 °C 210 °C 215 °C	 194 °C 206 °C 211 °C
Moisture weight gain (70°C/85%RH,equil)	0.80 %	0.84 %
DMA wet - Glass Transition - E' onset value - E" peak - Tan delta peak	 160 °C 170 °C 175 °C	 155 °C 175 °C 190 °C

(*) Laminate Data G0926 SD (AS4C J) E01 RTM6

For more information

Hexcel is a leading worldwide supplier of composite materials to aerospace and industrial markets.
Our comprehensive range includes:

- HexTow® carbon fibers
- HexForce® reinforcements
- HiMax™ multiaxial reinforcements
- HexPly® prepregs
- HexAM™ additive manufacturing
- HexMC® molding compounds
- HexFlow® RTM resins
- Redux® adhesives
- HexTool® tooling materials
- HexWeb® honeycombs
- Acousti-Cap® sound attenuating honeycomb
- Engineered core
- Engineered products
- Polyspeed™ laminates

For US quotes, orders and product information call toll-free 1-800-688-7734. For other worldwide sales office telephone numbers and a full address list, please go to:

http://www.hexcel.com/contact/salesoffice

ITA 065 M'18

A.4 Data sheet of Huikeshoven ELKM heating cable

Huikeshoven
Industrial Heating

eltherm®
innovations in heat tracing

PTFE-insulated
Heating Cable

Use on apparatus, vessels, pipes, valves, etc., in which low bending radii also allow compact tracing on small components across the entire surface.

Advantages:

- Highly flexible
- Small bending radius
- High operation temperature
- High chemical resistance
- Moisture proof

Applications:

- Vessels, pipes, valves
- Small components
- Can be used in many industrial areas
- Rotor blades
- Marble plates

Type **ELKM-A up to 260 °C**

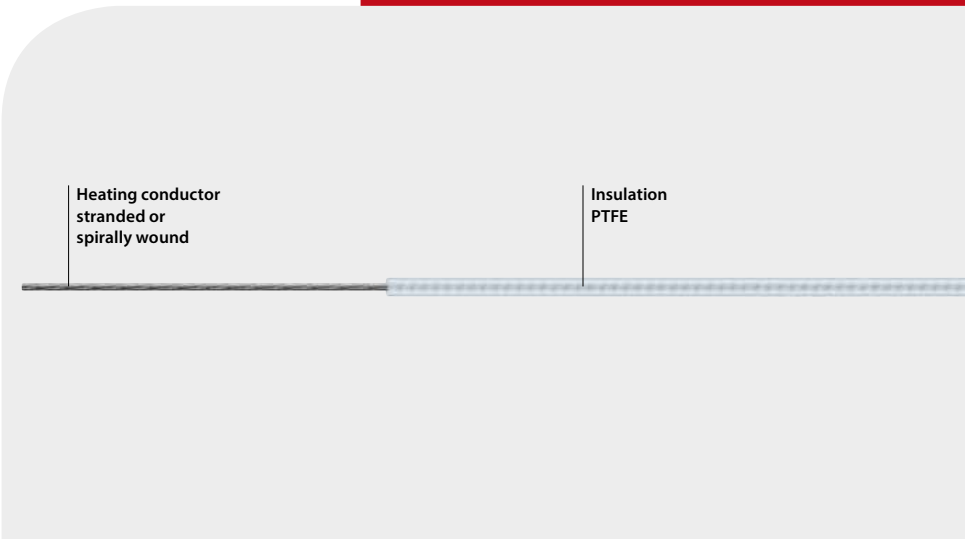

Huikeshoven
Industrial Heating

eltherm®
innovations in heat tracing

Technical Information

Type ELKM-A up to 260 °C

Data

Insulation	PTFE
Nominal voltage max.	750 V
Output, max.	30 W/m*
Operating temp., max.	260 °C
Bending radius, min.	2.5 x outer diameter
Installation temp., min.	-60 °C
Moisture proof	Yes
Heat conductor	Stranded, spirally wound for nominal resistance > 8,000 Ω/km

Standards

Manufactured according to	DIN VDE 0253

*Note: The output per meter of heating cable and the maximum possible operating temperatures depend on the respective application.
For individual cases, we recommend that you contact our engineers – we will be pleased to advise you.

Nominal resistance Ω/km	Outer diameter approx. (mm)	Weight approx. (g/m)	Temperature coefficient (x 10^{-3}/K)	Art. No.
1.95	5.8	112	4.30	0136002
2.90	4.6	73	4.30	0136006
4.40	4.2	54	4.30	0136004
7.20	3.1	33	4.30	0136007
10.00	3.0	31	4.30	0136008
11.70	2.7	30	4.30	0136010
15.00	2.6	19	4.30	0136012
25.00	2.5	17	3.00	0136016
31.50	2.9	23	1.60	0136020
50.00	2.6	17	1.60	0136030
65.00	2.4	14	1.60	0136032
80.00	2.7	20	0.90	0136038
100.00	2.5	17	0.90	0136042
157.00	2.5	17	0.45	0136049
180.00	2.2	12	0.90	0136052
200.00	2.4	14	0.45	0136054
260.00	2.2	12	0.45	0136058

Nominal resistance Ω/km	Outer diameter approx. (mm)	Weight approx. (g/m)	Temperature coefficient (x 10^{-3}/K)	Art. No.
280.00	2.1	10	0.38	0136059
328.00	2.5	16	0.18	0136061
360.00	2.1	10	0.45	0136064
430.00	2.3	13	0.18	0136066
480.00	2.2	12	0.18	0136068
600.00	2.1	10	0.18	0136076
800.00	2.0	9	0.18	0136080
1000.00	2.1	10	0.04	0136082
1470.00	2.1	9	0.04	0136092
1750.00	2.0	8	0.04	0136094
1900.00	2.2	12	0.04	0136096
2900.00	2.1	9	0.04	0136104
4000.00	2.0	8	0.04	0136114
4700.00	1.9	8	0.15	0136118
6000.00	1.9	7	0.20	0136124
7000.00	2.0	7	0.15	0136126
8000.00	2.0	7	0.15	0136128

Weight tolerances are possible for manufacturing reasons.
Nominal resistances up to 1,500,000 Ω/km upon request.
Resistance tolerance: +/- 5 %.

For applications with fixed external diameter, please contact our engineers first.

Cables shall neither intersect nor contact.
Provide protection by means of circuit breaker FI 30.
Please observe the standards IEC 62395-2, EN 60519-10.

Huikeshoven BV
Robijnstraat 6, NL-7554TB Hengelo (ov.)
Postbus 50, NL-7490 AB Delden
T : (++31)-(0)88-8898850

E :info@huikeshoven.nl
I :www.huikeshoven.nl

A.5 Data sheet of Araldite® LY 8615/ Aradur® 8615

HUNTSMAN
Enriching lives through innovation

Advanced Materials

Araldite® LY 8615 / Aradur® 8615

HOCHTEMPERATUR-EPOXID SYSTEM

ANWENDUNGSBEREICHE

Luftfahrt-Verbundwerkstoffe, Formwerkzeuge

EIGENSCHAFTEN

- Niedrige Viskosität, leicht injizierbar
- Lange Topfzeit
- Hochtemperaturbeständig (über 180°C)

BESCHREIBUNG

Araldite® LY 8615 / Aradur® 8615 Epoxidsystem ist ein niederviskoses Zweikomponenten-System für die Herstellung von hochwertigen Verbundwerkstoffen und Werkzeugen unter Verwendung des vakuumunterstützten Resin Transfer Molding (VARTM), Resin Transfer Molding (RTM), Seemans Composite Resin Injection Molding Process (SCRIMP℠) und anderer Infusionsverfahren. Die geringe Mischviskosität und die guten Benetzungseigenschaften von Araldite® LY 8615 / Aradur® 8615 ermöglichen eine gute Verarbeitung.

Die mit dem Araldite® LY 8615 / Aradur® 8615 produzierten Verbundwerkstoffe können nach der entsprechenden Nachhärtung eine Glasübergangstemperatur von über 180°C erreichen.

TYPISCHE GEBRAUCHSEIGENSCHAFTEN

Eigenschaften	Araldite® LY 8615 / Aradur® 8615	Testmethode
Farbe	Hellgelb, transparent	Visuell
Relative Dichte, Harz	1,22	ASTM D-792
Härter	0,94	
Viskosität bei 25°C (mPa.s)		ASTM D-2393
Harz	1.550	
Härter	120	
Gemisch	550	
Gelierzeit bei 25°C (h)	18	ASTM D-2471
Für 100 g		

HUNTSMAN
Enriching lives through innovation

MISCHUNGSVERHÄLTNIS

Araldite® LY 8615 / Aradur® 8615 100:50 Gewichtsanteile

Jede Komponente exakt (d. h. ±5%) in saubere Behälter abmessen. Harz und Härter gründlich miteinander mischen (mindestens zwei Minuten), dabei die Behälterwände, den Behälterboden und den Mischstab mehrmals abstreifen, um eine gleichmäßige Mischung zu gewährleisten.

AUSHÄRTUNG

- 24 h bei 35-40°C plus 3 h bei 180°C
oder
- 24 h bei 35-40°C plus 6 h bei 120°C plus 6 h bei 200°
falls nicht anders angegeben. Empfohlene Heizrate: 0,3°C/min

HINWEIS: Andere Härtungsprogramme können verwendet werden, um vergleichbare physikalische Eigenschaften zu erzielen. Bitte kontaktieren Sie Huntsman Advanced Materials im Internet unter www.huntsman.com/advanced_materials/, um Ihren Anwendungsfall zu besprechen.

HARZ-HÄRTERGEMISCH

TYPISCHE EIGENSCHAFTEN NACH DER HÄRTUNG:

Gehärtet für 24 h bei 35°C plus 2 h bei 120°C + 3 h bei 180°C. Getestet bei 25°C, falls nicht anders angegeben.

	Testwert	Testmethode
Relative Dichte	1,06	ASTM D-792
Härte, Shore D	87	ASTM D-2240
Ultimative Biegefestigkeit bei 25°C (MPa)	69	ASTM D-790
Biegemodul bei 25°C (GPa)	2,96	ASTM D-790
Tg durch DMA, E' Onset, trocken (°C)	217	ASTM D-4065
Druckfestigkeit bei 25°C (MPa)	251	ASTM D-695
Druckmodul bei 25°C (GPa)	2,2	ASTM D-695

VERBUNDWERKSTOFFE

TYPISCHE EIGENSCHAFTEN NACH DER HÄRTUNG:

1. Glassfaserverbundwerkstoff

Gehärtet für 24 h bei 35°C plus 2 h bei 120°C + 3 h bei 180°C. Getestet bei 25°C, falls nicht anders angegeben.

Verbundwerkstoff:

Gewebetyp:	Glasfasergewebe, satin 8, 300 g/m2
Gewebeausrichtung:	8 Lagen bei 0°
Laminatharzgehalt:	32,3%

HUNTSMAN
Enriching lives through innovation

	Testwert	Testmethode
Härte, Shore D	92	ASTM D-2240
Ultimative Biegefestigkeit bei 25°C (MPa)	695	ASTM D-790
Biegemodul bei 25°C (GPa)	42,9	ASTM D-790
Tg durch DMA, E' Onset, trocken (°C)	217	ASTM D-4065
Tg durch DMA, E' Onset, nass (°C)	189	ASTM D-4065
Wasseraufnahme* (%)	0,698	
Ultimative Druckfestigkeit bei 25°C (MPa)	430	ASTM D-695
Druckmodul bei 25°C (GPa)	77,9	ASTM D-695

*Heiß-/Nasskonditionierung für 48 h in kochendem Leitungswasser (98 bis 102°C). Probengewicht gemessen vor und nach dem Kochen der Probe zur Bestimmung der Gewichtszunahme in %.

2. Carbonfaserverbundwerkstoff

Härtung: 24 h bei 35°C plus 3 h bei 180°C

Verbundwerkstoff:

Gewebetyp:	Kohlenstofffasergewebe, satin 5, 375 g/m2
Gewebeausrichtung:	6 Lagen bei 0°
Laminatharzgehalt:	42% (Volumen)

	Testwert	Testmethode
Tg durch DMA, E' Onset, trocken, (°C)	192	
ILSS, trocken bei 25°C (MPa)	42	ISO 14130

VERFAHREN ZUR FORMENHERSTELLUNG

Schritt 1: Vorbereitung des Urmodelles

Das Modell mit einem geeigneten Reinigungsmittel reinigen.
Das Urmodell mit einem Dichtmittel und einem Trennmittel behandeln.

Schritt 2: Auftrag des Gelcoats (optional)

Wenn kein Gelcoat benötigt wird, direkt mit Schritt 3 fortfahren.
Huntsman empfiehlt die Verwendung des Gelcoats Rengel® SW 5200 + Ren® HY 5212 oder Ren® HY 5213.

HUNTSMAN
Enriching lives through innovation

	Rengel® SW5200/ Ren® HY5212	**Rengel® SW5200/ Ren® HY5213**
Mischungsverhältnis nach Gewichtsanteilen	100:20	100:16
Viskosität bei 25°C (mPa.s)	2000	1800
Topfzeit bei 25°C (h)	10 (500 ml)	4,5 (250 ml)
Haltezeit (h)	22 - 24	10 - 12

Den Gelcoat mit einem Pinsel in einer Schicht von mindestens 0,6 mm auftragen.

Schritt 3: Vorbereitung der Infusion
Gewebe, Abreißgewebe, Verteilmedium, Kanäle und Vakuumsack applizieren.
Die Infusionskanäle so anordnen, dass maximal 1 Meter Abstand zwischen den einzelnen Kanälen besteht.

Schritt 4: Mischen von Araldite® LY 8615 und Aradur® 8615 und Entgasen
Harz und Härter im Verhältnis 100:50 nach Gewichtsanteilen mischen.
Das gemischte Harz in einer Vakuumkammer mit 5-10 mbar Restdruck während 20 Minuten entgasen.

Schritt 5: Infusion bei Raumtemperatur

Durchzuführender Test vor Beginn der Infusion:
Die Vakuumpumpe stoppen und den Vakuumverlust messen. Dieser sollte weniger als 5 mbar in 10 Minuten betragen. Ziel des Tests ist es sicherzustellen, dass der Vakuumsack dicht ist.

Schritt 6: Härten unter Vakuum während 24 h bei 35-40°C.

Schritt 7: Aufbau der Trägerstruktur
Wir raten dazu, die Trägerstruktur vor der Entformung zu montieren. Die bei der Entformung auftretende Belastung kann eine Deformation des Werkzeugs verursachen.
Die Trägerstruktur kann aus Stahl oder Carbonversteifungen hergestellt werden.

Schritt 8: Entformung
Für die Entformung sollte ein thermoplastischer Kunststoffkeil verwendet werden, um eine Beschädigung des Werkzeugs zu verhindern.

Schritt 9: Nachhärtung
Huntsman empfiehlt eine Nachhärtung bis zu 180°C mit einer Heizrate von 0,3°C/Min.

B Publications

Journal Paper

[J1] J. Oelhafen, T. Mayr, F. Dorner, K. Moutzouris, J. Roths, and K. Drechsler. Fiber optic measurement system for fresnel reflection sensing: Calibration, uncertainty, and exemplary application in temperature-modulated isothermal polymer curing. *Journal of Lightwave Technology*, 36(4):939-945, 2018. ISSN 07338724. doi: 10.1109/JLT.2017.2757525.

Conference

[C1] J. Oelhafen, G. Obermeier, M. Heyer, D. Niefnecker, S. Zaremba, K. Drechsler. Methodology for viscosity measurement with fibre optic sensors for CFRP Manufacturing. *SICOMP Conference*, Gothenburg, 2015.

[C2] J. Oelhafen, R. Fernandez, D. Niefnecker, S. Zaremba, K. Drechsler, Flow front and cure monitoring with fibre optic sensors for thick CFRP laminates. In: *Proceedings of the International Conference on Composite Materials*, Copenhagen, July 19-24th 2015.

[C3] J. Oelhafen, T. Mayr, K. Moutzouris, J. Roths, and K. Drechsler. Calibration and uncertainty of a fibre optic measurement system for Fresnel reflectometer sensors. In Y. Chung, W. Jin, B. Lee, J. Canning, K. Nakamura, and L. Yuan, editors, *25th International Conference on Optical Fiber Sensors*, SPIE Proceedings. SPIE, 2017. doi: 10.1117/12.2260877.

[C4] J. Oelhafen, F. Muschaweckh, S. Zaremba, and K. Drechsler. Fibre optical temperature sensor for distributed sensing in composite moulds. *21st International Conference on Composite Materials*, 2017.

[C5] R. Engelhardt, J. Oelhafen, S. Ehard, A. Kollmannsberger, K. Drechsler. Manufacturing, testing and flight of a carbon fibre reinforced plastic rocket module with integrated fibre optical temperature sensors, *2nd Symposium on Space Educational Activities*, Budapest, Hungary, 2018.

[C6] R. Engelhardt, S. Ehard, J. Oelhafen, A. Kollmannsberger, R. Amann, P. Günzel, K. Drechsler. Development of a lightweight carbon composite rocket module with integrated fibre optical temperature sensors as part of experiment TESOS on REXUS 23, *24th ESA Symposium on European Rocket and Balloon Programmes and Related Research*, Essen, Germany, 2019.

[C7] R. Engelhardt, S. Ehard, T. Wolf, J. Oelhafen, A. Kollmannsberger, K. Drechsler. In situ joining of unidirectional tapes on long fiber reinforced thermoplastic structures by thermoplastic automated fiber placement for sounding rocket applications, *2nd CIRP Conference on Composite Material Parts Manufacturing*, Sheffield, United Kingdom, 2019.

Patent

[P1] J. Oelhafen, F. Muschaweckh. Temperatursensor und zugehöriges Herstellungsverfahren. German Patent Application. DE 10 2017 105285.2. 2017. (disclosed)

Bibliography

[1] *Ullmann's fibers*. WILEY-VCH, Weinheim, 2008. ISBN 9783527317721.

[2] Astm d4473-08(2016), standard test method for plastics: Dynamic mechanical properties: Cure behavior: Dynamic mechanical properties: Cure behavior, 2016.

[3] X. A. Aduriz, C. Lupi, N. Boyard, J.-L. Bailleul, D. Leduc, V. Sobotka, N. Lefèvre, X. Chapeleau, C. Boisrobert, and D. Delaunay. Quantitative control of rtm6 epoxy resin polymerisation by optical index determination. *Composites Science and Technology*, 67(15-16):3196–3201, 2007. ISSN 0266-3538. doi: 10.1016/j.compscitech.2007.04.008.

[4] S. G. Advani and E. M. Sozer. *Process modeling in composites manufacturing*, volume 59 of *Manufacturing engineering and materials processing*. Marcel Dekker, New York, 2003. ISBN 0-8247-0860-1.

[5] M. A. Afromowitz. Fiber optic polymer cure sensor. In *Optical Fiber Sensors*, page PD2. doi: 10.1364/OFS.1988.PD2.

[6] M. A. Afromowitz. Fiber optic polymer cure sensor. *Journal of Lightwave Technology*, 6(10):1591–1594, 1988. ISSN 07338724. doi: 10.1109/50.7920.

[7] M. A. Afromowitz and K.-Y. Lam. The optical properties of curing epoxies and applications to the fiber-optic epoxy cure sensor. *Sensors and Actuators A: Physical*, 23(1-3):1107–1110, 1990. ISSN 0924-4247. doi: 10.1016/0924-4247(90)87097-3.

[8] G. Ahlers-Hestermann and G. W. Ehrenstein. *Handbuch Kunststoff-Verbindungstechnik*. Hanser, München, 2004. ISBN 3-446-22340-1.

[9] Airbus. Process specification 80–t–31–2919: Manufacture of monolithic components by means of modified vacuum infusion process.

[10] V. Antonucci, M. Giordano, L. Nicolais, A. Calabrò, A. Cusano, A. Cutolo, and S. Inserra. Resin flow monitoring in resin film infusion process. *Journal*

of Materials Processing Technology, 143-144:687–692, 2003. ISSN 09240136. doi: 10.1016/S0924-0136(03)00338-8.

[11] V. Antonucci, A. Cusano, M. Giordano, J. Nasser, and L. Nicolais. Cure-induced residual strain build-up in a thermoset resin. *Internal Stresses in Polymer Composites*, 37(4):592–601, 2006. ISSN 1359-835X. doi: 10.1016/j.compositesa.2005.05.016.

[12] V. Antonucci, M. Giordano, A. Cusano, J. Nasser, and L. Nicolais. Real time monitoring of cure and gelification of a thermoset matrix. *Composites Science and Technology*, 66(16):3273–3280, 2006. ISSN 0266-3538. doi: 10.1016/j.compscitech.2005.07.009.

[13] E. Archer, J. Broderick, and A. T. McIlhagger. Internal strain measurement and cure monitoring of 3d angle interlock woven carbon fibre composites. *Composites Part B: Engineering*, 56(0):424–430, 2014. ISSN 1359-8368. doi: 10.1016/j.compositesb.2013.08.067.

[14] D. D. Archibald, C. E. Miller, L. T. Lin, and D. E. Honigs. Remote near-ir reflectance measurements with the use of a pair of optical fibers and a fourier transform spectrometer. *Applied Spectroscopy*, 42(8):1549–1558, 1988.

[15] J. Balvers and H. Bersee. Comparing flow-front propagation sensed by fbgs with pam-rtm simulation. In *The 10th International Conference on Flow Processes in Composite Materials*, 2010.

[16] J. M. Balvers. *In situ strain & cure monitoring in liquid composite moulding by fibre Bragg grating sensors*. Dissertation, Delft University of Technology, Delft, 2014.

[17] J. R. Bernstein and J. W. Wagner. Fiber optic sensors for use in monitoring flow front in vacuum resin transfer molding processes. *Review of Scientific Instruments*, 68(5):2156, 1997. ISSN 00346748. doi: 10.1063/1.1148065.

[18] R. P. Beukema, editor. *Embedding technologies of FBG sensors in composites: Technologies, applications and practical use*, volume 1, Dresden, 2012. ISBN 9783940283412.

[19] W. Bludau. *Lichtwellenleiter in Sensorik und optischer Nachrichtentechnik*. VDI-Buch. Springer Berlin Heidelberg, Berlin, Heidelberg, 1998. ISBN 978-3-642-72066-6.

[20] M. Born and E. Wolf. *Principles of optics: Electromagnetic theory of propagation, interference and diffraction of light*. Cambridge University Press, Cambridge and New York, 7th expanded ed. edition, 1999. ISBN 0521642221.

[21] A. R. Bunsell and J. Renard. *Fundamentals of fibre reinforced composite materials*. Series in materials science and engineering. Institute of Physics Pub., Bristol, 2005. ISBN 0750306890.

[22] A. Cadenato, J. M. Salla, X. Ramis, J. M. Morancho, L. M. Marroyo, and J. L. Martin. Determination of gel and vitrification times of thermoset curing process by means of tma, dmta and dsc techniques. *Journal of thermal analysis*, 49(1):269–279, 1997. ISSN 1572-8943. doi: 10.1007/BF01987448.

[23] L. P. Canal, M. Benavente, M. Hausmann, and V. Michaud. Process-induced strains in rtm processing of polyurethane/carbon composites. *Composites Part A: Applied Science and Manufacturing*, 78:264–273, 2015. ISSN 1359-835X. doi: 10.1016/j.compositesa.2015.08.018.

[24] W. Caspary. *Fehlertolerante Auswertung von Messdaten: Daten- und Modellanalyse, robuste Schätzung*. Oldenbourg, München, 2013. ISBN 9783486735796.

[25] J. Y. Chen, S. V. Hoa, C. K. Jen, and H. Wang. Fiber-optic and ultrasonic measurements for in-situ cure monitoring of graphite/epoxy composites. *Journal of Composite Materials*, 33(20):1860–1881, 1999. ISSN 00219983 (ISSN). doi: 10.1177/002199839903302001.

[26] P. E. Ciddor. Refractive index of air: new equations for the visible and near infrared. *Applied optics*, 35(9):1566–1573, 1996. ISSN 0003-6935. doi: 10.1364/AO.35.001566.

[27] R. O. Claus, R. Crotts, K. A. Murphy, R. P. Dahlgren, T. A. Tran, and S. H. Poland. Performance of miniaturized optical fiber interconnects between sensor-embedded composite panels. *Proceedings Volume 2072, Fiber Optic Physical Sensors in Manufacturing and Transportation*, pages 226–233, 1994. doi: 10.1117/12.166857.

[28] Claus, R. O., Bennett, K. D., A. M. Vengsarkar, and K. A. Murphy. Embedded optical fiber sensors for materials evaluation. *Journal of Nondestructive Evaluation*, 8(2):135–145, 1989. ISSN 0195-9298. doi: 10.1007/BF00565637.

[29] W. P. Cox and E. H. Merz. Rheology of polymer melts—a correlation of dynamic and steady flow measurements. In *International Symposium on Plastics Testing and Standardization*, pages 178–178–11. ASTM International, 100 Barr Harbor Drive, PO Box C700, West Conshohocken, PA 19428-2959, 1959. ISBN 978-0-8031-6105-4. doi: 10.1520/STP44206S.

[30] P. A. Crosby, G. R. Powell, G. F. Fernando, C. M. France, R. C. Spooncer, and D. N. Waters. In situ cure monitoring of epoxy resins using optical fibre sensors. *Smart Materials and Structures*, 5(4):415–428, 1996. ISSN 0964-1726. doi: 10.1088/0964-1726/5/4/005.

[31] P. A. Crosby, G. R. Powell, G. F. Fernando, D. N. Waters, C. M. France, R. C. Spooncer, and R. O. Claus. Comperative study of optical fiber cure-monitoring methods. In *Smart Structures and Materials '97*, SPIE Proceedings, pages 141–153. SPIE, 1997. doi: 10.1117/12.275731.

[32] A. Cusano, G. Breglio, M. Giordano, A. Calabrò, A. Cutolo, and L. Nicolais. An optoelectronic sensor for cure monitoring in thermoset-based composites. *Sensors and Actuators A: Physical*, 84(3):270–275, 2000. ISSN 0924-4247. doi: 10.1016/S0924-4247(00)00361-7.

[33] A. Cusano, G. Breglio, M. Giordano, A. Calabrò, A. Cutolo, and L. Nicolais. Optoelectronic characterization of the curing process of thermoset-based composites. *Journal of Optics A: Pure and Applied Optics*, 3(2):126–130, 2001. ISSN 1464-4258. doi: 10.1088/1464-4258/3/2/305.

[34] A. Cusano, A. Cutolo, M. Giordano, and L. Nicolais. Optoelectronic refractive index measurements: application to smart processing. *IEEE Sensors Journal*, 3(6):781–787, 2003. ISSN 1530437X (ISSN). doi: 10.1109/JSEN.2003.820319.

[35] M. Danisman, G. Tuncol, A. Kaynar, and E. M. Sozer. Monitoring of resin flow in the resin transfer molding (rtm) process using point-voltage sensors. *Composites Science and Technology*, 67(3-4):367–379, 2007. ISSN 0266-3538. doi: 10.1016/j.compscitech.2006.09.011.

[36] H. Dannenberg and W. R. Harp. Determination of cure and analysis of cured epoxy resins. *Analytical chemistry*, 28(1):86–90, 1956. ISSN 0003-2700. doi: 10.1021/ac60109a028.

[37] H. Darcy. *Les fontaines publiques de la ville de Dijon.* Dalmont, 1856.

[38] C. J. deBakker, G. A. George, N. A. St John, and P. M. Fredericks. The kinetics of the cure of an advanced epoxy resin by fourier transform raman and near-ir spectroscopy. *Spectrochimica Acta Part A: Molecular Spectroscopy*, 49(5-6):739–752, 1993. ISSN 05848539. doi: 10.1016/0584-8539(93)80098-U.

[39] D. Dickes. *Viscosity measurements with fibre optic sensors*. Bachelor thesis, Technical University Munich, 2016.

[40] E. Dietrich and A. Schulze. *Measurement process qualification: Gage acceptance and measurement uncertainty according to current standards*. Hanser Publications, Munich and Cincinnati, 2011. ISBN 9781569905050.

[41] DIN EN ISO 11357-1:2010-03. Plastics - differential scanning calorimetry (dsc) - part 1: General principles.

[42] DIN ISO 53019-1:2008-09. Viscometry - measurement of viscosities and flow curves by means of rotational viscometers - part 1: Principles and measuring geometry.

[43] C. Doyle, A. Martin, T. Liu, M. Wu, S. Hayes, P. A. Crosby, G. R. Powell, D. Brooks, and G. F. Fernando. In-situ process and condition monitoring of advanced fibre-reinforced composite materials using optical fibre sensors. *Smart Materials and Structures*, 7(2):145–158, 1998. ISSN 0964-1726. doi: 10.1088/0964-1726/7/2/002.

[44] J. P. Dunkers, K. M. Flynn, and R. S. Parnas. A mid-infrared attenuated total internal reflection cure sensor for control of resin transfer moulding of a preceramic polymer. *Composites Part A: Applied Science and Manufacturing*, 28(2):163–170, 1997. ISSN 1359-835X. doi: 10.1016/S1359-835X(97)89637-6.

[45] J. P. Dunkers, J. L. Lenhart, S. R. Kueh, J. H. van Zanten, S. G. Advani, and R. S. Parnas. Fiber optic flow and cure sensing for liquid composite molding. *Optics and Lasers in Engineering*, 35(2):91–104, 2001. ISSN 0143-8166. doi: 10.1016/S0143-8166(00)00110-X.

[46] B. Edlén. The refractive index of air. *Metrologia*, 2(2):71–80, 1966. ISSN 0026-1394. doi: 10.1088/0026-1394/2/2/002.

[47] B. Ellis. *Chemistry and technology of Epoxy Resins*. Blackie Academic & Professional, London, 1994. ISBN 0751400955.

[48] R. Engelbrecht. *Nichtlineare Faseroptik*. Springer Berlin Heidelberg, Berlin, Heidelberg, 2014. ISBN 978-3-642-40967-7. doi: 10.1007/978-3-642-40968-4.

[49] S. H. Eum, K. Kageyama, H. Murayama, K. Uzawa, I. Ohsawa, M. Kanai, H. Igawa, and D. D. Sampson. Process/health monitoring for wind turbine blade by using fbg sensors with multiplexing techniques. In *19th International Conference on Optical Fibre Sensors*, SPIE Proceedings. SPIE, 2008. doi: 10.1117/12.786240.

[50] Felix Kaufmann. *Development of a programme for monitoring the curing cycle of epoxy resin by means of fiber optic measurement.* Term project, Technical University Munich, 31.07.2014.

[51] G. N. M. Ferreira, A.-C. da Silva, and B. Tome. Acoustic wave biosensors: physical models and biological applications of quartz crystal microbalance. *Trends in biotechnology*, 27(12):689–697, 2009. ISSN 0167-7799. doi: 10.1016/j.tibtech.2009.09.003.

[52] Friebele, E. J., C. G. Askins, A. B. Bosse, A. D. Kersey, H. J. Patrick, W. R. Pogue, M. A. Putnam, Simon, W. R., F. A. Tasker, W. S. Vincent, and S. T. Vohra. Optical fiber sensors for spacecraft applications. *Smart Materials and Structures*, 8(6):813–838, 1999. ISSN 0964-1726. doi: 10.1088/0964-1726/8/6/310.

[53] J. Gao, Y. Li, M. Zhao, and G. Liu. Cure and glass transition temperature of the bisphenol s epoxy resin with 4,4-diaminodiphenylmethane. *Journal of Applied Polymer Science*, 78(4):794–799, 2000. ISSN 00218995.

[54] C. Garschke, C. Weimer, P. Parlevliet, and B. Fox. Out-of-autoclave cure cycle study of a resin film infusion process using in situ process monitoring. *Composites Part A: Applied Science and Manufacturing*, 43(6):935–944, 2012. ISSN 1359-835X. doi: 10.1016/j.compositesa.2012.01.003.

[55] G. A. George, P. Cole-Clarke, N. St. John, and G. Friend. Real-time monitoring of the cure reaction of a tgddm/dds epoxy resin using fiber optic ft-ir. *Journal of Applied Polymer Science*, 42(3):643–657, 1991. ISSN 00218995. doi: 10.1002/app.1991.070420310.

[56] M. Giordano, A. Laudati, M. Russo, J. Nasser, G. V. Persiano, and A. Cusano. Advanced cure monitoring by optoelectronic multifunction sensing system. *Thin Solid Films*, 450(1):191–194, 2004. ISSN 00406090. doi: 10.1016/j.tsf.2003.10.070.

[57] M. G. González, J. C. Cabanelas, and J. Baselga. Applications of ftir on epoxy resins - identification, monitoring the curing process, phase separation and

water uptake. In T. Theophanides, editor, *Infrared Spectroscopy - Materials Science, Engineering and Technology*. InTech, 2012. ISBN 978-953-51-0537-4. doi: 10.5772/36323.

[58] Q. Govignon, S. Bickerton, J. Morris, and P. A. Kelly. Full field monitoring of the resin flow and laminate properties during the resin infusion process. *Composites Part A: Applied Science and Manufacturing*, 39(9):1412–1426, 2008. ISSN 1359-835X. doi: 10.1016/j.compositesa.2008.05.005.

[59] Grattan, K. T. V. and T. Sun. Fiber optic sensor technology: an overview. *Sensors and Actuators A: Physical*, 82(1–3):40–61, 2000. ISSN 0924-4247. doi: 10.1016/S0924-4247(99)00368-4.

[60] A. K. Green and E. Shafir. Termination and connection methods for optical fibres embedded in aerospace composite components. *Smart Materials and Structures*, 8(2):269, 1999. ISSN 0964-1726.

[61] W. Griffioen. *Optical fiber mechanical reliability*. Eindhoven University of Technology, Eindhoven, 1995. ISBN 9038604947.

[62] T. M. A. Gronewold. Surface acoustic wave sensors in the bioanalytical field: recent trends and challenges. *Analytica chimica acta*, 603(2):119–128, 2007. ISSN 0003-2670. doi: 10.1016/j.aca.2007.09.056.

[63] N. Gupta and R. Sundaram. Fiber optic sensors for monitoring flow in vacuum enhanced resin infusion technology (verity) process. *Composites Part A: Applied Science and Manufacturing*, 40(8):1065–1070, 2009. ISSN 1359-835X. doi: 10.1016/j.compositesa.2009.04.022.

[64] P. J. Halley and M. E. Mackay. Chemorheology of thermosets: An overview. *Polymer Engineering & Science*, 36(5):593–609, 1996. ISSN 0032-3888. doi: 10.1002/pen.10447.

[65] F. M. Haran, J. K. Rew, and P. D. Foote. A strain-isolated fibre bragg grating sensor for temperature compensation of fibre bragg grating strain sensors. *Measurement Science and Technology*, 9(8):1163–1166, 1998. ISSN 0957-0233. doi: 10.1088/0957-0233/9/8/004.

[66] R. Hardis, J. L. P. Jessop, F. E. Peters, and M. R. Kessler. Cure kinetics characterization and monitoring of an epoxy resin using dsc, raman spectroscopy, and dea. *Composites Part A: Applied Science and Manufacturing*, 49 (0):100–108, 2013. ISSN 1359-835X. doi: 10.1016/j.compositesa.2013.01.021.

[67] M. Harsch. *Methoden und Ansätze zur spannungsarmen Vernetzung von Epoxidharzen*, volume Bd. 76 of *IVW-Schriftenreihe*. IVW, Kaiserslautern, als ms. gedr edition, 2008. ISBN 9783934930728.

[68] Helmut Schürmann. *Konstruieren Mit Faser-Kunststoff-Verbunden*. VDI-Buch. Springer-Verlag Berlin and Heidelberg GmbH & Co. KG, Berlin, 2nd edition, 2008. ISBN 978-3-540-72189-5.

[69] Hexcel. Hexflow rtm 6 product data sheet. URL `https://www.hexcel.com/user_area/content_media/raw/HexFlowRTM6DataSheetPDF.pdf`.

[70] Hexion Inc. Epikote™ system 600 product data sheet. URL `https://www.hexion.com/en-US/product/epikote-system-600`.

[71] K. O. Hill and G. Meltz. Fiber bragg grating technology fundamentals and overview. *Journal of Lightwave Technology*, 15(8):1263–1276, 1997. ISSN 07338724. doi: 10.1109/50.618320.

[72] T. Hochrein and I. Alig. *Prozessmesstechnik in der Kunststoffaufbereitung*. Vogel Fachbuch. Vogel Buchverlag, Würzburg, 1. aufl. edition, 2011. ISBN 9783834331175.

[73] D. Hunston. *Assessment of the State-of-the-art for Process Monitoring Sensors for Polymer Composites*. DIANE Publishing, 1992. ISBN 0941375986.

[74] ISO 22514-7:2012-09. Statistical methods in process management - capability and performance - part 7: Capability of measurement processes.

[75] JCGM. Jcgm 100:2008 (gum 1995 with minor corrections), evaluation of measurement data - guide to the expression of uncertainty in measurement (gum), 2008.

[76] D. J. Johnson, D. A. Compton, and P. L. Canale. Applications of simultaneous dsc/ftir analysis. *Thermochimica Acta*, 195:5–20, 1992. ISSN 00406031. doi: 10.1016/0040-6031(92)80042-U.

[77] Jörg Hoffmann. *Taschenbuch der Messtechnik*. Carl Hanser Verlag, [S.l.], 2015. ISBN 9783446442719.

[78] F. Juelich and J. Roths, editors. *Determination of the Effective Refractive Index of Various Single Mode Fibres for Fibre Bragg Grating Sensor Applications*, 2009. ISBN 978-3-9810993-6-2. doi: 10.5162/opto09/op2.

[79] W. Kaiser. *Kunststoffchemie für Ingenieure*. Carl Hanser Verlag GmbH & Co. KG, München, 2011. ISBN 978-3-446-43047-1. doi: 10.3139/9783446430495.

[80] H.-K. Kang, D.-H. Kang, C.-S. Hong, and C.-G. Kim. Simultaneous monitoring of strain and temperature during and after cure of unsymmetric composite laminate using fibre-optic sensors. *Smart Materials and Structures*, 12 (1):29–35, 2003. ISSN 0964-1726. doi: 10.1088/0964-1726/12/1/304.

[81] S. Kedenburg, M. Vieweg, T. Gissibl, and H. Giessen. Linear refractive index and absorption measurements of nonlinear optical liquids in the visible and near-infrared spectral region. *Optical Materials Express*, 2(11):1588, 2012. ISSN 2159-3930. doi: 10.1364/OME.2.001588.

[82] A. D. Kersey. A review of recent developments in fiber optic sensor technology. *Optical Fiber Technology*, 2(3):291–317, 1996. ISSN 1068-5200. doi: 10.1006/ofte.1996.0036.

[83] A. D. Kersey, M. A. Davis, H. J. Patrick, M. LeBlanc, K. P. Koo, C. G. Askins, M. A. Putnam, and Friebele, E. J. Fiber grating sensors. *Journal of Lightwave Technology*, 15(8):1442–1463, 1997. ISSN 07338724. doi: 10.1109/50.618377.

[84] C. J. Keulen, M. Yildiz, and A. Suleman. Multiplexed fbg and etched fiber sensors for process and health monitoring of 2-&3-d rtm components. *Journal of Reinforced Plastics and Composites*, 30(12):1055–1064, 2011. ISSN 07316844 (ISSN). doi: 10.1177/0731684411411960.

[85] L. Khoun, T. Centea, and P. Hubert. Characterization methodology of thermoset resins for the processing of composite materials — case study: Cycom 890rtm epoxy resin. *Journal of Composite Materials*, 44(11):1397–1415, 2009. ISSN 00219983 (ISSN). doi: 10.1177/0021998309353960.

[86] L. Khoun, R. de Oliveira, V. Michaud, and P. Hubert. Investigation of process-induced strains development by fibre bragg grating sensors in resin transfer moulded composites. *Composites Part A: Applied Science and Manufacturing*, 42(3):274–282, 2011. ISSN 1359-835X. doi: 10.1016/j.compositesa.2010.11.013.

[87] D. Kim, T. Centea, and S. R. Nutt. Out-time effects on cure kinetics and viscosity for an out-of-autoclave (ooa) prepreg: Modelling and monitoring. *Composites Science and Technology*, 100:63–69, 2014. ISSN 0266-3538. doi: 10.1016/j.compscitech.2014.05.027.

[88] J. G. Kim, K. H. Shin, H. S. Ryu, and J. W. Lee. Monitoring the change of viscosity during cure reaction of epoxy resins with resin position sensor. *Journal of Reinforced Plastics and Composites*, 21(2):139–152, 2002. ISSN 0731-6844. doi: 10.1177/0731684402021002353.

[89] M. S. Kim, C. S. Lee, and W. Hwang. Effect of the angle between optical fiber and adjacent layer on the mechanical behavior of carbon/epoxy laminates with embedded fiber-optic sensor. *Journal of Materials Science Letters*, 19(18):1673–1675, 2000. ISSN 02618028 (ISSN). doi: 10.1023/A:1006730630170.

[90] D. Kranbuehl, S. Delos, M. Hoff, P. Haverty, W. Freeman, R. Hoffman, and J. Godfrey. Use of the frequency dependence of the impedance to monitor viscosity during cure. *Polymer Engineering & Science*, 29(5):285–289, 1989. ISSN 00323888. doi: 10.1002/pen.760290504.

[91] R. K. Krishnaswamy and J. Janzen. Exploiting refractometry to estimate the density of polyethylene: The lorentz–lorenz approach re-visited. *Polymer Testing*, 24(6):762–765, 2005. ISSN 0142-9418. doi: 10.1016/j.polymertesting.2005.03.010.

[92] K.-Y. Lam and M. A. Afromowitz. Fiber-optic epoxy composite cure sensor i dependence of refractive index of an autocatalytic reaction epoxy system at 850 nm on temperature and extent of cure. *Applied Optics*, 34(25):5635, 1995. ISSN 0003-6935. doi: 10.1364/AO.34.005635.

[93] K.-Y. Lam and M. A. Afromowitz. Fiber-optic epoxy composite cure sensor ii performance characteristics. *Applied Optics*, 34(25):5639, 1995. ISSN 0003-6935. doi: 10.1364/AO.34.005639.

[94] J. Lange, N. Altmann, C. Kelly, and P. Halley. Understanding vitrification during cure of epoxy resins using dynamic scanning calorimetry and rheological techniques. *Polymer*, 41(15):5949–5955, 2000. ISSN 00323861. doi: 10.1016/S0032-3861(99)00758-2.

[95] S. Laurenzi and M. Marchetti. Advanced composite materials by resin transfer molding for aerospace applications. In N. Hu, editor, *Composites and Their Properties*. InTech, 2012. ISBN 978-953-51-0711-8. doi: 10.5772/48172.

[96] S. Le, F. Fang, and J. Zhao. Study on viscosity measurement using fiber bragg grating micro-vibration. *Measurement Science and Technology*, 24(1):015301, 2013. ISSN 0957-0233. doi: 10.1088/0957-0233/24/1/015301.

[97] B. Lee. Review of the present status of optical fiber sensors. *Optical Fiber Technology*, 9(2):57–79, 2003. ISSN 1068-5200. doi: 10.1016/S1068-5200(02)00527-8.

[98] H. Lee and K. Neville. *Handbook of epoxy resins*. McGraw-Hill handbooks. McGraw-Hill, 1967.

[99] N. A. Lee and G. D. Henson. Optical fiber strain relief apparatus. u.s. patent 5,355,429 a.

[100] J. S. Leng and A. Asundi. Real-time cure monitoring of smart composite materials using extrinsic fabry-perot interferometer and fiber bragg grating sensors. *Smart Materials and Structures*, 11(2):249–255, 2002. ISSN 0964-1726. doi: 10.1088/0964-1726/11/2/308.

[101] R. L. Levy and S. D. Schwab. Monitoring the composite curing process with a fluorescence-based fiber-optic sensor. *Polymer Composites*, 12(2):96–101, 1991. ISSN 0272-8397. doi: 10.1002/pc.750120205.

[102] N. Li, Y. Li, X. Hang, and J. Gao. Analysis and optimization of temperature distribution in carbon fiber reinforced composite materials during microwave curing process. *Journal of Materials Processing Technology*, 214(3):544–550, 2014. ISSN 09240136. doi: 10.1016/j.jmatprotec.2013.10.012.

[103] S. T. Lim and W. I. Lee. An analysis of the three-dimensional resin-transfer mold filling process. *Composites Science and Technology*, 60(7):961–975, 2000. ISSN 0266-3538. doi: 10.1016/S0266-3538(99)00160-8.

[104] Y. M. Liu, C. Ganesh, Steele, J. P. H., and J. E. Jones. Fiber optic sensor development for real-time in-situ epoxy cure monitoring. *Journal of Composite Materials*, 31(1):87–102, 1997. ISSN 0021-9983. doi: 10.1177/002199839703100106.

[105] R. Looser. *Statistische Messdatenauswertung: Praktische Einführung in die Auswertung von Messdaten mit Excel und spezifischer Statistik-Software für naturwissenschaftlich und technisch orientierte Anwender*. PC und Mathematik. Franzis, Poing, 2003. ISBN 3772354459.

[106] J. López, C. Ramírez, A. Torres, M. J. Abad, L. Barral, J. Cano, and F. J. Díez. Isothermal curing by dynamic mechanical analysis of three epoxy resin systems: Gelation and vitrification. *Journal of Applied Polymer Science*, 83 (1):78–85, 2002. ISSN 00218995. doi: 10.1002/app.10023.

[107] G. Luyckx. *Multi-axial strain monitoring of fibre reinforced thermosetting plastics using embedded highly birefringent optical fibre Bragg sensors*. Dissertation, Ghent University, 2009.

[108] M. Schwimmbeck. *Entwicklung eines kantenfilterbasierten faseroptischen Messsystems: Faseroptik und Gesamtintegration der Amplified Spontaneous Emission Lichtquelle*. Diploma thesis, Technical University Munich, 2011.

[109] N. G. MacCrum, C. P. Buckley, and C. B. Bucknall. *Principles of polymer engineering*. Oxford science publications. Oxford University Press, Oxford [u.a.], 1996. ISBN 0198561520.

[110] G. M. Maistros and C. B. Bucknall. Modeling the dielectric behavior of epoxy resin blends during curing. *Polymer Engineering & Science*, 34(20): 1517–1528, 1994. ISSN 00323888. doi: 10.1002/pen.760342002.

[111] G. M. Maistros and I. K. Partridge. Monitoring autoclave cure in commercial carbon fibre/epoxy composites. *Composites Part B: Engineering*, 29(3):245–250, 1998. ISSN 1359-8368. doi: 10.1016/S1359-8368(97)00020-6.

[112] I. H. Malitson. Interspecimen comparison of the refractive index of fused silica*,†. *Journal of the Optical Society of America*, 55(10):1205, 1965. ISSN 0030-3941. doi: 10.1364/JOSA.55.001205.

[113] B. A. Martin, S. W. Wenzel, and R. M. White. Viscosity and density sensing with ultrasonic plate waves. *Sensors and Actuators, A: Physical*, 22(1-3): 704–708, 1990. ISSN 09244247 (ISSN). doi: 10.1016/0924-4247(89)80062-7.

[114] J. N. Martin. Processes for engineering a system: An overview of the ansi/eia 632 standard and its heritage. *Systems Engineering*, 3(1):1–26, 2000. ISSN 1098-1241.

[115] R. J. Mathar. Refractive index of humid air in the infrared: Model fits. *Journal of Optics A: Pure and Applied Optics*, 9(5):470–476, 2007. ISSN 1464-4258. doi: 10.1088/1464-4258/9/5/008.

[116] T. Mayr. *Analysis of measurement accuracy of a fibre optical measurement device for isothermal cure monitoring*. Master thesis, Technical University Munich, 2016.

[117] T. S. Mesogitis, A. A. Skordos, and A. C. Long. Uncertainty in the manufacturing of fibrous thermosetting composites: A review. *Special Issue: 15th*

French National Conference on Composites - JNC15, 57(0):67–75, 2014. ISSN 1359-835X. doi: 10.1016/j.compositesa.2013.11.004.

[118] T. Mezger. *Das Rheologie-Handbuch*. Vincentz Network, Hannover, 4. aufl. edition, 2012. ISBN 3866308639.

[119] Mikhail N. Polyanskiy. Refractive index database. URL `https://refractiveindex.info`.

[120] A. Miño-Ron. *Development of an interface for fibre optic sensors embedded in composite structures*. Term paper, Technical University Munich, 31.10.2017.

[121] R. Montanini and L. D'Acquisto. Simultaneous measurement of temperature and strain in glass fiber/epoxy composites by embedded fiber optic sensors: I. cure monitoring. *Smart Materials and Structures*, 16(5):1718–1726, 2007. ISSN 0964-1726. doi: 10.1088/0964-1726/16/5/026.

[122] K. Moutzouris, M. Papamichael, S. C. Betsis, I. Stavrakas, G. Hloupis, and D. Triantis. Refractive, dispersive and thermo-optic properties of twelve organic solvents in the visible and near-infrared. *Applied Physics B*, 116 (3):617–622, 2014. ISSN 0946-2171. doi: 10.1007/s00340-013-5744-3.

[123] M. Mulle, F. Collombet, P. Olivier, and Y.-H. Grunevald. Assessment of cure residual strains through the thickness of carbon–epoxy laminates using fbgs, part i: Elementary specimen. *Composites Part A: Applied Science and Manufacturing*, 40(1):94–104, 2009. ISSN 1359-835X. doi: 10.1016/j.compositesa.2008.10.008.

[124] U. Müller, M. Philipp, M. Thomassey, R. Sanctuary, and J. Krüger. Temperature modulated optical refractometry: A quasi-isothermal method to determine the dynamic volume expansion coefficient. *Thermochimica Acta*, 555:17–22, 2013. ISSN 00406031. doi: 10.1016/j.tca.2012.12.011.

[125] A. K. Nair, V. R. Machavaram, R. S. Mahendran, S. D. Pandita, C. Paget, C. Barrow, and G. F. Fernando. Process monitoring of fibre reinforced composites using a multi-measurand fibre-optic sensor. *Sensors and Actuators B: Chemical*, 212:93–106, 2015. ISSN 09254005. doi: 10.1016/j.snb.2015.01.085.

[126] M. Neitzel, P. Mitschang, and U. Breuer, editors. *Handbuch Verbundwerkstoffe: Werkstoffe, Verarbeitung, Anwendung*. Hanser, München, 2., aktualisierte und erw. aufl., [elektronische ressource] edition, 2014. ISBN 978-3-446-43697-8.

[127] M. W. Nielsen, J. W. Schmidt, J. H. Hattel, T. L. Andersen, and C. M. Markussen. In situ measurement using fbgs of process-induced strains during curing of thick glass/epoxy laminate plate: Experimental results and numerical modelling. *Wind Energy*, 16(8):1241–1257, 2013. ISSN 10954244 (ISSN). doi: 10.1002/we.1550.

[128] D. J. O'Brien and S. R. White. Cure kinetics, gelation, and glass transition of a bisphenol f epoxide. *Polymer Engineering & Science*, 43(4):863–874, 2003. ISSN 00323888. doi: 10.1002/pen.10071.

[129] M. J. O'Dwyer, G. M. Maistros, S. W. James, R. P. Tatam, and I. K. Partridge. Relating the state of cure to the real-time internal strain development in a curing composite using in-fibre bragg gratings and dielectric sensors. *Measurement Science and Technology*, 9(8):1153–1158, 1998. ISSN 0957-0233. doi: 10.1088/0957-0233/9/8/002.

[130] J. Oelhafen, T. Mayr, K. Moutzouris, J. Roths, and K. Drechsler. Calibration and uncertainty of a fibre optic measurement system for fresnel reflectometer sensors. In Y. Chung, W. Jin, B. Lee, J. Canning, K. Nakamura, and L. Yuan, editors, *25th International Conference on Optical Fiber Sensors*, SPIE Proceedings, page 103235O. SPIE, 2017. doi: 10.1117/12.2260877.

[131] J. Oelhafen, F. Muschaweckh, S. Zaremba, and K. Drechsler. Fibre optical temperature sensor for distributed sensing in composite moulds. *21st International Conference on Composite Materials*, 2017.

[132] J. Oelhafen, T. Mayr, F. Dorner, K. Moutzouris, J. Roths, and K. Drechsler. Fiber optic measurement system for fresnel reflection sensing: Calibration, uncertainty, and exemplary application in temperature-modulated isothermal polymer curing. *Journal of Lightwave Technology*, 36(4):939–945, 2018. ISSN 07338724. doi: 10.1109/JLT.2017.2757525.

[133] R. A. Oliveira, J. Canning, K. Cook, M. Nashqbandi, and A. Pohl. Compact dip-style viscometer based on the acousto-optic effect in a long period fiber grating. *Sensors and Actuators B: Chemical*, 157(2):621–626, 2011. ISSN 09254005. doi: 10.1016/j.snb.2011.05.035.

[134] T. A. Osswald and N. Rudolph. *Polymer rheology: Fundamentals and applications*. Hanser Publications, Cincinnati, 2015. ISBN 9781569905173.

[135] A. Othonos, K. Kalli, D. Pureur, and A. Mugnier. Fibre bragg gratings. In H. Venghaus, editor, *Wavelength Filters in Fibre Optics*, pages 189–269.

Springer Berlin Heidelberg, Berlin, Heidelberg, 2006. ISBN 978-3-540-31770-8.

[136] J. C. Owens. Optical refractive index of air: dependence on pressure, temperature and composition. *Applied optics*, 6(1):51–59, 1967. ISSN 0003-6935.

[137] R. S. Parnas. *Liquid composite molding*. Hanser [u.a.], Munich [u.a.], 2000. ISBN 3446213945.

[138] N. Pearce, F. J. Guild, and J. Summerscales. An investigation into the effects of fabric architecture on the processing and properties of fibre reinforced composites produced by resin transfer moulding. *Composites Part A: Applied Science and Manufacturing*, 29(1-2):19–27, 1998. ISSN 1359-835X. doi: 10.1016/S1359-835X(97)00028-6.

[139] E. R. Peck and K. Reeder. Dispersion of air. *Journal of the Optical Society of America*, 62(8):958, 1972. ISSN 0030-3941. doi: 10.1364/JOSA.62.000958.

[140] G. R. Powell, P. A. Crosby, D. N. Waters, C. M. France, R. C. Spooncer, and G. F. Fernando. In-situ cure monitoring using optical fibre sensors - a comparative study. *Smart Materials and Structures*, 7(4):557–568, 1998. ISSN 0964-1726. doi: 10.1088/0964-1726/7/4/017.

[141] Y.-J. Rao. In-fibre bragg grating sensors. *Measurement Science and Technology*, 8(4):355–375, 1997. ISSN 0957-0233. doi: 10.1088/0957-0233/8/4/002.

[142] W. Reuter. *Hochleistungs-Faser-Kunststoff-Verbunde mit Class-A-Oberflächenqualität für den Einsatz in der Fahrzeugaussenhaut*, volume Bd. 19 of *IVW-Schriftenreihe / Institut für Verbundwerkstoffe GmbH - Kaiserslautern*. IVW, Kaiserslautern, als ms. gedr edition, 2002. ISBN 3934930158.

[143] L. Robert and G. Dusserre. Anisothermal thermosetting resin cure monitored by optical fiber refractometer. *Polymer Engineering & Science*, 54(3):626–635, 2014. ISSN 00323888. doi: 10.1002/pen.23596.

[144] Roberts, S. S. J. and R. Davidson. Cure and fabrication monitoring of composite materials with fibre-optic sensors. *Composites Science and Technology*, 49(3):265–276, 1993. ISSN 0266-3538. doi: 10.1016/0266-3538(93)90108-S.

[145] P. Royston. Approximating the shapiro-wilk w-test for non-normality. *Statistics and Computing*, 2(3):117–119, 1992. ISSN 1573-1375. doi: 10.1007/BF01891203.

[146] H. Saechtling and E. Baur. *Saechtling-Kunststoff-Taschenbuch*. Hanser, München, 30 edition, 2007. ISBN 9783446403529.

[147] S. D. Schwab, R. L. Levy, and G. G. Glover. Sensor system for monitoring impregnation and cure during resin transfer molding. *Polymer Composites*, 17(2):312–316, 1996. ISSN 0272-8397. doi: 10.1002/pc.10616.

[148] S. D. Senturia and N. F. Sheppard. Dielectric analysis of thermoset cure. In K. Dušek, editor, *Epoxy Resins and Composites IV*, volume 80 of *Advances in Polymer Science*, pages 1–47. Springer Berlin Heidelberg, Berlin, Heidelberg, 1986. ISBN 978-3-540-16423-4.

[149] S. S. Shapiro and M. B. Wilk. An analysis of variance test for normality (complete samples). *Biometrika*, 52(3/4):591, 1965. ISSN 00063444. doi: 10.2307/2333709.

[150] N. Shito. Specific volume, dielectric properties, and mechanical properties of cured epoxy resins in the glass-transition region. *Journal of Polymer Science Part C: Polymer Symposia*, 23(2):569–582, 1968. ISSN 04492994. doi: 10.1002/polc.5070230213.

[151] W. R. Simon and W. R. Pogue. Apparatus for ingress and egress of fiber optic sensor leads from the surface of composite parts and a method for the manufacture thereof. u.s. patent 6,173,090 b1.

[152] J. O. Simpson and S. A. Bidstrup. Rheological and dielectric changes during isothermal epoxy-amine cure. *Journal of Polymer Science Part B: Polymer Physics*, 33(1):55–62, 1995. ISSN 08876266. doi: 10.1002/polb.1995.090330106.

[153] W. B. Spillman and E. Udd. *Fiber Optic Sensors: An Introduction for Engineers and Scientists*. John Wiley & Sons Incorporated, 2006. ISBN 978-0-470-06810-6.

[154] H. Su and X. G. Huang. Fresnel-reflection-based fiber sensor for on-line measurement of solute concentration in solutions. *Sensors and Actuators B: Chemical*, 126(2):579–582, 2007. ISSN 09254005. doi: 10.1016/j.snb.2007.04.008.

[155] N. Takeda, Y. Okabe, J. KUWAHARA, S. KOJIMA, and T. OGISU. Development of smart composite structures with small-diameter fiber bragg grating sensors for quantitative evaluation of delamination length in cfrp

laminates using lamb wave sensing damage detection. *Composites Science and Technology*, 65(15-16):2575–2587, 2005. ISSN 0266-3538. doi: 10.1016/j.compscitech.2005.07.014.

[156] A. Talaie, T. Kosaka, N. Oshima, K. Osaka, Y. Asano, and T. Fukuda. Report on a simultaneous ion viscosity, strain and impedance measurement technique using a novel integrated dielectric, optical fiber and piezoelectric sensing element for the online characterization of smart structures. *Smart Materials and Structures*, 10(2):326–331, 2001. ISSN 0964-1726. doi: 10.1088/0964-1726/10/2/319.

[157] H. Teil, S. A. Page, V. Michaud, and J.-A. E. Månson. Ttt-cure diagram of an anhydride-cured epoxy system including gelation, vitrification, curing kinetics model, and monitoring of the glass transition temperature. *Journal of Applied Polymer Science*, 93(4):1774–1787, 2004. ISSN 00218995. doi: 10.1002/app.20631.

[158] M.-T. Ton-That, K. C. Cole, C.-K. Jen, and D. R. França. Polyester cure monitoring by means of different techniques. *Polymer Composites*, 21(4):605–618, 2000. ISSN 0272-8397. doi: 10.1002/pc.10216.

[159] F. Trochu, E. Ruiz, V. Achim, and S. Soukane. Advanced numerical simulation of liquid composite molding for process analysis and optimization. *Composites Part A: Applied Science and Manufacturing*, 37(6):890–902, 2006. ISSN 1359-835X. doi: 10.1016/j.compositesa.2005.06.003.

[160] S. Vacher, J. Molimard, H. Gagnaire, and A. Vautrin. A fresnel's reflection optical fiber sensor for thermoset polymer cure monitoring. *Polymers and polymer composites*, 12(4):269–276, 2004. ISSN 0967-3911.

[161] G. van Assche, A. van Hemelrijck, H. Rahier, and B. van Mele. Modulated differential scanning calorimetry: Isothermal cure and vitrification of thermosetting systems. *Thermochimica Acta*, 268:121–142, 1995. ISSN 00406031. doi: 10.1016/0040-6031(95)02693-2.

[162] VDA - Verband der Automobilindustrie. Volume 5: Capability of measurement processes, 2010.

[163] W.-C. Wang, S. S. Yee, and P. G. Reinhall. Optical viscosity sensor using forward light scattering. *Sensors and Actuators B: Chemical*, 25(1-3):753–755, 1995. ISSN 09254005. doi: 10.1016/0925-4005(95)85167-4.

[164] R. W. Warfield and M. C. Petree. Properties of crosslinked polymers as evidenced by electrical resistivity measurements. *Die Makromolekulare Chemie*, 58(1):139–159, 1962. ISSN 0025116X. doi: 10.1002/macp.1962.020580108.

[165] R. M. Waxler and G. W. Cleek. The effect of temperature and pressure on the refractive index of some oxide glasses. *Journal of Research of the National Bureau of Standards Section A: Physics and Chemistry*, 77A(6):755, 1973. ISSN 0022-4332. doi: 10.6028/jres.077A.046.

[166] H. H. Winter. Can the gel point of a cross-linking polymer be detected by the g' – g" crossover? *Polymer Engineering and Science*, 27(22):1698–1702, 1987. ISSN 0032-3888. doi: 10.1002/pen.760272209.

[167] G. Wisanrakkit, J. K. Gillham, and J. B. Enns. The glass transition temperature (tg) as a parameter for monitoring the cure of an amine/epoxy system at constant heating rates. *Journal of Applied Polymer Science*, 41(78):1895–1912, 1990. ISSN 00218995. doi: 10.1002/app.1990.070410743.

[168] D. L. Woerdeman, K. M. Flynn, J. P. Dunkers, and R. S. Parnas. The use of evanescent wave fluorescence spectroscopy for control of the liquid molding process. *Journal of Reinforced Plastics and Composites*, 15(9):922–943, 1996. ISSN 07316844 (ISSN). doi: 10.1177/073168449601500904.

[169] D. L. Woerdeman, J. K. Spoerre, K. M. Flynn, and R. S. Parnas. Cure monitoring of the liquid composite molding process using fiber optic sensors. *Polymer Composites*, 18(1):133–150, 1997. ISSN 0272-8397. doi: 10.1002/pc.10268.

[170] R. D. Yates and D. J. Goodman. *Probability and stochastic processes: A friendly introduction for electrical and computer engineers*. John Wiley & Sons, Hoboken, NJ, third edition edition, 2014. ISBN 1-118-32456-0.

[171] T. Zeh. *Optical fiber Bragg sensors: Measurement systems and signal processing*. Reports on measurement and sensor systems. Shaker, Aachen, 2005. ISBN 978-3-8322-4355-5.

[172] Y. Zhu, C. Wang, J. Wang, W. He, and G. Gao. Long-period gratings in-situ sensing for flow monitoring in liquid composite molding. *J. Mater. Sci. Technolog.*, (21):234–28, 2005.